



## REVIEW ARTICLE

10.1002/2016RG000529

## Key Points:

- Analysis methods for processing large GPS networks are described, and interpretation and access to products are discussed
- Detailed comparisons of analysis results from PBO and other GPS processing groups are given
- The estimation of scale changes (a common practice) has large impacts on vertical motion estimates

## Correspondence to:

T. A. Herring,  
tah@mit.edu

## Citation:

Herring, T. A., T. I. Melbourne, M. H. Murray, M. A. Floyd, W. M. Szeliga, R. W. King, D. A. Phillips, C. M. Puskas, M. Santillan, and L. Wang (2016), Plate Boundary Observatory and related networks: GPS data analysis methods and geodetic products, *Rev. Geophys.*, 54, doi:10.1002/2016RG000529.

Received 18 JUL 2016

Accepted 1 OCT 2016

Accepted article online 6 OCT 2016

## Plate Boundary Observatory and related networks: GPS data analysis methods and geodetic products

Thomas A. Herring<sup>1</sup>, Timothy I. Melbourne<sup>2</sup>, Mark H. Murray<sup>3</sup>, Michael A. Floyd<sup>1</sup>, Walter M. Szeliga<sup>2</sup>, Robert W. King<sup>1</sup>, David A. Phillips<sup>4</sup>, Christine M. Puskas<sup>4</sup>, Marcelo Santillan<sup>2</sup>, and Lei Wang<sup>1</sup>

<sup>1</sup>Department of Earth, Atmospheric, and Planetary Sciences, Massachusetts Institute of Technology, Cambridge, Massachusetts, USA, <sup>2</sup>Department of Geological Sciences, Central Washington University, Ellensburg, Washington, USA, <sup>3</sup>Department of Earth and Environmental Science, New Mexico Institute of Mining and Technology, Socorro, New Mexico, USA, <sup>4</sup>UNAVCO, Boulder, Colorado, USA

**Abstract** The Geodesy Advancing Geosciences and EarthScope (GAGE) Facility Global Positioning System (GPS) Data Analysis Centers produce position time series, velocities, and other parameters for approximately 2000 continuously operating GPS receivers spanning a quadrant of Earth's surface encompassing the high Arctic, North America, and Caribbean. The purpose of this review is to document the methodology for generating station positions and their evolution over time and to describe the requisite trade-offs involved with combination of results. GAGE GPS analysis involves formal merging within a Kalman filter of two independent, loosely constrained solutions: one is based on precise point positioning produced with the GIPSY/OASIS software at Central Washington University and the other is a network solution based on phase and range double-differencing produced with the GAMIT software at New Mexico Institute of Mining and Technology. The primary products generated are the position time series that show motions relative to a North America reference frame and secular motions of the stations represented in the velocity field. The position time series themselves contain a multitude of signals in addition to the secular motions. Coseismic and postseismic signals, seasonal signals from hydrology, and transient events, some understood and others not yet fully explained, are all evident in the time series and ready for further analysis and interpretation. We explore the impact of analysis assumptions on the reference frame realization and on the final solutions, and we compare within the GAGE solutions and with others.

### 1. Introduction

#### 1.1. Advances From the Plate Boundary Observatory

The Plate Boundary Observatory (PBO) is the core network of 1100 continuously operating Global Positioning System (GPS) stations managed as part of the Geodesy Advancing Geosciences and EarthScope (GAGE) Facility, the geodetic component of the National Science Foundation (NSF) EarthScope project. It is designed to provide open data access to study the three-dimensional strain rate across the active plate boundary zone between the North America and Pacific tectonic plates, including the Juan de Fuca plate, in the western United States and, through incorporation of associated networks, in neighboring countries [Silver *et al.*, 1998]. Although the broad kinematics of the North America-Pacific plate boundary, over the scale of the boundary itself, were previously known, the GAGE Facility has provided a density of stations appropriate for elucidating the details of how tectonic motions are accommodated on more regional spatial scales and daily, or even subdaily, temporal scales. A deeper understanding of faulting as well as volcanic processes throughout the western United States is only possible with an appropriate density of observations relative to the scale over which phenomena of interest occur, in both space and time. Silver *et al.* [1998] first postulated that this improvement of our geophysical knowledge and understanding would not be possible without a large, dense, dedicated network, such as that provided by the PBO, and the accurate and precise products generated from its operation. This is extremely important in areas such as Southern California and the San Francisco Bay Area, where myriad fault systems intersperse and interact within short distances compared to the plate boundary as a whole. Regional networks including the Southern California Integrated GPS Network (SCIGN) and the Bay Area Regional Deformation Network have previously provided dense geodetic networks acquiring GPS data in specific areas of interest but not across the entire North America-Pacific plate boundary. Therefore, until the advent of the PBO and its accompanying suite of self-consistent products, the commonality and relationship between different areas

©2016. The Authors.

This is an open access article under the terms of the Creative Commons Attribution-NonCommercial-NoDerivs License, which permits use and distribution in any medium, provided the original work is properly cited, the use is non-commercial and no modifications or adaptations are made.

along the same plate boundary, and consequent synthesis to advance scientific understanding and application, might be overlooked.

For example, prior to the PBO, *Dragert et al.* [2001] documented the occurrence of a “silent slip event” within the Cascadia subduction zone below southern Vancouver Island of British Columbia and the Olympic Peninsula of Washington State. Their study used just 14 GPS stations over an area of about 650 km by 650 km. Similar subsequent phenomena in the same area, accompanied by nonvolcanic microearthquakes, were termed “episodic tremor and slip” events by *Rogers and Dragert* [2003]. Since then, the PBO has provided an augmented network and core data that have led to the recording of tens of these episodes throughout the entire Cascadia subduction zone southward to northern California, not just in the small area near the western U.S.-Canada border [*Aguilar et al.*, 2009; *Gomberg et al.*, 2010]. Their distribution and recurrence of tremor and slip are vital to understanding how segmented the Cascadia subduction zone may be or whether it is capable of supporting much larger earthquakes in the future [e.g., *Brudzinski and Allen*, 2007; *Chapman and Melbourne*, 2009; *Holtkamp and Brudzinski*, 2010].

The availability of data and products in real or near real time across a dense network has enabled the launch of initiatives such as the Southern California Earthquake Center’s Transient Detection Exercise [*Lohman and Murray*, 2013]. This has enabled a routine, operational assessment of nonsecular phenomena, whether they are due to, for example, the initiation of a fault creep episode or a volcanic inflation episode. Both phenomena have a direct impact on hazard assessment in immediate and surrounding areas.

Other operational capabilities include an immediate release of displacements detected at PBO stations after moderate or larger earthquakes. These estimates may be used as they are, or the original raw data may be reprocessed by anyone for consistency with other approaches. For example, after the 21 August 2014 South Napa earthquake, one of the largest to occur within the PBO network to date, local GPS data were used to constrain models of seismic rupture [*Barnhart et al.*, 2015; *Dreger et al.*, 2015] and reprocessed alongside survey-mode GPS and interferometric synthetic aperture radar (InSAR) data to study afterslip phenomena and its relationship to the coseismic slip distribution [*Wei et al.*, 2015; *Floyd et al.*, 2016]. These studies each contribute to our knowledge of the process of the earthquake rupture itself and the coseismic and postseismic parts of the earthquake cycle.

The coverage of PBO stations extends to include volcanic provinces such as Yellowstone, where a wealth of new data has contributed to advances in our understanding of this region over many time scales. Continuously, changing patterns of deformation associated with decadal-scale inflation episodes have been reported by *Chang et al.* [2010], among others, using PBO stations in conjunction with InSAR observations. The density of precise GPS observations provided by the PBO allows a meaningful comparison and combination of geodetic techniques and aids in the interpretation of episodic data acquisition techniques like InSAR that may otherwise alias time-dependent deformation. Rapid (subannual) deformation episodes have also been captured, in association with observed seismic swarms, using PBO stations [e.g., *Farrell et al.*, 2010]. On the opposite end of the temporal spectrum, more subtle, long-period signals have also been extracted from time series, such as those following earthquakes near Yellowstone [e.g., *Chang et al.*, 2013], which have led to insights about the rheology and behavior of the deeper lithosphere throughout that region. Each of these phenomena over each of these time scales would not necessarily be separable without the dedicated precise products made available continuously from the PBO.

The high quality of geodetic data and products from the PBO has spurred new analysis methods that have also revealed heretofore undetected details of physical processes [e.g., *Ji and Herring*, 2013]. *Ji and Herring* [2011] showed that subtle inflation and deflation signals may be detected by using PBO stations monitoring Aleutian volcanoes in Alaska. This, again, has implications for hazard assessment in the absence of eruptive or seismic phenomena, as these episodes inform our knowledge of volcanic chamber depth, size, and deformation history.

These types of studies primarily use geodetic positioning, but there are many other applications already in use and the potential for other applications that are still being developed. The station positions determined in the analysis and products described in this paper are locations averaged over 24 h periods with latencies of 24 h to 6 months depending on data retrieval latency. However, in the event of a large earthquake, high-rate (1 Hz or 5 Hz with PBO data) kinematic positioning is also downloaded, which allows the position time history of the earthquake displacements to be determined and analyzed (e.g., *Larson et al.* [2003], *Vigny et al.* [2005],

*Delouis et al.* [2010], *Shao et al.* [2011], and many others). These high-rate solutions are possible in real time if the data are being telemetered in real time, and position estimates from these data can be used for rapid determination of large ground displacements with applications to earthquake and tsunami early warning [e.g., *Bock et al.*, 2004; *Blewitt et al.*, 2006; *Falck et al.*, 2010; *Wright et al.*, 2012] if the data are also available with low latency. In some examples of tsunami warning, the high-rate GPS receivers are located on ocean buoys [e.g., *Kato et al.*, 2005]. In the PBO region, the Cascadia subduction zone is being instrumented for tsunami early warning [e.g., *Crowell et al.*, 2012]. The combination of GPS receivers with accelerometers can greatly improve the sensitivity of the waveform estimates, and such systems are also being deployed in the PBO region [e.g., *Bock et al.*, 2011].

The availability of a large, continental-scale, unified data set has produced these new insights to geophysical phenomena over many spatial and temporal scales but also the development of innovative uses of the data from the receivers. For example, a path-dependent effect on the GPS observations can often be seen clearly in the signal-to-noise ratio (SNR) where the interference between the direct and reflected signals results in an oscillatory pattern in the SNR that can be related to the geometry and reflection characteristics of the reflecting surface. SNR variations have been used to infer snow depth around GPS antennas [*Larson et al.*, 2009; *Nievinski and Larson*, 2014a, 2014b], soil moisture [e.g., *Larson et al.*, 2008], and vegetation index [*Small et al.*, 2010]. Carrier phase measurements can also be used for these types of studies as well with the added complexity of needing a very accurate a priori model for the phase [e.g., *Ozeki and Heki*, 2012]. This probing of surface conditions through GPS reflectometry (i.e., satellite to surface to receiver pathways) to measure soil moisture, snow depth, vegetation moisture index, and other features provides crucial information regarding the water cycle and water resources [e.g., *Fu et al.*, 2015]. This enables the verification of the reliability of ground methods and provides a means by which to estimate snow depths, for example, away from traditional, and sparse, meteorological stations in areas that might otherwise be inaccessible.

The PBO has also supported ever-expanding uses of Global Navigation Satellite Systems (GNSS) data beyond geoscience. The surveying and civil engineering communities also use these data in a postprocessing mode and, increasingly, as real-time data streams [e.g., *Peyret et al.*, 2000; *Leick et al.*, 2015]. PBO stations are used as base stations, relative to which kinematic and short duration static stations are referenced.

The primary focus of this paper is to detail the methods used to generate position time series and related products from the GPS data generated by the PBO and related networks, which provide millimeter-level measurements of surface and near surface displacements associated with many different physical processes. We do not present new analyses and interpretations based on GAGE data and products. However, we cite many studies that have used GAGE data and products throughout this paper and we refer readers to those works for more detailed information about the scientific investigations that have been enabled by the operation of GAGE. For a list of publications using geodetic data from the UNAVCO community, see <http://www.unavco.org/science/community-publications/community-publications.html>. Furthermore, for more detailed snapshots of scientific discoveries made using geodetic data, see <http://www.unavco.org/science/snapshots/snapshots.html>.

## 1.2. High-Quality Geodetic Observations for EarthScope

Advances in our understanding of crustal, subaerial, and atmospheric processes derive from hypotheses that are tested by using direct observations of the Earth. Geodetic data form the principal measurements of most, if not all, contemporary studies of the deformation of Earth's surface. In addition to positioning results generated with different sampling and averaging intervals, the propagation delay of GPS microwave signals through the atmosphere to the antenna depends on water vapor content in the atmosphere, which is difficult to model. This water vapor sensitivity of GPS delay measurements has been used to study water vapor and precipitable water in the atmosphere [e.g., *Radhakrishna et al.*, 2015] and as an additional data source for numerical weather forecasting [e.g., *Bevis et al.*, 1992; *Rocken et al.*, 1997; *Wolfe and Gutman*, 2000; *Vey et al.*, 2010].

The ionosphere has been studied with GPS to gain a better understanding of the dynamics of the system [e.g., *Mannucci et al.*, 1998; *Orús et al.*, 2002]. Ionospheric delay variations have also been associated with propagating waves in the atmosphere and ionosphere excited by coseismic motions [e.g., *Calais and Minster*, 1995] and the tsunamis generated by large earthquakes [e.g., *Liu et al.*, 2006; *Galvan et al.*, 2011].

There are potentially many other applications of the data and results generated from the analyses of GPS and other Global Navigation Satellite System (GNSS) data that are still to be developed. The phase residuals from the GPS positioning process possibly combined with signal strength measurements could give more insights into the refractive and diffractive character of the medium through which the GPS signal propagates. Analysis of GPS raypaths through volcanic plumes is one possible application of these more detailed and specific models [e.g., *Houlié et al.*, 2005]. Additional avenues of research could be opened with the additional frequencies and satellite systems that become available with the newer generations of GNSS satellites and receivers. The open data and product policy associated with the PBO project allows all investigators to exploit these data.

The application of knowledge gained through analysis of GPS data extends well beyond the immediate scientific community, informing geoscientists and engineers involved in basic research, applied research (such as for earthquake hazard analyses, water resource management, and civil engineering), and public policy makers, who may use such results to plan for disaster preparedness, mitigation, and environmental monitoring. All of these applications rely on dedicated networks of geodetic instruments that are widespread, dense, operated over a long time, and record high-quality GPS/GNSS data continuously at a high rate, which are made freely available in real or near real time. To date, scientific studies have often been conducted by using small geodetic networks developed and maintained by individual or collaborating researchers or institutions. These data and associated metadata may or may not be available to the broader scientific community or the public at large. The value of a community network, and its potential uses as demonstrated in the works cited above and many others, gave rise to the PBO [e.g., *Silver et al.*, 1998]. This was initiated to provide geodetic data from a dedicated network of stations and products that are consistently processed, accurate, precise, and publicly available for free in real or near real time to all potential users. The variety of the potential users warrants a community approach to provide unified network installation, operations, maintenance, data management, and processing.

Coordinated efforts to produce geodetic products from global-, continental-, and regional-scale networks have existed since at least 1994, notably with the advent of the International GNSS Service (IGS). Other examples of geodetic networks designed to provide high-quality and high-level products in support of the geodetic community are the EUREF Permanent Network, GNSS Earth Observation Network System (GEONET), and Baseline Inferences for Fennoscandian Rebound Observations Sea Level and Tectonics (BIFROST). GEONET, which includes 1200 stations, is operated by the Geospatial Information Authority of Japan (<http://www.gsi.go.jp/ENGLISH/index.html>). Operating since 1994, the primary design goals of GEONET include support for national survey infrastructure and studies of seismic and volcanic activity [e.g., *Sagiyama*, 2004]. This network provided key data for analysis of the M9.0 11 March 2011 Tohoku earthquake [e.g., *Nishimura et al.*, 2011; *Simons et al.*, 2011]. Data from the BIFROST (Baseline Inferences for Fennoscandian Rebound Observations Sea Level and Tectonics) network, which includes about 40 stations covering Norway, Sweden, and Finland, was initiated in 1993 and led to the first three-dimensional crustal velocity solutions associated with glacial isostatic recovery [*Johansson et al.*, 2002].

However, some of these networks, as well as others of similar origin, rely on the collaboration and generosity of individual institutions and station operators to provide their data publicly in real time, as well as their maintenance of stations and data flows. The equipment used throughout the networks are therefore often heterogeneous, and the products are often designed more for use among geodetic scientists rather than by public agencies or industry, or individuals who may be interested in using final position or velocity estimates. The motivation and approach of the PBO, however, was to provide as homogeneous as possible a network of stations and products, all through one central agency and data access platform. Data streams and products are openly available for immediate and direct public use in various technical and intuitive formats, the latter of which require minimal technical knowledge.

The PBO is the largest scientific geodetic network in North America. We report on all aspects of the PBO from its inception to the presentation of current results, along with some advice and caveats for users of the products or those wishing to recreate them independently. The intention of this paper is not to perform detailed scientific analysis on the results but to document the routine operational procedures, technical achievements, and uses of the observation network, including some considerations revealed by the results. We discuss the network of instruments and associated monuments, data gathering, processing procedures, and generation and dissemination of geodetic products.

Following in this introductory section, we first describe the rationale and history of the PBO network, and roles of the institutions involved in the GAGE Facility. We also provide details of the work flow from geodetic sensor to data products accessible by the community. In section 2, we present the specific details of the analysis methods employed to process the raw (“Level 1”) data at each of the contributing institutions and at each stage in the work flow. In section 3, we describe the creation and dissemination of the GAGE Facility time series and velocity (“Level 2”) products. This is accompanied by a discussion of pertinent perturbations of the network, such as equipment changes and offsets due to the occurrence of earthquakes, both of which are common across a network of nearly 2000 stations and must be accounted for fully, correctly, and consistently. In section 4, we present a description of the geodetic results and discuss some important quality issues and perspectives from the various geographical regions covered that are evident in GAGE Facility products from long-running stations. Although thorough geophysical modeling, interpretation, and discussion of the processing results are beyond the scope of this paper, we nevertheless show several examples that demonstrate the diverse power of these community products. In section 5, we provide a set of considerations to users of the GAGE Facility products or those that process raw GPS data. These considerations are based on our collective experience with the network, data, and products presented here. This section is relevant to anyone developing, maintaining, or using data or products from a geodetic network of any size, not just those that are included by the GAGE Facility. We conclude section 5 by looking to the future of this endeavor and describe lessons learned during the course of the operations, maintenance, and processing of the network to date, a summary of the main results, and some final thoughts on the future of GNSS processing and prospects for enhanced data products and services. Finally, we refer the reader to Table A1, which contains expansions for the acronyms used throughout this manuscript.

### 1.3. Rationale and History of Community Geodetic Analyses and Products

UNAVCO operates the National Earth Science Geodetic Facility, known as the Geodesy Advancing Geosciences and EarthScope (GAGE) Facility, for the U.S. National Science Foundation (NSF) through a Cooperative Agreement. The GAGE GPS Analysis Centers (ACs) at the New Mexico Institute of Mining and Technology (NMT) and Central Washington University (CWU), and the GAGE GPS Analysis Center Coordinator (ACC) at the Massachusetts Institute of Technology (MIT), analyze data and continuously generate a suite of GPS data products from more than 2170 GPS stations across North America and the Caribbean. The GAGE GPS ACC/ACs, originally referred to as the PBO GPS ACC/ACs, were established in 2005 as part of the PBO Major Research Equipment and Facilities Construction (MREFC) project funded by the NSF and managed by the UNAVCO, which provides the overall management of the ACC/ACs and the data products they produce. These products include daily station position estimates, time series, velocity estimates, coseismic offsets, and tropospheric (zenith delay) parameters as described in detail in sections 2 and 3. They are based solely on GPS L1 and L2 phase and code observations at this time. Multiconstellation GNSS observables, even if the deployed receiver is capable of recording and/or streaming them, are not currently analyzed by the GAGE ACs. The term “GPS” is therefore used specifically throughout this text when discussing data analysis and data products. The term “GNSS” is only used when specifically discussing multiconstellation GNSS instrumentation and/or data flow.

Construction of the PBO core network of 1100 continuously operating GPS stations was completed in 2008, at which time the PBO MREFC construction phase transitioned into Operations and Maintenance (O&M), which spanned from 2008 to 2013. Continuation of the PBO GPS ACC/ACs in O&M mode focused on analyzing data from the 1100 core PBO GPS stations. During this time, new EarthScope science questions emerged [e.g., *Williams et al.*, 2010] and there was community interest in adding more stations to the PBO GPS analysis to provide increased spatial coverage away from the actively deforming Pacific-North America plate boundary to improve reference frame realization and to characterize nonplate boundary effects such as glacial isostatic adjustments and intraplate deformation.

This increase in spatial coverage was realized in 2012, near the close of the first PBO O&M stage, when plans were developed to add more than 500 non-PBO GPS stations to the PBO analysis. These additional stations, collectively referred to as “expanded analysis” stations, were selected based on location, data availability, data quality, and metadata accuracy. Also, at this time, stations from regional government, community, and other investigator networks, such as all stations from the Southern California Integrated GPS Network (SCIGN), were added to the analysis. Nearly 180 stations in the Caribbean and Mexico were

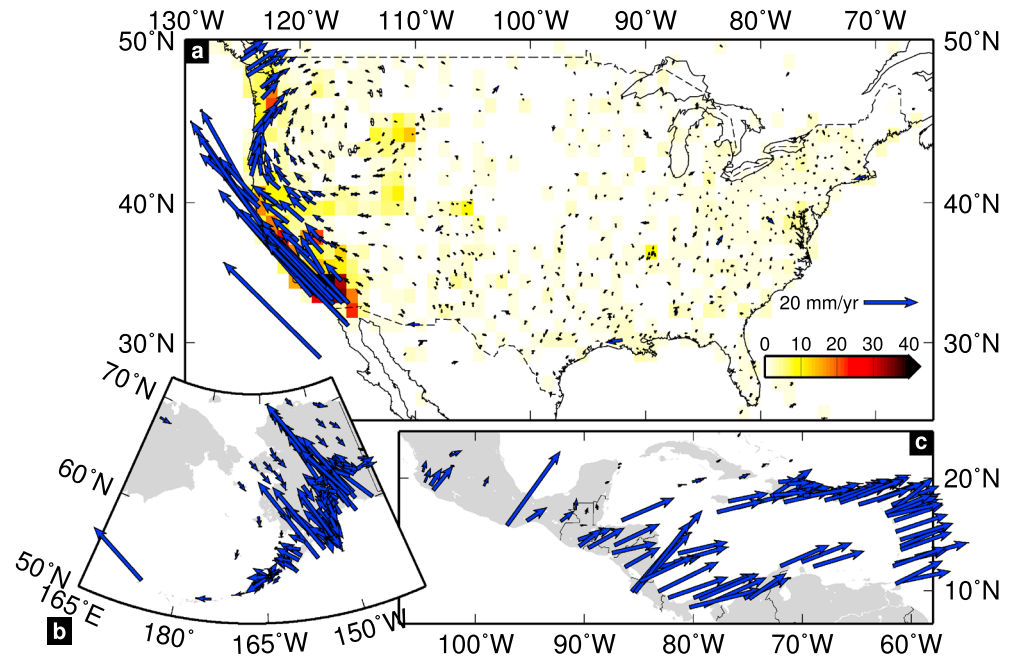


**Figure 1.** Horizontal velocities from the GAGE solution in (a) the contiguous United States, (b) Alaska, and (c) the Caribbean. The solution is decimated for clarity in Figure 1a, where only approximately 15% of the stations in the solution are shown west of 110°W. Velocity uncertainties are plotted at 95% confidence but are imperceptibly small at this scale. The background color map in Figure 1a shows the station density per square degree of the processed network in the contiguous U.S.

ultimately also added to the analysis as part of the NSF-funded Continuously Operating Caribbean GPS Observational Network (COCONet) [Braun *et al.*, 2012] and Trans-boundary Land and Atmosphere Long-term Observational and Collaborative Network (TLALOCNet) projects. In 2013 PBO O&M activities were incorporated into the current GAGE Facility. GPS data analysis continued, and the “PBO” ACC/ACs became known as the “GAGE” ACC/ACs.

The GAGE products comprise more than 2170 total GPS stations (as of 1 January 2016), including currently active as well as inactive stations with available data starting in 1996. One of the primary products generated by the GAGE analyses are the estimates of the secular motions of the stations. The current GAGE velocity solution is shown in Figure 1, and its generation is discussed in section 3. The density of stations is such that the solution is decimated for clarity in the western United States. The color background in Figure 1a shows the density of stations. The velocity field shows the expected features for the tectonics of the North America region: the large relative motions expected across the San Andreas Fault system, subduction in Cascadia, along the Aleutian Islands and in the Caribbean are clearly seen. The more diffuse motions throughout the Basin and Range province and around Yellowstone National Park are also visible. The coverage and precision of the velocity solution also reveal the horizontal and vertical motions associated with glacial isostatic adjustment and many other subtler motions induced by a variety of mechanisms.

#### 1.4. Data Source: Networks and Instrumentation

Data analyzed by the GAGE ACC/ACs originate from GPS stations in networks operated by UNAVCO including PBO (Figures 1a and 1b), COCONet and TLALOCNet (Figure 1c), and from networks operated by various other research groups, universities, and government agencies. Stations operated by UNAVCO were installed to meet specific geophysical research criteria based on geographic location and feature standardized instrument configurations (e.g., receiver type and antenna type), monumentation, metadata, and data flow. The importance of complete and accurate metadata cannot be overstated as station configuration changes can affect a time series directly due to, for example the introduction of offsets due to antenna changes, or indirectly due to inappropriate processing parameters being applied during raw data analysis. Stations from networks not operated by UNAVCO, the expanded analysis stations, are heterogeneous in terms of their

originally intended application, instrumentation, monumentation, metadata, and data flow. Data from some expanded analysis stations can potentially be of lower quality than from core PBO and other GPS stations installed and operated by UNAVCO. As of April 2016, for the preceding 6 months the ACs processed an average of 1709 stations with 1 day latency, 1801 with 2 to 3 week latency, 1844 with 12 week latency, and 1884 with 26 week latency with the latency being driven by data being downloaded from receivers.

#### 1.4.1. Plate Boundary Observatory (PBO) Stations

The 1100 core PBO stations are primarily located in the western U.S. and Alaska at sites specifically intended to support high-quality geodetic observations of geophysical processes (Figures 1a and 1b). GPS station locations were guided by EarthScope community science advisory committees and were classified according to transform, subduction, extension, and magmatic system tectonic regimes. By design, PBO station density correlates with regions of highest strain rate, in particular: the San Andreas Fault system, especially in Southern California (a transform boundary); above the Cascadia subduction zone; throughout the Basin and Range (an extensional province); and around Yellowstone National Park (a volcanic center). Each of these regions has a density of stations of approximately 10–20 per square degree of arc (midyellow background in Figure 1a) and over 40 per square degree of arc around Los Angeles and adjacent counties (dark red and black in Figure 1a). This is equivalent to interstation distances of approximately 20–30 km and less than 15 km, respectively (assuming an even geometric distribution). Correspondingly, the network density is lower in areas where strain rates are lower, such as across the eastern two-thirds of the continental United States, and where geography reduces the available land for station siting, such as along the Aleutian Islands and throughout the Caribbean.

Optimally, PBO stations are located on bedrock with good sky view. Dedicated geodetic monuments were installed to maximize stability. For example, of the 1100 core PBO stations, 569 use deep-drilled braced monuments [Langbein *et al.*, 1995] and 441 are short-drilled braced monuments, with the remainder including pillar, wellhead, permafrost thermopile, and a small number of building roof installations. All PBO core stations were originally outfitted with Trimble NetRS receivers and Dorne-Margolin element choke-ring antennas with SCIGN radomes. While most PBO stations were constructed by UNAVCO during the PBO MREFC award period, 223 preexisting stations were upgraded by UNAVCO to PBO specifications and integrated into the network as part of the “PBO-NUCLEUS” project. Recently, some PBO stations have been upgraded to GNSS capability with Trimble NetR9 receivers, all of which have Global Navigation Satellite System (GNSS) tracking enabled starting in early 2016, with additional stations to be upgraded with Septentrio PolaRx5 multiconstellation GNSS receivers in 2016. Standardized equipment configurations and quality control practices are key features of the networks managed by UNAVCO, and this greatly facilitates data access and quality control through the use of common interfaces.

#### 1.4.2. COCONet and TLALOCNet Stations

Compared to the PBO network, in which the geographic distribution of stations was optimized as much as possible to observe specific geophysical processes, the COCONet geometry in the eastern Caribbean is limited in part by the geographic distribution of islands on which to install stations. Nevertheless, COCONet station locations were strategically selected to provide as spatially dense a network as possible with limited resources while addressing the specific science goals associated with solid Earth processes such as plate kinematics and dynamics, and plate boundary interaction and deformation, including earthquake cycle processes. COCONet also provides precise estimates of column-integrated tropospheric water vapor to enable better forecasting of the dynamics of tropospheric moisture associated with the yearly Caribbean hurricane cycle and provides a regional framework for future atmospheric science objectives. When possible, COCONet stations were also collocated with tide gauges to facilitate comparisons of sea level height in a global reference frame. Eighty one of the COCONet stations were built or refurbished by UNAVCO and feature the same basic hardware, data, and metadata configurations and standards as the PBO. The remainder comprise contributed stations installed and maintained by COCONet partner organizations. These stations have heterogeneous instrumentation, monumentation, metadata management configurations, and data flow. At the time of this submission, there are 145 COCONet stations being analyzed as part of the GAGE ACC/AC stream.

The locations of TLALOCNet stations are optimized as much as possible to support geophysical and atmospheric research investigations with a focus on the development of the tropical monsoon and moisture transfer from the Pacific Ocean to the North American continent, and examination and characterization of elastic

strain accumulation and episodic tremor and slip along the Middle America Trench in Mexico. Most TLALOCNet stations have been built or refurbished to PBO standards by UNAVCO, with some stations also being contributed primarily by UNAVCO's NSF Major Research Instrumentation (MRI) project partner, Universidad Nacional Autónoma de México (UNAM). Additional COCONet and TLALOCNet stations continue to come online at the time of this submission. Accordingly, the number of stations processed by the GAGE ACC/ACs will continue to increase. At the time of this submission, 36 TLALOCNet stations are analyzed as part of the GAGE ACC/AC stream.

#### 1.4.3. Expanded Analysis Stations

The remainder of stations in the GAGE analysis originate from networks not directly operated or managed by UNAVCO. These are collectively referred to as expanded analysis stations and provide increased spatial coverage away from the actively deforming plate boundary as well as increased spatial density within the PBO region. Specific objectives for the expanded analysis stations were to provide (1) a backbone network of stations to yield a minimum spacing of 100–200 km covering the entire North American continent and (2) denser groupings of stations in regions of geophysical interest not covered by PBO stations, such as known seismic zones in the eastern U.S. and Canada, areas of ongoing glacial isostatic adjustment (GIA), and undersampled regions within the PBO footprint. Stations from global and regional networks are also analyzed to help improve North America plate reference frame realization. There are two main classes of expanded analysis stations: (1) those from networks designed for geophysical applications and (2) those from networks designed for more general applications such as monitoring civil engineering infrastructure.

Specific stations from networks managed by government agencies, community, and principal investigators whose configurations are optimized for geophysical research or as geodetic reference frame stations were preferentially selected for expanded GAGE analysis. These stations include all stations in the GAGE region from the Southern California Integrated GPS Network (SCIGN), the NASA Global Geodetic Network (GGN), the International GNSS Service (IGS) network, the Rio Grande Rift network, the GPS Array for Mid America, the Basin and Range Geodetic Network (BARGEN), the Idaho National Laboratory (INL) network, the Pacific Northwest Geodetic Array (PANGA), the Western Canada Deformation Array, SuomiNet, GulfNet, and stations near the epicenter of the 23 August 2011 *M*5.8 Mineral, Virginia, earthquake. These networks have heterogeneous equipment configurations as a whole, but they are often internally consistent, and a requirement for selection was that they have and report good metadata overall. UNAVCO provides some level of support for the operation of many of the stations in these networks.

In contrast to stations associated with the networks discussed immediately above (e.g., SCIGN), most of the expanded analysis stations in the eastern U.S. were not installed with geophysical research objectives in mind. Nevertheless, these stations help provide key geographic distribution and network densification across the North American continent. Most of these expanded stations are part of the National Oceanic and Atmospheric Administration's (NOAA) National Geodetic Survey (NGS) Continuously Operating Reference Station (CORS) network.

#### 1.5. Data and Data Flow

The GPS, and increasingly GNSS, receivers at the stations in the networks generate multifrequency pseudorange and phase data, and signal-to-noise ratio (SNR) measurements for the satellites being tracked. The standard GPS data collection rate for networks operated by UNAVCO, including PBO, COCONet, and TLALOCNet, is one sample every 15 s. Data are stored in files that span one GPS time (GPST) day (00:00:00 GPST to 00:00:00 GPST) and are downloaded daily. Most UNAVCO stations also record data at 1 and 5 samples per second in a temporary buffer, which are downloaded after an earthquake or other significant geophysical event. These high-rate data are not routinely processed by the GAGE ACs. In addition, more than 450 of the GPS stations managed by UNAVCO stream 1 Hz data in real time, but these streams are not processed by the GAGE ACs and these data will not be addressed in this paper. Raw GPS data from stations managed by UNAVCO are transmitted, often in a vendor-specific proprietary format, to the UNAVCO Data Center by various means of telecommunication including internet, radio and, in some cases, by satellite links. Metadata are carefully tracked and maintained in a dedicated database at UNAVCO.

Data flow consists of the following primary components: (1) collection and transfer of Level 0 (raw) GPS data from field instruments to the UNAVCO Data Center; (2) generation of Level 1 (Receiver Independent Exchange (RINEX)) data including file translation, quality checks, archiving, distribution, and metadata

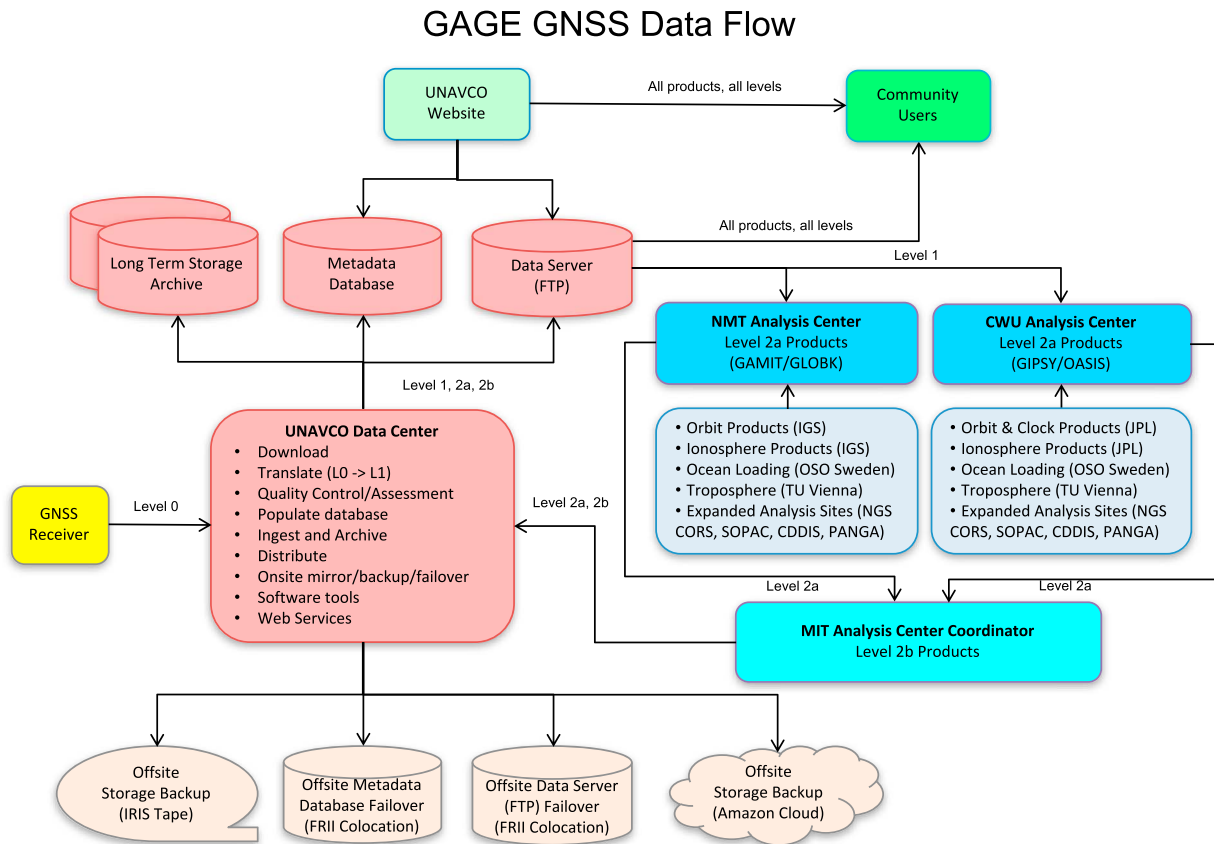


**Figure 2.** GAGE GNSS data flow.

management at UNAVCO; (3) generation of Level 2a products by the ACs, including loosely constrained position solutions; and (4) generation of Level 2b products by the ACC, including position solutions, time series, and velocities realized in a well-defined terrestrial reference frame, and offset estimates due to earthquakes, equipment changes, and other discontinuities. The raw GPS data are converted to RINEX version 2.11 format and quality-checked using the *teqc* software [Estey and Meertens, 1999]. The ACC transfers all Level 2a and 2b products to the UNAVCO Data Center (<http://www.unavco.org/data/data.html>) for subsequent archiving and distribution to the user community by UNAVCO. Level 2b data products undergo additional quality assessment at UNAVCO including the generation of quality assessment products using tools developed by the University of Nevada at Reno Geodesy Laboratory. Data products from all levels are distributed currently via FTP, HTTP and Web services. Offsite FTP and redundant (“failover”) systems are provided by Front Range Internet, Inc. (FRII). Additional offsite data storage and backups are provided by Amazon Cloud and the Incorporated Research Institutions for Seismology (IRIS) Data Management Center (DMC). Figure 2 provides an illustration of this data flow schema.

Most data analyzed by the ACs are obtained directly from the UNAVCO archive as described above and shown in Figure 2. For stations archived by UNAVCO but not operated by UNAVCO, steps 1 and 2 in the above data flow description are combined, as Level 1 (RINEX) data are typically provided by network operators instead of Level 0 (raw) data. For the ~350 expanded analysis stations not archived by UNAVCO, the ACs download Level 1 (RINEX) data and metadata directly from alternate station operators or data centers including the NGS, the NASA Crustal Dynamics Data Information System (CDDIS), the U.S. Geological Survey (USGS), the Scripps Orbit and Permanent Array Center (SOPAC), and PANGA.

All data products resulting from these analyses are archived and distributed by UNAVCO and made available on a free and open basis to the community with no artificial delay in accordance with NSF, EarthScope, and UNAVCO data policies [e.g., Pritchard et al., 2012].

**Table 1.** Processing Models Common Between the ACs<sup>a</sup>

Processing Parameter	Model
Second-order Ionosphere	Not applied for rapid orbit solution
Subdaily Earth Rotation Model	IERS 2010
Solid Earth tides	IERS 2010/IERS2003
Ocean tidal loading	FES2004 convolved with Green's functions by the ocean tide loading Web service at Chalmers University of Technology
Atmospheric nontidal loading	Not applied
Atmospheric tidal loading	Not applied
A priori atmospheric parameters (pressure, temperature, and zenith delay)	For final orbit solution: VMF1 pressure, temperature, zenith delay
Tropospheric mapping function	For final orbit solution: VMF1 grid

<sup>a</sup>Full model descriptions are given in the GAGE data analysis plan (<https://www.unavco.org/data/gps-gnss/derived-products.html>).

## 2. Analysis Methods

### 2.1. Analysis Centers

Two independent Analysis Centers (ACs) were originally specified during early planning of the PBO for a number of reasons. First, it was widely recognized that GPS analysis algorithms and software packages continued to evolve and that routine comparison of independent solutions offered the only feasible way rapidly to discover, diagnose, and fix analysis issues whose manifestation could be very difficult to predict otherwise. Avoidable mistakes, such as flawed station metadata from the field or introduced during processing, take on meaningful significance when handling thousands of stations daily, but fortunately lend themselves to automatic detection. Subtle errors, such as flawed models or incorrect parameterizations used during processing, can affect long-term time series and derived velocities but are more difficult to detect automatically and require a second analysis, as independent as possible, with which to compare. In 10 years of practice, comparison of solutions has proven very useful by revealing processing issues that would likely not have been identified without routine and automatic comparison. Second, it was felt that having two geographically distributed analysis centers greatly reduced the risk of loss due to catastrophic failure at one analysis center. In practice, this too was borne out when water leaks at one analysis center destroyed servers. The damaged computers required several months to replace.

The two GAGE Facility ACs, one using the GPS Inferred Positioning System, Orbit Analysis and Simulation Software (GIPSY/OASIS) (CWU) and one using the GPS At MIT (GAMIT) (NMT) software package, provide loosely constrained, nonfiducial solutions following standard and widely used GPS data processing strategies. The methodology and algorithms behind precise point positioning with ambiguity-resolution based on external wide-lane phase bias estimates as used in GIPSY are described in *Zumberge et al.* [1997] and *Bertiger et al.* [2010], while the methodology and algorithms behind the double-differencing used in GAMIT are documented in *Dong et al.* [1998] and *Herring et al.* [2015]. Below, we briefly describe the generation of nonfiducial solutions by each of the two analysis centers. Table 1 documents external products, including the models for atmospheric delay and mapping functions, tide, and tidal loading models, that are common between ACs.

We discuss below general aspects of the processing models used for the GAGE analyses. The full description of the processing algorithms, including updates, is given on the GAGE-derived product Web site in the GAGE data analysis plan (<https://www.unavco.org/data/gps-gnss/derived-products.html>).

### 2.2. New Mexico Tech GAMIT Solution

The GAGE Analysis Center at NMT analyzes the GPS observables using version 10.6 of the "GPS At MIT"/Global Kalman filter (GAMIT/GLOBK) software, developed primarily by MIT [*Herring et al.*, 2015]. The GAMIT software component can estimate station positions, atmospheric delays, satellite orbits, and Earth orientation parameters from ionosphere-free linear combination GPS phase observables using double-differencing techniques to eliminate phase biases caused by drifts in the satellite and receiver clock

oscillators. GPS pseudo range observables are used to constrain clock timing offsets to within  $1 \mu\text{s}$ , which is adequate to keep errors in the doubly differenced phase observations below 1 mm. Pseudo range observations are also used to improve automated editing of the phase data and assist in the resolution of integer phase ambiguities. GAMIT incorporates a weighted least squares algorithm to estimate the station position and satellite orbit parameters, first using constrained a priori station positions (nominally at the 0.05 m level) to aid phase ambiguity resolution, and then using weakly constrained station positions (at the 100 m level) to generate position and covariance solutions that can then be combined with the GLOBK software. GLOBK uses Kalman filtering techniques to estimate station positions, time series, velocities, and transient deformation.

For the GAGE analysis, satellite orbit parameters are fixed to the IGS rapid or final orbit product values. Second-order ionospheric corrections are applied in the final-orbit solutions based on the formulation of *Fritsche et al.* [2005]. To perform the double-differencing of the phase observables, GAMIT must perform estimates using a defined network of stations. For computational efficiency, the GAGE network is divided into subnetworks, each currently with 80 or fewer stations. For the final-orbit solutions, which include ~1800 stations, the subnetworks typically have 50 stations, resulting in ~36 individual network solutions. The stations in each subnetwork are determined every day based on station availability and are chosen by geographic location to minimize station baseline lengths, which improves integer phase ambiguity resolution. To allow combination of the subnetworks into a single full-network solution using GLOBK, tie stations (two for the final-orbit solutions with 3 week latency) are included that are common to nearby subnetworks. Due to the large geographic extent of the GAGE network, an additional solution is performed that includes one station from each subnetwork, which stabilizes the rigidity of the full-network solution. For the final-orbit solutions with 12 and 26 week latency, which typically have fewer than 80 new stations, a single subnetwork solution of the new stations, plus ~6 stations in common with the 3 week final-orbit solution, is estimated. This single subnetwork solution is then combined by the ACC with the 3 week final-orbit solution using GLOBK to provide the 12 and 26 week full-network solution.

Integer phase ambiguities are generally well resolved in all the subnetwork solutions. Greater than 90.6% of wide-lane ambiguities (difference in cycles between the L2 and L1 phase observables), and greater than 85.2% of narrow-lane (L1) ambiguities, are resolved in 95% of the solutions. In the best 30% of the solutions, 99.6% of the wide-lane and 96.5% of the narrow-lane ambiguities are resolved. In some cases, fewer ambiguities (72–85%) are resolved, apparently due to specific firmware versions in some receivers.

### 2.3. Central Washington University GIPSY Solution

Solutions using the precise point positioning (PPP) technique are produced using GIPSY/OASIS II version 6.3 software, developed by the Jet Propulsion Laboratory (JPL), and JPL version 2.1 orbit solutions [*Zumberge et al.*, 1997]. Daily solutions for individual station position and covariances employ ambiguity resolution using imposed wide-lane phase bias (WLPB) constraints derived from the global GPS network and provided by JPL, as described by *Bertiger et al.* [2010]. Ocean tide loading effects are accounted for in all position products with ocean loading displacements coefficients calculated by using the ocean tide loading Web service run by Chalmers University of Technology using the FES2004 ocean tide model and include corrections for center of mass motion (ocean plus solid Earth). Estimates of zenith wet delay derived from gridded reanalysis of European Centre for Medium-Range Weather Forecast data are included through the Vienna Mapping Functions grids (VMF1) [*Boehm et al.*, 2006]. Incorporation of second-order ionospheric effects [*Kedar et al.*, 2003] requires estimates of the global total electron content (TEC) and the orientation of the magnetic dipole field of the Earth. Global TEC estimates from JPL in the form of Ionosphere Map Exchange format (IONEX) files (<ftp://cddis.gsfc.nasa.gov/pub/gps/products/ionex>) are preferred and generally used. IONEX files provided by the IGS are used when JPL products are unavailable. Estimates of the magnetic dipole field of the Earth are calculated from the IGRF11 model (<http://www.ngdc.noaa.gov/IAGA/vmod/igrf.html>) [*Finlay et al.*, 2010]. For the purposes of calculating the second-order ionospheric correction, the Earth's ionosphere is modeled as a 600 km high thin shell.

Neither phase nor range differencing between stations is employed in GIPSY so stations are processed individually and asynchronously, which allows efficient parallelization during processing. Solutions are run daily

**Table 2.** Processing Models That Differ Between the ACs

Model	CWU	NMT
Processing strategy	Precise point positioning	Double-differencing
Date sampling	5 min	2 min
Orbits and clocks	JPL rapid and final orbits and clocks	IGS rapid and final orbits
Second-order ionospheric products	JPL IONEX files, beginning GPS Week 1817 (05 November 2014)	IGS IONEX files, beginning GPS week 1849 (14 June 2015).
Atmospheric zenith delay and gradient estimates	Stochastic process with process noise uncertainties of 3 mm/√h in zenith wet delay and 0.3 mm/√h in zenith wet delay gradient	Two-hour interval zenith wet delay piecewise linear function with process noise uncertainty constraint of 20 mm/√hr. Twelve-hour interval zenith wet delay gradients with a priori constraint of 10 mm at 10° elevation.
Elevation angle cutoff	15°	10°
Phase elevation weighting	Constant	Site dependent constant and 1/sin (elevation angle) terms
A priori atmospheric parameters (pressure, temperature, and zenith delay)	For rapid orbit solution: nominal wet tropospheric delay constant 0.1 m, nominal dry tropospheric delay exponential model	For rapid orbit solution: GPT2, 50% relative humidity
Tropospheric mapping function	For rapid orbit solution: NIELL	For rapid orbit solution: GPT2 wet mapping function

with rapid orbit and clock corrections and WLPB estimates and run weekly as final products become available. Processing with rapid orbit products does not include VMF1 zenith wet delay information or second-order ionospheric corrections to maintain consistency with the orbit products provided by JPL. Rapid-orbit station positions are expressed as fiducial positions, i.e., constrained to their a priori coordinates consistent with the IGS rapid processing standards, within the IGS realization (IGb08) of the International Terrestrial Reference Frame [Altamimi *et al.*, 2011]. In comparison, weekly and supplemental data processing with final orbit and clock products do include second-order ionospheric corrections from JPL and a priori zenith wet delay information using VMF1 data and results in fiducial-free positions in the satellite reference frame of the day, defined by JPL.

#### 2.4. Differences Between Analyses

Two main strategies are employed in the initial phase processing by the two analysis centers: double-differencing [e.g., Bock *et al.*, 1986] and precise point positioning [Zumberge *et al.*, 1997]. One immediate difference in external product requirements for precise point positioning is the need for estimates of satellite clocks as well as precise satellite orbits, which are not required a priori for double-differencing. In the ACs' processing, the GIPSY processing uses orbits, clocks, and WLPBs produced by JPL [Bertiger *et al.*, 2010; Desai *et al.*, 2014], while the GAMIT processing uses IGS orbit products [e.g., Beutler *et al.*, 1999]. The difference in orbit (and clock products) arises because the IGS reprocessed clocks, needed for processing pre-2010 data, inherit the scale from the International Terrestrial Reference Frame 2005 realization (ITRF2005) system, and are inconsistent with ITRF2008 products (see section 5.6). The JPL clocks and orbits used in the CWU processing are generated in the ITRF2008 system.

Aside from the principal strategies in processing pseudorange and carrier phase data, considerable effort has been made to ensure that the remaining processing parameters used at each analysis center match as closely as possible. Table 2 describes some of the major processing model decisions that are common between the analysis centers and some processing parameter choices that differ between the analysis centers. The most significant of these differences is that in phase data weighting. At present, a constant phase weighting over all elevation angles is used in the GIPSY processing. In contrast, the GAMIT processing uses a phase variance,  $\sigma^2$ , computed from

$$\sigma^2 = a^2 + \frac{b^2}{\sin^2(\varepsilon)} \quad (1)$$

where  $\varepsilon$  is the elevation angle, and the coefficients  $a$  and  $b$  are estimated from a least squares fit to the scatter of the postfit phase residuals. In addition, differences in elevation cutoff angle have arisen with 15° being

used in the GIPSY processing and  $10^\circ$  being used in the GAMIT processing. Other notable differences include the a priori tropospheric parameters and the tropospheric mapping functions used in the rapid orbit processing. For CWU, the rapid orbit processing employs the tropospheric mapping function of *Niell* [1996], a constant a priori nominal wet delay of 0.1 m and an exponential model for the nominal a priori dry delay ( $Z_d$ ) according to the following function:

$$Z_d = 1.013 \times 2.27 \times e^{(-0.116 \times 10^{-3} \times h)} \quad (2)$$

where  $h$  is the height above the ellipsoid in meters and  $Z_d$  is in units of meters. In contrast, NMT uses a global pressure and temperature model, GPT2 [Lagler *et al.*, 2013], with 50% relative humidity for the nominal wet and dry delays.

### 2.5. Combination Solution

The daily analyses from the two ACs are submitted as Solution Independent Exchange (SINEX) format files [IERS, 2005], which contain station position estimates and variance-covariance information. These SINEX files are combined in a common reference frame with a weighted least squares approach. The combined solution uses the file naming code “PBO” to differentiate them from the input AC solutions, denoted as “CWU” and “NMT.” The treatment of the SINEX files from the two ACs is slightly different because the methods used to generate their initial loosely constrained position estimates are different. The RMS scatters of the position time series from individual analyses are similar, but the data noise models differ, resulting in the CWU position estimates having standard deviations  $\sim 2.6$  times smaller than the NMT values. We therefore re-scale the covariance matrices from the two ACs to weight the solutions equally (described in detail below). The alignment of the frames between the two analyses is performed in the combination step by allowing the position estimates to rotate and translate. In addition, gross error detection is performed during the combination stage to remove any stations whose estimates differ by more than 0.5 m from the a priori values. In the event of a large earthquake, the a priori coordinates are updated shortly after the earthquake to avoid having stations with large displacement being deleted from the final combined solution. The individual operations used in the combination are discussed in detail below. Finally, the daily solutions from each AC and from their combination are aligned to a common reference frame by estimating the rotations and translations needed to minimize the position residuals at a specified set of reference frame stations. Since 2008, the number of reference frame stations has usually been  $\sim 575$ . Details of this procedure are discussed in section 3.

The NMT version 2.01 SINEX files are delivered with weak constraints ( $\pm 100$  m) applied to the coordinates and are considered to be fiducial-free solutions. These SINEX files have a full variance covariance matrix. The CWU version 1.00 SINEX files are from precise point positioning with fixed satellite clock and orbit estimates. The standard deviations of station coordinates in the SINEX files are small (typically 1–3 mm) although they are from fiducial-free solutions. In addition, the covariance matrices for the GIPSY-derived SINEX files have no station-to-station covariance values. In order to make the GIPSY-derived SINEX files loosely constrained and to complete in the whole covariance matrix, we add to the block diagonal covariance matrix in the SINEX files a covariance matrix which allows the system to rotate and translate. The addition of this covariance matrix allows the solutions to rotate and translate to align to different reference frame realizations without the need for explicit rotation and translation parameters in the Kalman filter state vector. The added covariance matrices allow translation and rotation with standard deviations of  $\sim 1$  m at the surface of the Earth. The formulation of this additional covariance is based on the standard propagation of variance-covariance matrices methodology. The changes in Cartesian coordinates of a station,  $i$ , located at  $X_i$ ,  $Y_i$ , and  $Z_i$  due to rotations,  $\Delta\phi_x$ ,  $\Delta\phi_y$ , and  $\Delta\phi_z$ , about the global XYZ axes, with the sign convention and angle definitions (pole position and UT1-UTC) of the standard Earth orientation parameters, are

$$\begin{pmatrix} \Delta X_i \\ \Delta Y_i \\ \Delta Z_i \end{pmatrix} = \begin{pmatrix} Z_i & 0 & Y_i \\ 0 & -Z_i & -X_i \\ -X_i & Y_i & 0 \end{pmatrix} \begin{pmatrix} \Delta\phi_x \\ \Delta\phi_y \\ \Delta\phi_z \end{pmatrix} \quad (3)$$

where  $\Delta X_i$ ,  $\Delta Y_i$ , and  $\Delta Z_i$  are the changes to the Cartesian coordinates. The covariance matrix contribution for two stations  $i$  and  $j$  due to rotation and translations with a priori variances  $\sigma_\phi^2$  and  $\sigma_t^2$  is given by

$$\begin{pmatrix} \sigma_{X_i}\sigma_{X_j} & \sigma_{X_i}\sigma_{Y_j} & \sigma_{X_i}\sigma_{Z_j} \\ \sigma_{X_i}\sigma_{Y_j} & \sigma_{Y_i}\sigma_{Y_j} & \sigma_{Y_i}\sigma_{Z_j} \\ \sigma_{X_i}\sigma_{Z_j} & \sigma_{Y_i}\sigma_{Z_j} & \sigma_{Z_i}\sigma_{Z_j} \end{pmatrix} = \begin{pmatrix} (Z_i Z_j + Y_i Y_j)\sigma_\phi^2 + \sigma_t^2 & -Y_i X_j \sigma_\phi^2 & -Z_i X_j \sigma_\phi^2 \\ -X_i Y_j \sigma_\phi^2 & (Z_i Z_j + X_i X_j)\sigma_\phi^2 + \sigma_t^2 & -X_i Y_j \sigma_\phi^2 \\ -X_i Z_j \sigma_\phi^2 & -Y_i Z_j \sigma_\phi^2 & (X_i X_j + Y_i Y_j)\sigma_\phi^2 + \sigma_t^2 \end{pmatrix} \quad (4)$$

The variances assigned to the rotation and translations are equivalent to 1 m<sup>2</sup> at the Earth's surface. The NMT analysis is already loosely constrained and so we do not change its covariance matrix. However, because the IGS orbits are fixed, the origin of the GPS terrestrial frame is well determined, and hence, we explicitly estimate daily translation parameters, rather than add translational variance, so that the solutions are insensitive to translation of the reference frame.

The procedures used to generate the daily GAGE products are the same for all four latencies in the GAGE products. The rapid solution latency is typically 24 h and is generated when the IGS rapid products become available. Rapid solutions are generated daily. The final analysis latency is 2–3 weeks and is generated when the IGS final orbits become available. These analyses are performed in 1 week batches. Two additional analyses are performed with 12 week and 26 week latency; stations whose data were not available at the time of the original 2–3 week final orbit analysis run are added to these solutions. These longer latency solutions are referred to supplemental and supplemental 6 month solutions. In addition, campaign processing may be added as requested by users. Infrequently, full time-span reprocessing analyses are performed when there are significant updates to the models used in GPS processing that need to be incorporated in the analysis of the phase and range data. For example, these reprocessing analyses have been performed when the IGS antenna phase center models were updated to align the GPS system to the latest International Terrestrial Reference Frame and at times when deficiencies in the original analyses needed to be corrected. The current GAGE analysis is consistent with ITRF2008 [Altamimi *et al.*, 2011] but will need to be updated pending publication of the ITRF2014 reference frame. The latest results generated will have the most complete and up to data analyses.

As mentioned in section 2.4, two different schemes are used by the ACs for weighting the phase and range data, and two different sampling intervals are used in the estimation. NMT uses an elevation angle-dependent phase data standard deviation with the values used for each station determined from the postfit phase residuals. The pseudo ranges are not directly used in the NMT geodetic parameter estimation. Phase measurements are sampled every 2 min in the estimator. CWU uses a fixed phase standard deviation, independent of the elevation angle, and the RMS scatter of the phase data at individual stations. The estimator uses 5 min phase and pseudorange measurement samples. These differences in the noise models and sampling rates in the geodetic analysis result in the need to scale the variance-covariance matrices included in the SINEX files from each processing center. The scale factors are determined such that the average values of the  $\chi^2/f$ , where  $f$  is the number of degrees of freedom, of the fits to the coordinate differences at the reference frame stations (typically 575 per day) are near unity. Fixed scale factors for all NMT and CWU solutions of 0.7 and 4.8, respectively, are used. When the two AC results are combined, these factors, applied to variances, are doubled so that the individual AC and combined GAGE solutions have similar standard deviations for the geodetic parameter estimates.

The GAGE individual AC and the combined daily solutions are aligned to the GAGE realization of the North American plate by using typically 500–600 reference frame stations. A hierarchical list of reference frame stations is constructed based on a grid with 150 km node spacing placed over the entire geographical region covered by the GAGE network, spanning longitudes from 165° to 311° and latitudes from 7°N to 77°N. In each grid cell stations are ranked based on their time series process noise values. During frame alignment stations with lower process noise from each cell are chosen as reference frame stations. In the current realization, up

to 604 stations could be used with a typical number being about 575 stations. The loosely constrained solutions, in which the reference frame is not realized, are rotated and translated to align to the North America reference frame. During reference frame realization, the vertical components are down weighted by a variance factor of 1000 in determining the reference frame transformation parameters. An IGS08 (IGb08) no-net-rotation (NNR) frame solution is also generated by using similar algorithms but by rotating and translating the time series generated in the North America frame (NAM08). IGb08 is a refinement of the IGS08 system, which was the IGS implementation of ITRF2008 (see discussion in acronyms in Appendix A).

For each day and analysis latency, six SINEX files are made available in the GAGE product area. Three of these are referred to as loosely constrained files. These include the original two SINEX files submitted by the ACs and the combined SINEX file with loose constraints applied. The other three files are referred to as frame-resolved files, and these have been aligned, through rotation and translation, to the GAGE NAM08 reference frame with a variance-covariance matrix that represents the uncertainties in this frame. Separate frame-resolved SINEX files are available for each AC and the combined solution to allow for easy comparison.

While network translation and rotation are explicitly estimated during reference frame realization, network scale changes are not explicitly estimated in the GAGE frame realization. Not estimating scale changes affects the nature of the time series of height estimates from the GAGE analysis when compared to analyses performed by other groups that do estimate scale changes. This mostly affects the amplitude of position variations throughout a time series, for example, due to seasonal signals, as these variations become absorbed by coincident variations in position vector scaling estimates that tend to suppress such signals toward fitting a given linear velocity model. On a sphere, a change in the radius of the sphere scales all the features on the surface of the sphere by the ratio of the radius change to the radius of the sphere. A change in radius is the same as changing the heights of all the points on the surface of the sphere by the change in radius. For a spherical body, and very nearly for the Earth, there is a direct correspondence between uniform changes in height and the scale of features on the surface. The scale change to height change conversion is proportional to the mean radius of the Earth (6371 km). Analyses that estimate scale changes when aligning to a terrestrial reference frame that has only secular motions effectively absorb the average of the height differences between the estimates and the a priori values into the scale estimates. For global GPS analyses, the changes in global-scale estimates are  $\pm 0.5$  ppb corresponding to average height changes of  $\pm 3.2$  mm [Altamimi *et al.*, 2011]. In a continental-scale network, such as that processed by the GAGE Facility analysis stream, even larger average height changes are likely to be absorbed as scale changes. Methods of mitigating the effects of height variations are discussed in Collilieux *et al.* [2011]. Since the GAGE analyses do not estimate scale changes, the large annual signals plus shorter time scale variations in heights are retained in the time series. Other institutions that do estimate scale will typically have smaller annual signals than the GAGE signals as a result. Issues concerning the impact of scale estimation are discussed in more detail in the scale treatment analysis document at <http://www.unavco.org/revgeophys2016>.

### 3. Products Generation

#### 3.1. Time Series Generation

The current GAGE North America reference frame, NAM08, is based on rotating IGb08 position estimates into the North America frame using the rotation rate vector from Altamimi *et al.* [2012] ( $X$ ,  $Y$ , and  $Z$  axes of 0.009722,  $-0.18390$ , and  $-0.02778$  deg/Myr). This rotation rate vector corresponds to an Euler pole at  $8.5784^{\circ}\text{S}$ ,  $86.9738^{\circ}\text{W}$  at a rate of  $0.1862$  deg/Myr. The origin of the GAGE reference frame is center of figure [Blewitt, 2003], as is ITRF2008 and the products generated by the IGS. In order to convert from a center of figure to a center of mass system, Altamimi *et al.* [2012] estimate translation rates as  $(T_x, T_y, T_z) = (0.41, 0.22, 0.41)$  mm/yr. The initial frame is realized by aligning the GAGE combined velocity solution to IGb08 rotated to the North America frame, NAM08, using 34 stations (ALRT, AMC2, BARH, BILL, BOGT, BREW, BRMU, CHUR, CRO1, DUBO, EISL, EPRT, FLIN, GODE, GUAT, INVK, KELY, MANA, MAUI, MDO1, MKEA, NAIN, NANO, NLIB, NRC1, PIE1, PRDS, QIKI, RESO, SCH2, SSIA, STJO, THU3, and USNO). The positions and velocities of the GAGE stations generated from this solution are then used as the basis of the daily NAM08 frame realization ([ftp://data-out.unavco.org/pub/products/position/gage\\_gps.igs08.txt](ftp://data-out.unavco.org/pub/products/position/gage_gps.igs08.txt)). Fits to the time series aligned to NAM08, including earthquake offsets, postseismic motion assuming logarithmic decay as a function time since the main shock, any known antenna phase center discontinuity offsets and annual signals are used to generate the

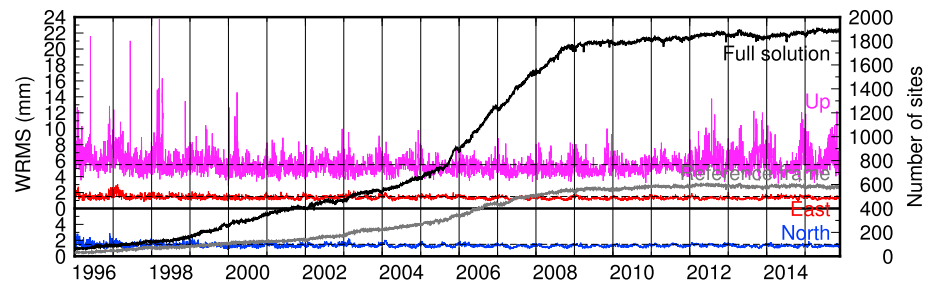


**Figure 3.** Evolution of the GAGE processed network over time. The weighted root-mean-square residual of the fit to the reference frame is shown in east (red), north (blue), and up (magenta) components, where the number of stations used to align the processed network to the reference frame is shown by the gray line. The total number of stations contained in the processed solution is shown by the black line.

nonsecular components of the NAM08 reference frame *postfit* coordinate file. These coordinate files contain estimates of annual sine and cosine terms in the local topocentric frame, but these annual terms are not used during reference frame realization.

The daily position estimates are generated by aligning to the coordinates of the reference stations computed at 12:00 GPS time (GPST) on the day of the data being processed as described in section 2.5.

The AC SINEX files for the supplemental analyses only contain a small number of stations but the reference frame-resolved SINEX files from these analyses and the combined loose and reference frame resolved SINEX files contain all stations processed up to the time of the analysis. In general, the latest available SINEX file (from the UNAVCO website) should always be used to obtain the most complete set of analysis results. When reprocessing is performed, the reprocessed SINEX files and time series entries supersede all previous versions of the products (<ftp://data-out.unavco.org/pub/products/>). Also available in the archived products are earlier realizations of both the North America and global reference frames. Until 2014, the PBO analyses used the Stable North America Reference Frame (<https://www.unavco.org/projects/past-projects/snarf/snarf.html>) and the IGS05 NNR frame. Analyses in these systems included scale change estimates because at that time the ground- and satellite-based antenna calibration models were in a state of flux related to the conversion from relative antenna calibrations to absolute calibrations; this state of flux led to scale differences between realizations of the reference frame necessitating their estimation.

The evolution of the number of stations being processed and used in the reference frame realization, along with the weighted root-mean-square (WRMS) scatter of the fits to reference frame stations, are shown in Figure 3. Over the full 20 year processed data span of the GAGE Facility analysis, the average WRMS fit to the reference frame stations is 1.2, 1.1, and 5.4 mm in north, east, and up. The WRMS fit improves by ~15% between pre-2000 and post-2000. There is an increase in the WRMS fit after about 2012, and this could arise from the “aging” of the ITRF2008 system. Reference frame fits often degrade as the reference site coordinates are projected beyond the time of the last data used to define the reference frame. In our case, this is not the direct reason because the coordinates and velocities of the GAGE reference frame stations are regularly updated. The most likely reason for the degradation is the errors in the phase center offset values for the satellites launched since the analyses used for the ITRF2008 system [Rebischung *et al.*, 2016]. This topic is discussed in more detail in section 5.5.

### 3.2. Treatment of Discontinuities and Postearthquake Deformation

Two classes of discontinuities are included in the GAGE analyses: (1) those due to equipment changes or damage and (2) those due to earthquakes. The former class are identified in two ways: using known changes in the antenna and/or radome setup at a station and through a posteriori visual inspection of time series for abrupt changes in position. These abrupt changes are often due to equipment damage or partial antenna failure at a station. Discontinuities are allowed for all equipment changes, even when the same model of antenna (i.e., only change in serial number) is replaced. For many antennas, offsets, especially in horizontal coordinates, are often seen when an antenna is replaced. Discontinuities for earthquakes are introduced when the earthquake magnitude is sufficiently large and the distance from epicenter sufficiently close that

displacements in excess of 1 mm are expected. We use the following empirical formula that approximate the radius of influence of an earthquake,

$$d = 2.5 \times 10^{-3} \times 5^M \quad (5)$$

where  $M$  is the magnitude of the earthquake as reported by the USGS National Earthquake Information Center (NEIC). All stations within  $d$  km of the epicenter are then examined for coseismic offsets. When coseismic offsets are detected, the dependence of the coseismic offset is assumed to decay as distance from epicenter squared. We apply this empirical formula simply as a guide as to narrow down the number of time series that need manual inspection. When earthquake rupture models are available these are used to better assess which stations are likely to be displaced by more than 1 mm. For many earthquakes, the coseismic offset due to the earthquake is all that needs to be estimated. For larger earthquakes, postseismic motions can often be observed in the time series and these motions are modeled as logarithmic functions,  $\ln(1 + \Delta t/\tau)$ , with time constants  $\tau$ , empirically estimated, that depend on the specific earthquake. Table 3 tabulates the earthquakes along with their characteristics that are included in the GAGE analyses through January 2016.

The list of discontinuities related to equipment changes is too large (~1500 for this paper) to reproduce here. Lists are continually updated and are available in the ancillary files at the UNAVCO website (<http://www.unavco.org/revgeophys2016>).

There are also apparent discontinuities and anomalous position estimates in the GAGE time series related to snow and ice accumulations on the antennas. When GAGE velocity fields are estimated, these anomalous points are removed from the time series. In some cases, there are more anomalous data than normal data (as judged by viewing the time series), and in these cases many of the anomalous data might be retained because they do not fall outside of the editing criteria used. The list of position estimates removed from the velocity field analysis is very large (~40,000 entries) and is available at the URL given above.

While offsets in the time series due to discontinuities are estimated in the velocity field analyses, none of the offsets are removed from GAGE time series files. The secular rates, annual signals, and the postseismic deformation models are also not removed. Most of the anomalous data are also retained in the time series. The GAGE Facility time series are meant to catalog the observed position of any station for a specific day as it was estimated through the analysis system. When a position is anomalous as a result of snow or ice accumulation on the antenna, the position estimate is sensitive to processing method (i.e., the CWU and NMT estimates are likely to differ more than normally observed); nevertheless, the position estimate is included to alert users that data are available and that they have been processed. Users may wish to eliminate these data from their analyses. These anomalous position estimates in the GAGE Facility time series may benefit from further analysis. Other anomalies not explicitly accounted for in modeling the time series are the effects of vegetation growing near the antenna (e.g., CN34, P158, and P316). Many of the anomalous data cases are documented online in the UNAVCO GAGE Facility processing notes (<http://www.unavco.org/revgeophys2016>).

### 3.3. GAGE Velocity Solution Generation

Two steps, SINEX file combination via Kalman filter and time series analysis, are performed to generate velocity fields from the individual GAGE AC solutions and the combined AC analyses. Initial solutions are derived with minimal assumptions by using the SINEX file combination via Kalman filter. This initial solution provides time series that are then analyzed to estimate various station-dependent parameters, such as stochastic noise levels, position offsets, and postseismic position decay. The time series analysis method is less computationally burdensome and is used to bootstrap parameters for the computationally more intensive SINEX file combination method.

The more computationally intensive, and therefore time-consuming method, is the estimation using the full variance-covariance matrices contained in the daily SINEX files from the ACs. This method is described in *Dong et al.* [1998]. We apply a forward running Kalman filter in which the state vector includes the positions and velocities for each station. A single GPS location may have multiple station names because of offsets in the position estimates, and this list is used as input to the Kalman filter. As input to this forward-running Kalman filter, we use the loose position estimates from the two ACs as they may be freely rotated and translated, thus eliminating the need to include Earth orientation parameters in the state vector. At each epoch,

**Table 3.** GAGE Analysis Earthquakes

# <sup>a</sup>	C <sup>b</sup>	M <sup>c</sup>	$\phi^d$ (deg)	$\lambda^d$ (deg)	Date <sup>e</sup>	Time <sup>f</sup> H min	Radius <sup>g</sup> (km)	$\tau^h$ (days)
1	HT	7.1	34.590	243.730	16-10-1999	09 46	237.4	10.0
2	NI	6.8	47.149	237.273	28-02-2001	18 55	149.6	-
3	01	6.8	59.030	204.880	28-07-2001	07 32	149.6	-
4	02	4.0	33.920	241.730	28-10-2001	16 27	9.6	-
5	DN	7.9	63.520	212.560	03-11-2002	22 12	839.4	10.0
6	FJ	8.3	41.810	143.910	25-09-2003	19 50	1000.0	5.0
7	CA	6.6	35.710	238.900	22-12-2003	19 15	110.6	2.0
8	05	4.8	35.740	238.930	17-03-2004	23 53	13.7	-
9	PA	6.0	35.887	239.676	28-09-2004	17 15	83.2	2.0
10	06	7.2	41.290	234.050	15-06-2005	02 50	277.5	-
11	07	4.5	33.175	244.370	02-09-2005	01 28	11.5	-
12	08	5.0	59.394	208.253	05-02-2006	16 16	15.8	-
13	09	6.7	19.878	204.065	15-10-2006	17 08	128.5	-
14	11	6.7	13.550	269.380	13-06-2007	19 29	128.5	-
15	12	5.6	37.430	238.230	31-10-2007	03 04	28.5	-
16	13	7.2	51.360	180.490	19-12-2007	09 30	277.5	-
17	14	5.1	34.810	243.580	06-12-2008	04 18	17.2	-
18	15	6.3	14.550	268.860	03-05-2009	16 21	71.3	-
19	16	7.3	16.730	273.780	28-05-2009	08 24	324.5	-
20	17	5.9	32.440	244.830	30-12-2009	18 48	41.3	-
21	18	6.5	40.650	235.310	10-01-2010	00 27	95.3	-
22	GU	7.2	32.298	244.710	04-04-2010	22 40	500.0	10.0
23	26	5.8	32.700	244.079	15-16-2010	04 26	36.3	-
24	27	6.7	52.876	190.152	18-07-2010	05 56	128.5	-
25	19	5.5	33.020	244.450	26-08-2012	20 57	35.0	-
26	20	7.3	12.140	271.410	27-08-2012	04 37	324.5	-
27	21	7.6	10.100	274.690	05-09-2012	14 42	521.0	2.0
28	22	6.5	10.070	274.700	24-10-2012	00 45	95.3	-
29	23	5.4	36.310	239.140	21-10-2012	06 55	22.9	-
30	24	7.5	55.370	225.380	05-01-2013	08 58	444.7	-
31	25	8.2	54.700	153.400	24-05-2013	05 47	1355.4	-
32	28	7.0	51.610	184.639	30-08-2013	16 25	203.3	-
33	29	6.8	40.829	234.866	10-03-2014	05 19	200.0	-
34	30	5.1	33.919	242.056	29-03-2014	04 10	17.2	-
35	31	6.6	49.846	232.556	24-04-2014	03 11	110.6	-
36	32	7.9	51.797	178.760	23-06-2014	20 54	839.4	-
37	33	5.9	58.358	222.870	25-07-2014	10 55	41.3	-
38	34	6.0	38.220	237.687	24-08-2014	10 21	55.0	-
39	35	6.7	56.594	203.570	29-05-2015	07 01	128.5	-
40	36	6.9	52.376	190.554	27-07-2015	04 50	174.3	-
41	37	7.1	59.658	206.548	24-01-2016	10 31	237.4	-

<sup>a</sup>Number sign is a sequential number.

<sup>b</sup>C is the two-character code used in the GAGE extended station name.

<sup>c</sup>M is the magnitude of earthquake from the NEIC catalog (type of magnitude depends on catalog entry).

<sup>d</sup> $\phi$  and  $\lambda$  are latitude and longitude of the NEIC reported epicenter.

<sup>e</sup>Date is calendar date.

<sup>f</sup>Time is hours and minutes (UTC).

<sup>g</sup>Radius is the distance from the epicenter to stations that were considered to be affected by a coseismic offset for that event.

<sup>h</sup> $\tau$ , if given, is the time constant of logarithmic functional representation of the postseismic signal. No postseismic parameters were estimated for earthquakes with a hyphen entry.

during the update phase of the Kalman filter, a priori positions and velocities are computed including (if necessary) the postseismic logarithmic decay estimates obtained from previous time series analysis. The stochastic noise on the station positions is modeled as a random walk with station location specific parameters determined from analysis of previously generated station time series. At the end of the forward Kalman filter run, the positions and velocities can be aligned to any reference frame using the same algorithms as used in the daily time series reference frame realization, with appropriate rotation and translation rates added. Velocities of differently named stations at the same location are also equated in this final reference frame realization analysis.

Temporally correlated noise in the position time series in the GAGE velocity field analyses are characterized by random walks (spectral index  $-2$ ) combined with white noise (spectral index  $0$ ). Nearly all analyses of the GPS time series show that a more appropriate characterization would be closer to flicker noise (spectral index  $-1$ ) and white noise [see, e.g., Zhang *et al.*, 1997; Langbein and Johnson, 1997; Williams *et al.*, 2004; Mao *et al.*, 1999; Amiri-Simkooei *et al.*, 2007; Langbein, 2008]. Random walk spectra have been observed in two-color electronic distance measurements [Langbein, 2004], but the noise level observed in this work tends to be lower than that seen in GPS analyses. Incorporation of a flicker noise model into an estimation strategy is difficult, and the computations are much more time-consuming than the incorporation of a random walk, which can be easily formulated as a sequential estimator [see, e.g., Williams, 2008]. The computational cost motivates us to formulate process noise as a random walk, and we attempt to set the random walk process noise (RWPN) levels so that for the duration of data being processed, the standard deviations of the velocity estimates is similar to that obtained from lower spectral index process noise models.

Once an initial time series solution has been generated, the position time series method is used to fit velocities along with offsets, postseismic coefficients where needed, and optionally annual sine and cosine coefficients to these GPS time series. This time series estimator can either be weighted-least-squares or a Kalman filter. Since these analyses process data from one station at a time they run very fast but they do require that a reference frame be defined prior to estimating station velocity and other parameters. The parameters determined from this analysis are then used in subsequent SINEX file combinations via the Kalman filter, producing improved estimates of station position and velocity.

The full GAGE analysis is an iteration of the two methods discussed above. The initial analysis uses the full SINEX files to define a reference frame (only the smaller number of reference frame stations need be included in this analysis, which speeds up the runtime), and these reference frame stations are used to generate daily position time series at all stations. The time series analysis is then used to refine the stochastic and postseismic models for the stations, which are then used in a repeated reference frame analysis. In practice, since the GAGE analyses have been performed for a number of years, the position time series analysis from the previous reference frame analysis (yearly re-computation) is used for the stochastic and postseismic model estimation.

The very large number of stations and the length of observation in the GAGE network make a standard parameterized run of the reference frame Kalman filter impractical (i.e., a state vector with position and velocity estimates for all stations and updated daily with a sequential Kalman filter). With position and velocity estimates for almost 6000 stations (each discontinuity introduces a new set of station parameters) and 20 years of data, we estimate that it would take many years for a sequential Kalman filter run to completion on a standard (circa 2015) desktop computer. To speed up the run, we modify the analysis method to allow a series of smaller Kalman filter runs, which then can be run in parallel. The reference frame analysis uses a network approach similar to the methods used to create networks for GAMIT processing of large networks (see discussion above). The process noise models, in the form of random walk time-step variances or process noise (RWPN), are generated by analysis of the position residuals from fitting the time series for each station. Stations that have process noise values greater than  $100.0 \text{ mm}^2/\text{yr}$  are not included in this velocity solution so that they do not contaminate nearby stations. Ten stations are excluded based on this criterion (AC30, AV05, BOMG, P323, P656, SUMM, SMM1, SMM2, TNMZ, and TTSF). An additional five stations were excluded due to short spans of data (CN32, CN53, HVHS, LKHG, and TNCC). Some of this latter group are stations installed near the end of 2015. We also impose a minimum RWPN value of  $0.05 \text{ mm}^2/\text{yr}$ , which results in 563 stations having computed RWPN values less than this value. The details of the methods used to generate the process noise values and to detect daily outliers are given in the GAGE analysis documentation (<http://www.unavco.org/data/gps-gnss/derived-products.html>).

The total GAGE time series presented in this paper contain 7,418,670 station-days. The outlier criteria remove 8339 (0.11%) of NMT and 31372 (0.42%) of CWU station-days from the final combined solution. Because of the long run times associated with the SINEX velocity solutions, we currently run them using only day 3 of each GPS week (i.e., 1 day/week). When the correlated noise models are used and the additional days of each GPS week are included, we find that the additional data have little effect on the estimates of the velocities or their standard deviations (i.e., comparison of results from different days of the week or using all 7 days in the week shows differences of less than 0.5 times the standard deviations of the estimates).

**Table 4.** Statistics of Differences in North (N), East (E), and Up (U) Velocities Between Velocity Fields Determined by Different Analysis Methods<sup>c</sup>

Analysis 1 <sup>a</sup>	Analysis 2 <sup>a</sup>	# <sup>b</sup>	N Mean (mm/yr)	N WRMS (mm/yr)	N NRMS	E Mean (mm/yr)	E WRMS (mm/yr)	E NRMS	U Mean (mm/yr)	U WRMS (mm/yr)	U NRMS
PBO GKNA	CWU GKNA	2130	-0.01	0.06	0.26	-0.00	0.06	0.26	0.04	0.24	0.35
PBO GKNA	NMT GKNA	2136	0.01	0.05	0.22	-0.00	0.05	0.25	-0.03	0.18	0.27
CWU GKNA	NMT GKNA	2129	0.01	0.10	0.46	0.00	0.11	0.50	-0.07	0.40	0.59
PBO GKNA	PBO TSLS	2137	-0.01	0.14	0.82	0.00	0.14	0.82	0.03	0.42	0.77
PBO GKNA	PBO TSKF	2130	-0.01	0.15	0.80	0.00	0.14	0.75	0.12	0.49	0.85
PBO GKNA	CWU TSLS	2130	-0.00	0.15	0.88	-0.00	0.15	0.89	-0.00	0.50	0.89
PBO GKNA	CWU TSKF	2123	-0.01	0.16	0.80	-0.00	0.15	0.77	0.07	0.51	0.87
PBO GKNA	NMT TSLS	2136	-0.00	0.16	0.96	0.00	0.16	0.96	-0.27	0.66	1.18
PBO GKNA	NMT TSKF	2128	-0.02	0.17	0.88	-0.00	0.16	0.84	-0.34	0.70	1.20
PBO GKNA	PBO GKIG	2137	-0.01	0.07	0.33	0.22	0.24	1.10	-0.24	0.27	0.40
PBO GKNA	CWU GKIG	2130	-0.03	0.10	0.46	0.22	0.25	1.15	-0.19	0.32	0.47
PBO GKNA	NMT GKIG	2136	-0.01	0.08	0.37	0.20	0.23	1.07	-0.30	0.38	0.56
PBO GKNA	PBO 2014	2066	-0.03	0.19	1.16	-0.00	0.20	1.17	-0.05	0.55	1.01

<sup>a</sup>The codes for the analyses are of the form: CCC TTY where CCC is the center NMT, CWU, or the combined PBO analysis; TT is the type of analysis: GK, GLOBK SINEX Kalman filter; TS, time series fit; and YY is a combination of method and reference frame: LS, least squares, KF, Kalman filter; NA, NAM08, IG, IGB08 rotated to NA. The final entry PBO 2014 is the earlier PBO full solution generated in November 2014.

<sup>b</sup># is the number of common stations in the solutions.

<sup>c</sup>No transformation parameters between the fields have been estimated.

The subnetwork Kalman filter runs that speed up the processing for the reference frame solution divide the ~2137 stations analyzed into 29 networks each with approximately 77 station locations included in each sub-network. (The final number of estimated parameters for each network depends on the number of position discontinuity estimates needed at each station. The networks need from 99 to 288 individual station names to accommodate the discontinuities.) There is no overlap between the stations in the first 28 networks. A 29th network is created to tie all the other 28 networks into a single solution. To form the stations in the 29th network, three stations for each network are chosen so as to minimize the trace of the covariance matrix of the estimates of rotation and translation using these stations. Weights are assigned to each station in accord with the expected variance of the velocity estimate for the station (i.e., combination of the RWPN and duration of data at the station). If equal weights are given to each station, this algorithm is the same as choosing the three stations that cover the largest area. The analyses of the 29 networks can be run in parallel, and this takes a few hours to run on a standard desktop computer. The combination of the 29 networks uses ~9 Gb of memory. The separate Kalman filter runs for the NMT and CWU solutions, along the equating of velocities (with a constraint of  $\pm 0.01$  mm/yr) at stations with discontinuities, take about a day of CPU time. The NMT and CWU velocity solutions are then merged to form the PBO solution combined solution. This combination uses ~18 Gb of memory. The velocity combinations use loose constraints, and we align to the reference frame at the end of the combination. We generate four reference frame realizations: (1) a North America frame aligned to our current NAM08 frame using ~1072 stations in our hierarchical list of reference frame stations, (2) a North America frame aligned to IGB08 rotated into the North America frame using the 37 stations originally used in ITRF2008 to define the North American plate, and (3) and (4), which are the same as (1) and (2), except the reference velocities are in the IGB08 NNR reference as opposed to a North America-fixed one.

The full GLOBK SINEX velocity solution allows us to re-align the reference frames based on the combination of all of the data collected between 1996 and the current day (14 November 2015, GPS Week 1870, for the analysis in this paper). The estimation of velocities from the position time series is much faster, but the daily solutions need to be aligned to the reference frame each day based on an earlier realization of the reference frame. The current NAM08 frame was originally aligned to the reference frame using data through August of 2014—about a year and half before the current solution. Table 4 compares the WRMS scatters and the square root of the chi-square per degree of freedom, referred to as the normalized root-mean-square (NRMS) scatter, of the differences between the velocity estimates obtained by the two GAGE ACs and the combination of the two ACs using different analysis methods. The footnotes for Table 4 explain the naming scheme used to describe the solutions. There are the three analysis types, NMT, CWU, and their combination, PBO. The velocity estimates are generated with three different methods: (1) GLOBK SINEX combinations (GK), (2) time series analyses using a weighted least squares estimator (LS), and (3) time series analyses using a

**Table 5.** Statistics of Differences in North (N), East (E), and Up (U) Velocities Similar to Table 4 Except We Limit the Comparisons to Stations That Have Horizontal and Vertical Velocity Standard Deviations That are Both Below the Median Horizontal (0.16 mm/yr) and Vertical (0.54 mm/yr) Velocity Standard Deviations<sup>a</sup>

Analysis 1 <sup>b</sup>	Analysis 2 <sup>b</sup>	# <sup>c</sup>	N Mean (mm/yr)	N WRMS (mm/yr)	N NRMS	E Mean (mm/yr)	E WRMS (mm/yr)	E NRMS	U Mean (mm/yr)	U WRMS (mm/yr)	U NRMS
PBO GKNA	CWU GKNA	706	-0.01	0.04	0.23	-0.00	0.04	0.26	0.02	0.16	0.32
PBO GKNA	NMT GKNA	706	0.01	0.03	0.21	-0.00	0.04	0.25	-0.02	0.13	0.26
CWU GKNA	NMT GKNA	706	0.01	0.07	0.43	0.00	0.08	0.49	-0.04	0.28	0.56
PBO GKNA	PBO TSLS	706	-0.01	0.10	0.79	0.01	0.09	0.74	-0.02	0.30	0.74
PBO GKNA	PBO TSKF	706	-0.02	0.10	0.72	0.01	0.09	0.61	0.07	0.37	0.86
PBO GKNA	CWU TSLS	706	-0.01	0.10	0.83	0.01	0.10	0.77	-0.06	0.35	0.83
PBO GKNA	CWU TSKF	706	-0.02	0.10	0.71	0.01	0.09	0.60	0.01	0.37	0.84
PBO GKNA	NMT TSLS	706	-0.01	0.10	0.85	0.01	0.10	0.77	-0.24	0.55	1.30
PBO GKNA	NMT TSKF	706	-0.02	0.11	0.75	0.01	0.09	0.63	-0.29	0.58	1.33
PBO GKNA	PBO GKIG	706	-0.00	0.07	0.40	0.22	0.24	1.44	-0.23	0.25	0.50
PBO GKNA	CWU GKIG	706	-0.02	0.08	0.48	0.23	0.25	1.48	-0.19	0.26	0.51
PBO GKNA	NMT GKIG	706	0.00	0.07	0.42	0.21	0.23	1.40	-0.28	0.33	0.66
PBO GKNA	PBO 2014	706	-0.03	0.11	0.90	0.01	0.12	0.97	-0.07	0.36	0.88

<sup>a</sup>There are less than 1065 stations because both horizontal and vertical sigma conditions must be satisfied. Analysis codes are same as Table 4.

<sup>b</sup>Same as Table 4.

<sup>c</sup>Same as Table 4.

Kalman filter of the position time series as opposed to SINEX files. The time series LS analysis is used to generate the monthly GAGE “snapshot” velocity fields found in the online GAGE product area. The GK analysis can be aligned to the current NAM08 frame (NA) or be realigned to the IGB08 frame (IG). In all analyses, the same process noise models, discontinuities, and postseismic nonlinear models (based on time series analyses) are used. The comparisons do not re-align the velocity fields in any way. The WRMS and NRMS values are based on the simple difference between the estimates. The numbers of stations included in the analyses do not match because the GK analyses exclude stations with large process noise values and sites with large velocity standard deviations (component sum > 100 mm/yr) are not included. The specific sites excluded under this latter condition are dependent on the processing method. Table 5 shows the same type of comparison when we restrict the stations to the best 706 stations, as defined by their velocity standard deviations of each topocentric component being less than the median values for that component. The NRMS values are very consistent with those in Table 4 suggesting that even for the stations with the smallest standard deviations, the velocity estimates agree with each other in accordance with their standard deviations.

The agreement between the different methods to estimate velocities is very good overall, with the WRMS difference in the horizontal components < 0.2 mm/yr (including the comparison to the PBO 2014 velocity solution) and in the height component < 0.7 mm/yr. The NRMS scatter of the differences is often less than unity showing that the error bars are somewhat larger than the differences. The comparison between this solution and the earlier 2014 PBO solution yields NRMS values that are a little larger than unity.

The official GAGE velocity solution is aligned to our current realization of the NAM08 frame to maintain consistency and to avoid discontinuities due to changes in reference frame. The current ITRF2008/IGb08 is now about 5 years old and will soon be replaced by ITRF2014 (probably late 2016). We will evaluate aligning the GAGE solution with the revised realization of the ITRF when it is released.

## 4. Analysis of the Results

### 4.1. Comparison of NMT and CWU Solutions

The comparison of the velocity estimates from CWU and NMT analyses shows that the secular rate estimates from each analysis match at the level of 0.11 mm/yr in north and east and 0.40 mm/yr in height when all stations are included in the comparison (Table 4). When stations with velocity standard deviations less than the median standard deviations are compared, the WRMS differences between the velocity estimates reduces to < 0.08 in north and east and 0.28 mm/yr in height (Table 5). Here we consider in more detail the nature of the comparison between the two analyses. First, we compare the differences in velocity estimates and then the differences in position estimates. Figure 4 shows histograms of the differences in velocity estimates from the two GAGE analysis centers. Overall, these differences appear to be Gaussian in shape with little

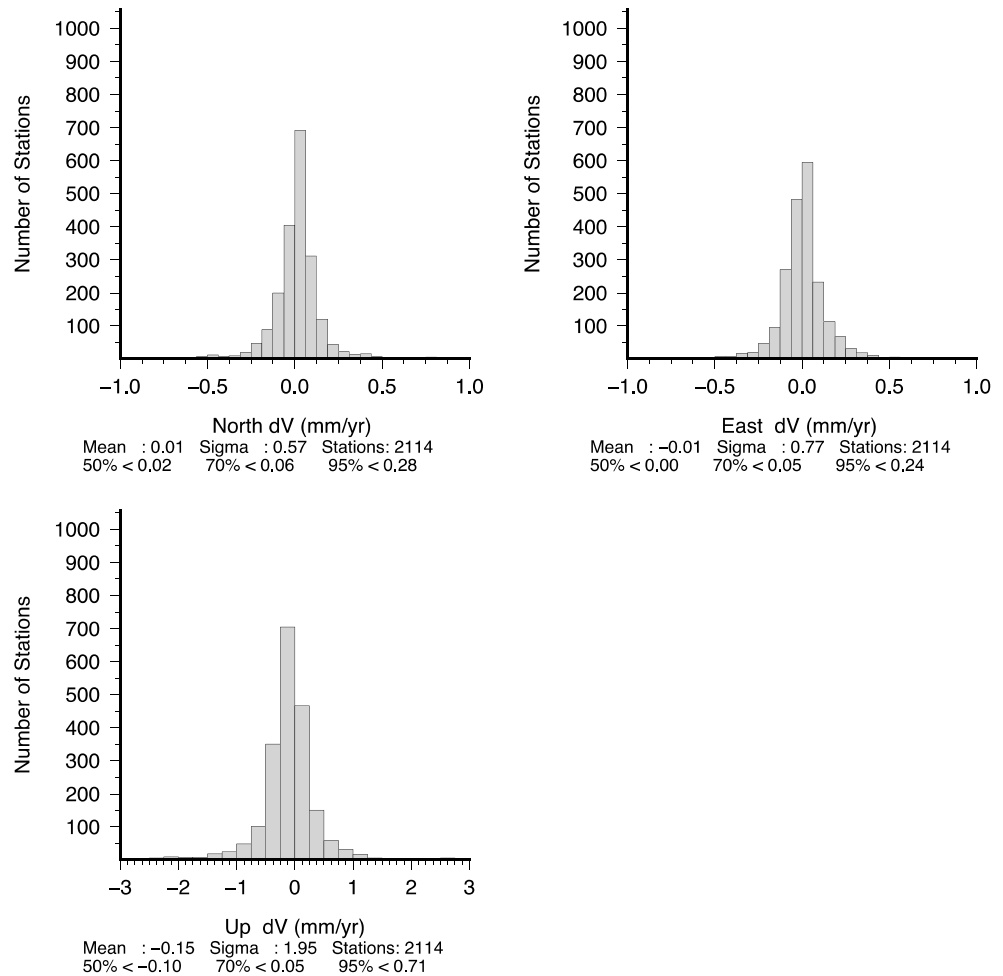


**Figure 4.** Histograms of the differences in velocity estimates between the NMT and CWU analyses. The mean vertical rate difference is not equal to the value in Table 4 because the value in Table 4 is a weighted mean difference, whereas here it is an arithmetic mean.

skewness. The mean difference in the height velocity from the histogram ( $-0.15$  mm/yr) differs slightly from that reported in Table 4 ( $-0.07$  mm/yr) because the table reports the weighted mean of the height velocity differences.

We can also examine the differences in the daily position estimates. For each station, we differentiate the time series of the position estimates and find the weighted mean differences in north, east, and height. The histograms of the weighted mean of the differences are shown in Figure 5. In the horizontal components, the mean, and median differences are small and less than or equal to 0.10 mm. The mean height differences show a small bias of  $-0.65$  and  $-0.81$  mm for the mean and median differences. The observation that the horizontal components are unbiased is not unexpected, since each daily position estimate is aligned to the same reference frame; we note that this alignment is made with  $\sim 575$  stations while the histograms are generated for all 2154 stations in the analysis.

Although the mean of height differences between the analyses by the two ACs are small, the temporal behavior of the height differences is complex as shown Figure 6. Here we show the time series of the averages of the height differences at the reference frame stations for NMT, CWU, and combined analyses and the differences of the means between the AC analyses and the PBO combined solution. The curves have been offset in order to show the patterns more easily. Two aspects of the figure are very clear. The PBO combined mean height difference (MHD) (black curve) nearly tracks the CWU MHD estimates (blue curve) exactly. This tracking is very clear in the time series that shows the difference between the CWU and PBO MHD values

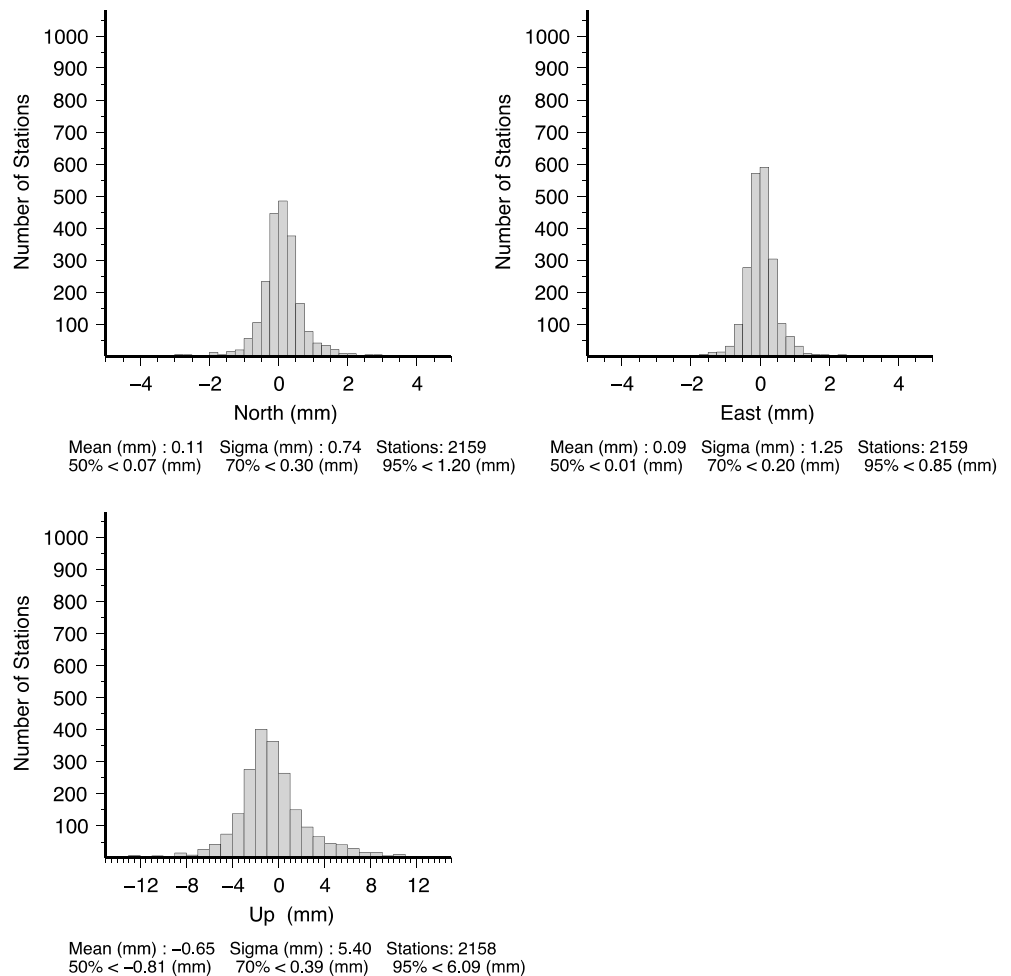


**Figure 5.** Histograms of the mean position differences between NMT and CWU analysis. These histograms are generated by differencing the times series for each station and finding the weighted mean of the differences. The sense here is NMT-CWU.

(magenta, offset  $-20$  mm). The other feature of Figure 6 is that the NMT analysis shows long-term systematic differences, which at times can exceed 10 mm for extended periods of time. Between 1999 and 2003, the mean difference for NMT is  $-5.9$  mm compared to  $-0.4$  mm for CWU. The period from 1999 to 2003 also covers the period of the sunspot maximum in solar cycle 23 [e.g., *Nandy et al.*, 2011]. We initially inferred that that this correlation may arise because of the neglect of higher-order ionospheric delay corrections [Kedar et al., 2003; Hernández-Pajares et al., 2007] in the reprocessing. Trial re-processing of data over this time frame with higher-order ionospheric delay corrections applied shows that this neglect is not the direct cause of the offset. (Higher-order ionospheric delay corrections are applied in standard processing since 05 November 2014 for CWU and 14 June 2015 for NMT.). Analysis of the behavior of the NMT solution reveals that the offset arises because of scale-like correlations in the position estimates and strong correlations between network translations and scale. We believe that the bias in the NMT GAMIT solution arises because the GAGE network only covers one quadrant of the globe. The double difference operator in GAMIT, which effectively estimates all receiver and satellite clocks, results in scale-like correlations that ultimately manifest in the height estimate difference (i.e., common-mode errors in the clock estimates will project as common height offsets in all the stations). Explicitly constraining a scale estimate is one way of reducing the effects of these correlations but that would impose a condition that the mean height differences at the reference frame stations be zero. The solution that we are now testing reduces these correlations by combining the NMT GAMIT solution with overlapping stations from a global double-difference network analysis. We are evaluating the use of the MIT submissions to IGS operational and reprocessing campaigns for this purpose. Initial analyses do show that the NMT MHD are reduced to levels similar to the CWU PPP solutions when the covariance matrix and position

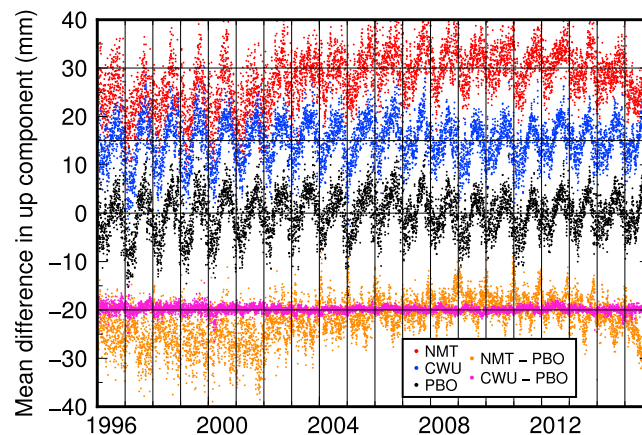


**Figure 6.** Estimates of daily averages of the height differences at the reference frame stations (varies between 30 in 1996 to more than 500 after 2008) between the estimated values and the reference frame linear (plus postseismic) a priori values. Several different results are shown as indicated in the legend. The red dots are the NMT analysis shifted by 30 mm, the blue dots are CWU shifted by 15 mm, and the black dots are the combined PBO solution. The orange and magenta dots show the differences between the NMT and CWU analyses and the PBO combined analysis shifted by  $-20$  mm. See text for discussion of why the PBO average height differences so closely follows the CWU estimates.

estimates for the sites common between the GAGE analyses and MIT IGS analyses are included in the combined solution. For the CWU GIPSY PPP solutions, the satellite clock values are fixed based on a global analysis from the NASA Global Geodetic Network (GGN), and these fixed clocks reduce the effect of these correlations on individual station height position estimates.

As mentioned above, the impact of the correlations in the NMT solutions can be seen if scale change parameters are explicitly estimated. Although the typical standard deviation of the height estimates in the NMT and CWU solutions are similar (due to the reweighting factors discussed in section 2.5), the standard deviations of scale estimates differ by a factor of  $\sim 5$ . For this reason, the mean height differences in the combined solution are dominated by the CWU contribution. The CWU solution dominates for parameter estimates that average over a large number of stations, such as scale. The coordinates of individual stations behave more like the simple average of the two solutions.

Histograms of the weighted RMS scatter of the differences in position estimates between the CWU and NMT analyses are shown in Figure 7. The median WRMS scatter of the differences is less than 1 mm in north and east and less than 5.5 mm in height. The stations with the largest WRMS differences and NRMS differences are given in Table 6. Some of the stations with large WRMS differences have values of the NRMS scatter below unity, indicating that the overall noise level at these stations is high. In some cases, these large differences are associated with poor sky view at the station that arises because of obstructions from vegetation, landforms (e.g., hills and cliffs), and structures. In other cases, partial antenna failures have occurred yielding incomplete raw GPS observations. In these cases, enough data are collected to allow position estimates to be obtained by the ACs, but these estimates are corrupted. In some cases, these antenna failures show large seasonal deviations in the horizontal coordinates.

We can also compare the WRMS scatters of the position time series fits for the CWU, NMT, and combined PBO results. The medians of the WRMS scatters of the position NEU time series are given in Table 7. We see in the table that the combined solution has WRMS scatters that are less than or equal to each AC showing that even with just two ACs, the combination has reduced or equal scatter over the two contributing solutions. We also note that despite the large scatter in the mean height estimates (Figure 6) from the NMT solution compared to the CWU solution, the WRMS scatter in height of individual stations is slightly smaller for the NMT solution (and smallest for the combined solution).

#### 4.2. Spatial Distribution of the Quality of Position Estimates and Phase Data Noise

There are multiple statistics that we could use to assess how the quality of the position estimates of the stations used in the GAGE analysis depends on where the stations are located. As a general trend, stations in regions with little vegetation and low humidity (exemplified by the Basin and Range province) have smaller WRMS scatters of position estimates than stations in regions with large amounts of vegetation and high humidity (such as the Caribbean), as first noted by Mao *et al.* [1999]. Different metrics for assessing the quality of the station position estimates are shown in Figures 8–12. An overall spatial pattern of performance metrics of the stations, as judged by RMS scatter of different geodetic quantities, is similar for all of the metrics. Figure 8 shows the station averages of the phase residual RMS scatter over  $\sim 15$  months starting in late

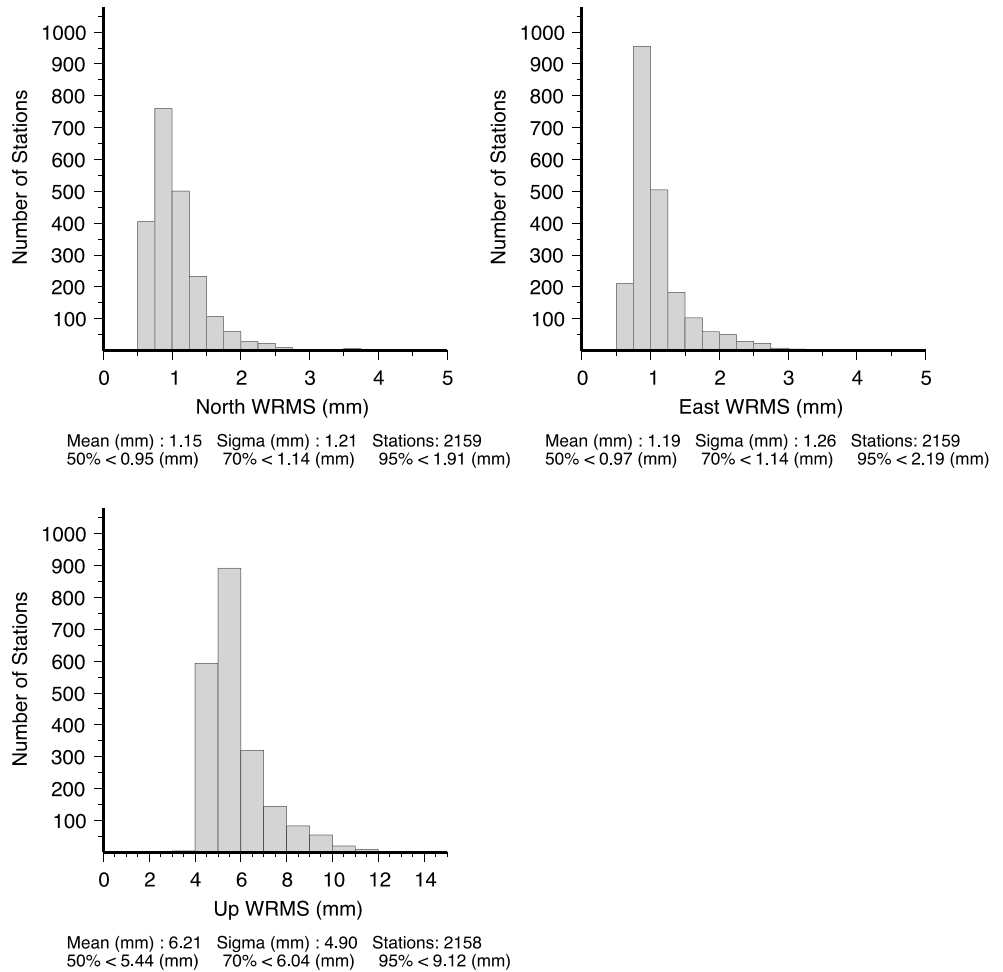


**Figure 7.** Histograms of the WRMS scatters of the differences between the positions estimates from the CWU and NMT analyses.

2014 and continuing through early 2016 (this interval was chosen to show recent data processing and to span over a year). The means of the phase residual RMS scatters shown in these figures averages over the seasonal component of changes in RMS scatter (i.e., during the summer months, the RMS scatter of the phase residuals is larger than during the winter months for most stations). The values shown are the average of the CWU and NMT daily estimates of the phase residual RMS scatter (in general, the estimates from analysis centers show similar values). There are also seasonal changes in the scatter of the phase residuals, but these are not shown. The general sense from the figure is that regions with more humid weather conditions and vegetation have high phase residuals. A similar conclusion can also be reached from Figure 9, which shows the WRMS scatter of the north position estimates after fitting for the parameters in the GAGE velocity model. The pattern of the WRMS of the east position residuals is similar, and as shown in Figure 10 the east position WRMS scatter values are very similar to the north values. In general, the phase residual RMS scatter is positively correlated with the position WRMS scatter. One region where there is a difference between the phase RMS scatter and position WRMS scatter is Alaska. The phase residuals in Alaska are similar in size to the western United States but the position residuals are larger. The reason for the additional scatter is not clear, but it could be due to the neglect of higher-order ionospheric delay terms, which have not been removed over most of duration of the analysis presented here. When ITRF2014 becomes finalized and the GAGE data are re-processed, the higher-order ionospheric delay corrections will be applied as they been in the operational analysis since 05 November 2014. The WRMS scatters of the vertical position estimates are shown in Figure 11, and a similar geographic distribution of the values can be seen. The other measure of nature of the time series noise is the estimates of the random walk noise in the horizontal position estimates used in the

**Table 6.** Summary of the Stations With the Largest Differences Between the NMT and CWU Analyses<sup>a</sup>

Station	No. of Days	Mean Difference (mm)	WRMS Scatter of Differences (mm)	NRMS Scatter of Differences
Sorted by North WRMS				
LONG	7110	1.20	3.59	0.83
BLYN	4555	-0.04	3.61	0.78
WDCB	1595	1.90	3.99	0.63
LOZ1	2680	-3.68	7.16	0.95
EISL	2673	-0.68	8.57	0.89
Sorted by East WRMS				
LOZ1	2680	-2.09	4.76	0.75
MHMS	5749	3.00	4.83	1.46
HCES	4767	2.35	4.90	1.51
P561	3807	9.76	5.08	0.95
EISL	2641	-1.10	12.33	1.32
Sorted by Height WRMS				
COUP	3297	-13.03	26.22	2.46
NJCM	3151	17.19	31.68	2.88
NJOC	3390	14.04	33.06	3.29
SGU1	1337	8.48	35.89	3.66
LOZ1	2676	22.43	36.04	0.87
Sorted by North NRMS				
AC33	2704	-1.05	3.22	0.94
QHTP	4905	0.67	2.63	0.94
LOZ1	2680	-3.68	7.16	0.95
P656	1195	-0.89	3.25	0.97
LJRN	5376	-2.71	3.53	1.08
Sorted by East NRMS				
AV04	3347	0.23	3.58	1.14
EISL	2641	-1.10	12.33	1.32
LJRN	5374	-0.63	3.85	1.35
MHMS	5749	3.00	4.83	1.46
HCES	4767	2.35	4.90	1.51
Sorted by Height NRMS				
PTAL	4876	13.37	18.20	1.95
COUP	3297	-13.03	26.22	2.46
NJCM	3151	17.19	31.68	2.88
NJOC	3390	14.04	33.06	3.29
SGU1	1337	8.48	35.89	3.66

<sup>a</sup>Values are sorted for the largest WRMS differences (mm) and NRMS differences. Only stations with more 1000 measurements are included.

GAGE velocity analysis. These values are shown in Figure 12. The lowest levels of the random walk estimates are in the drier portions of the Basin and Range Province, which probably is related to water vapor in the atmosphere, the generally low amount of vegetation growing near the stations, and minimal changes in groundwater usage (i.e., small anthropogenic hydrologic loading signals).

**Table 7.** Median Values of the WRMS Scatter of Position Time Series for the GAGE ACs and the Combined PBO Analysis From the Fits in the GAGE Time Series Velocity Analysis<sup>a</sup>

Analysis	No. of Stations	Median N (mm)	Median E (mm)	Median U (mm)
CWU	2160	1.32	1.28	6.02
NMT	2169	1.11	1.18	5.83
PBO	2170	1.11	1.13	5.38

<sup>a</sup>Data spanning 1999 to 14 November 2015 are used in these statistics. The numbers of stations differ slightly because of small differences in the list of stations processed by each AC.

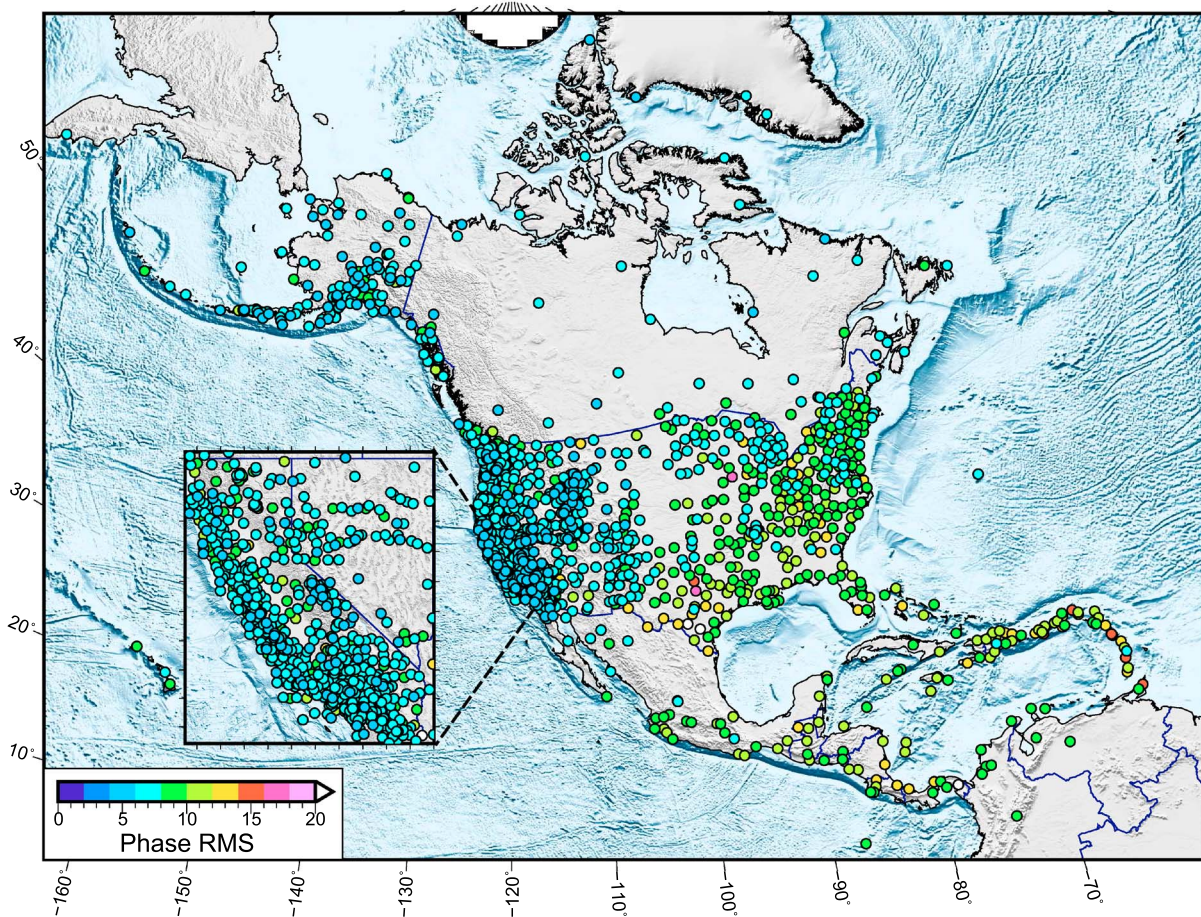


**Figure 8.** Average root-mean-square (RMS) scatter of the phase residuals in millimeter for 1969 stations from which data are available during the period from 23 November 2014 to 28 February 2016.

#### 4.3. Nature of the Phase Residuals at Individual Stations

The residuals of the phase observations can be used to assess data quality and environmental characteristics at each station. The typical RMS scatter of ionosphere-free linear-combination residuals is  $\sim 6\text{--}9$  mm [Herring *et al.*, 2015], but the residuals vary in azimuth and elevation above the horizon depending on the multipath scattering environment near the antenna. We have found that the elevation dependence of the phase residuals, averaged over all azimuths, provides a useful measure of the phase modeling and multipath effects at each site (Figure 13). Station P473, whose antenna is installed on a small ridge surrounded by uneven ground, is an example of a site located in a good scattering environment where the azimuthal-averaged phase residuals are low (0.3 mm average) at all elevation angles (Figures 13a and 13b). Station P502, located in a flat, grassy field, has higher, oscillating phase residuals (up to 10 mm) at low elevations, presumably due to multipath effects from reflections off the nearby ground surface (Figures 13c and 13d). Station CRFP, whose antenna is installed on a flat roof near the corner of a slightly elevated metallic covering, is an example of a poor scattering environment that causes large phase residuals at elevations up to  $40^\circ$  above the horizon (Figures 13e and 13f). In addition to these multipath assessments, unusually large phase residuals have enabled us to identify incorrect antenna models.

The pattern of phase residuals typically remains relatively constant over time, as shown by the examples in Figure 13, so large multipath effects usually do not bias estimates of station displacements. However, multipath can vary over time due to several causes, including vegetation growth, snow and soil moisture effects [e.g., Larson *et al.*, 2008, 2009], or man-made alterations to the site such as adding new buildings or temporarily parking a vehicle near the antenna, which should be considered when evaluating potential transient deformation signals.

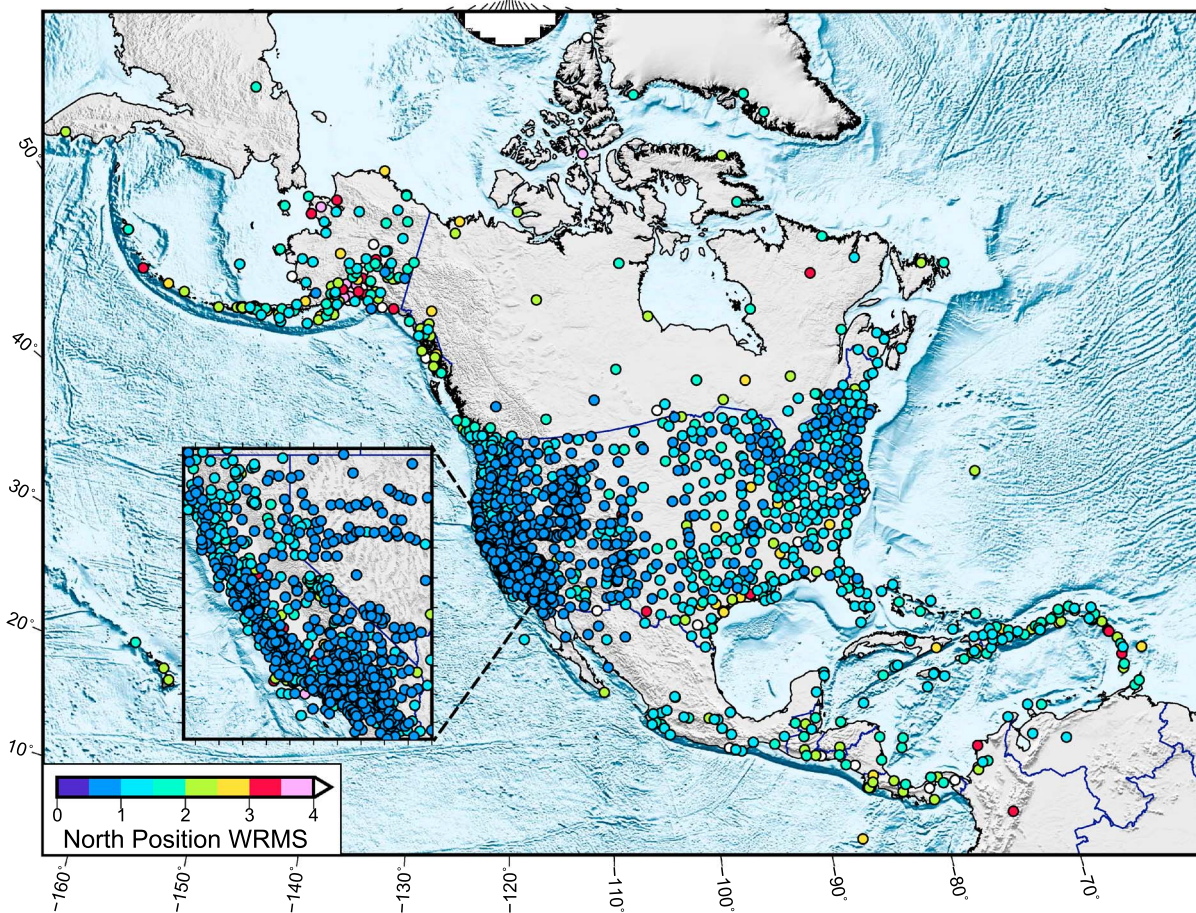


**Figure 9.** WRMS scatter of the north position residuals (mm) after removing linear trends, offsets, annual sine and cosine terms, and in some case postseismic logarithmic terms. There are 2137 stations shown, and the values are based on GAGE analysis from 1996 to 2015.

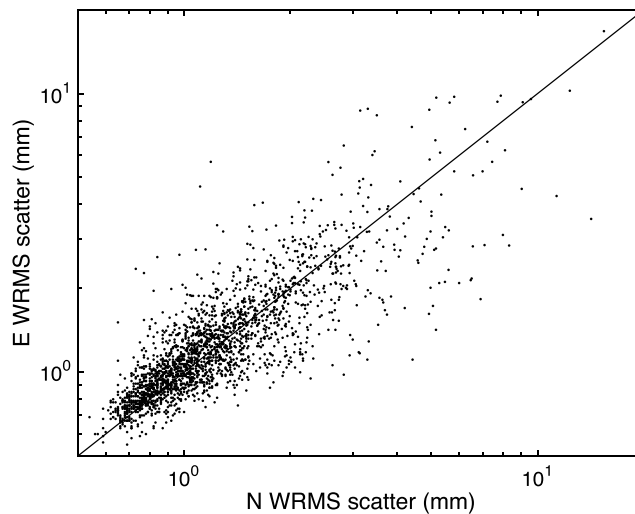


**Figure 10.** Log-log plot of the north and east WRMS scatter of the 2137 stations in the GAGE analysis of data collected between 1996 and the end of 2015. The solid line shows a one-to-one correlation.

#### 4.4. Impact of Antenna Changes

In the GAGE analysis presented here, we have catalogued 1412 antenna changes as a result of known equipment changes and identified 116 offsets in station position estimates for unknown reasons (up to 14 November 2015). In many cases, the unknown offsets likely correspond to the onset of partial failure of an antenna or some other disturbance. In general, changes in antennas can lead to both horizontal and vertical changes in position, with the horizontal change often being larger than those observed in the vertical component. When the GAGE velocity fields are generated, offsets at the epoch of each antenna change are estimated. The GAGE time series data

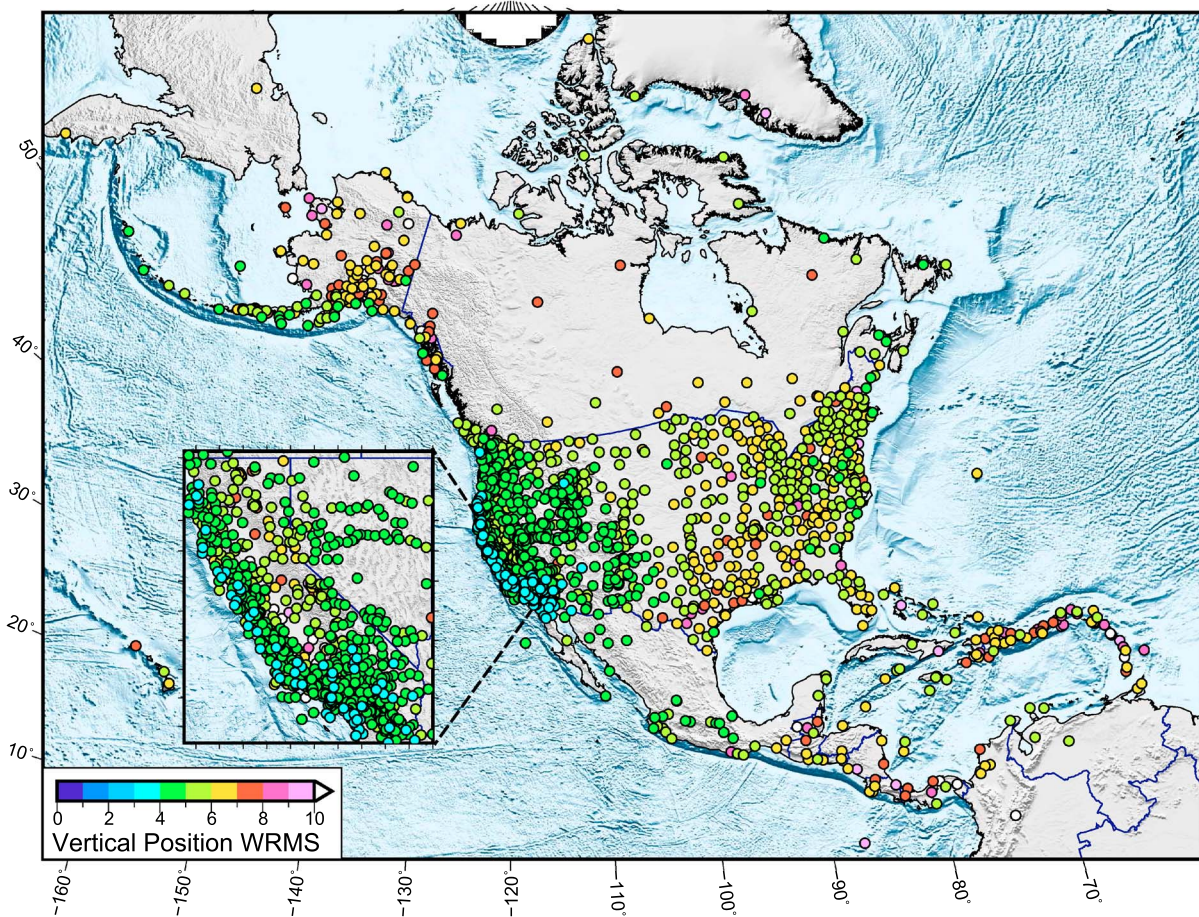


**Figure 11.** WRMS scatter of the height position residuals (mm) after removing linear trends, offsets, annual sine and cosine terms, and in some case postseismic logarithmic terms. The scale used here is larger than that in Figure 9, reflecting the larger uncertainty in height.

products do not attempt to remove these offsets in order to preserve the original position time series. The epochs of individual station offsets are available through the UNAVCO website and are updated monthly in the GAGE products area. As part of the supplemental material for this paper, we provide tables of the changes associated with the most common antenna changes (listed in Table 8). These offsets are estimated with the time series Kalman filter with station-specific process noise models. In some cases, the estimates can be corrupted by poor data or large gaps in the data at the time of the antenna change. In some rare cases, the replacement antenna was subsequently found to be not functioning correctly (poor quality data but still enough to allow a daily position estimate), and this results in a large offset (e.g., P135 on 04 June 2015 TRM29659.00 changed to TRM59800.80). Accordingly, these estimated offsets should always be validated before being applied to and thus removed from the position time series.

Table 8 gives a summary of the offset statistics for the common changes made over the course of the GAGE analysis. In general, no clear patterns emerge, with horizontal offsets often being incoherent between different stations. The height offsets are more likely to show a common trend, but this too is not always the case. One of the most coherent patterns, however, was the change from the UNAV to SCIS radome. In nearly all cases, this change resulted in an  $\sim 2$  mm north and east shift (both positive) and a drop of  $\sim 5$  mm. Some of the largest offsets are due to failed or damaged antennas, and the estimated offset after the antenna is replaced brings the station position back to its previous value prior to the assumed antenna failure. An example is the change at P110 on 07 May 2009 when an antenna that had multiple bullet holes was replaced. In general, time series must be examined to understand fully the effects of antenna and radome changes.

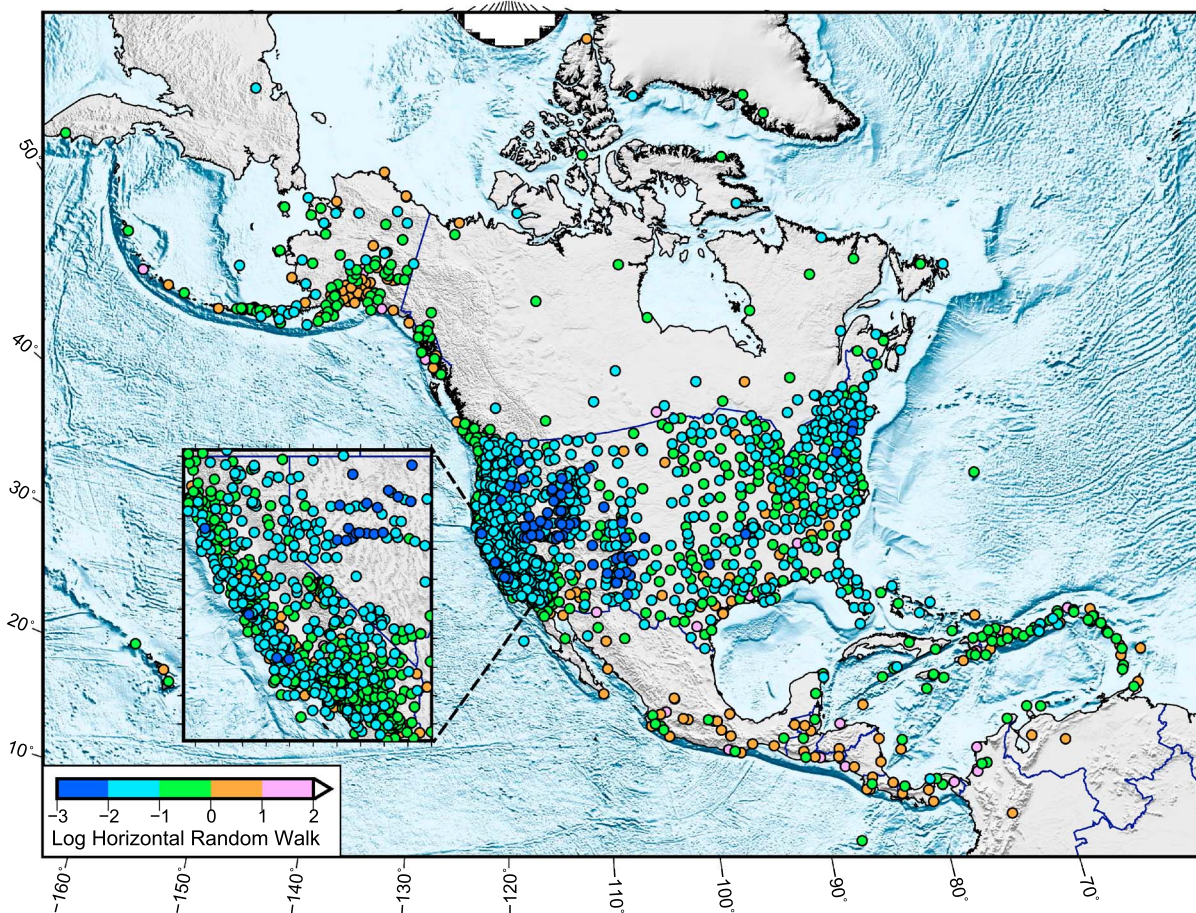


**Figure 12.** A measure of the temporal correlations in the time series based on the estimates of the process noise random walk variances for the site horizontal position residuals. Values are shown as  $\log(\text{mm}^2/\text{yr})$ .

#### 4.5. Analysis of Vertical Motions

Estimates of the vertical velocity for decade-long time series of geodetic data sets are now becoming statistically significant [e.g., *Wahr et al., 2013*] and thus are being used to interpret glacial isostatic adjustment [e.g., *Calais et al., 2006; Sella et al., 2007*]. Similarly, vertical motions due to fluid movements and loading, including those from snow [e.g., *Ouellette et al., 2013*], surface water [e.g., *Elósegui et al., 2003*], and aquifers [e.g., *Amos et al., 2014; Borsa et al., 2014*], are now measurable due to better precision and are separable from other physical processes. The vertical secular velocity estimates from the GAGE NAM08 analysis are shown in Figure 14. The figure clearly shows the GIA signal including the collapse of the fore bulge south of the Canadian border [e.g., *Peltier, 2004; Argus et al., 2014; Peltier et al., 2015*] and vertical signals related to a combination of tectonics of the subduction zone in Alaska and the recent melting of glaciers in the same region [*Sauber and Molnia, 2004; Larsen et al., 2005; Freymueller et al., 2008; Elliott et al., 2010*], and groundwater usage and drought in the western United States [*Borsa et al., 2014*]. When interpreting the vertical changes and comparing results between different analysis groups, it is important to be aware of how estimates of scale changes are handled when defining regional reference frames (see section 2.5).

We explore in more detail the nature of the estimates of the changes in height in the GAGE analysis by comparing to analyses by other groups, all of which use the GIPSY processing system. Time series are readily available with Cartesian coordinates and station component variance-covariance matrices from both JPL and the University of Nevada, Reno (UNR). The URLs from which we have obtained data are (1) [ftp://sideshow.jpl.nasa.gov/pub/JPL\\_GPS\\_Timeseries/repro2011b/raw/position/xyzseries](ftp://sideshow.jpl.nasa.gov/pub/JPL_GPS_Timeseries/repro2011b/raw/position/xyzseries) with file name extent .xyzseries for JPL, (2) [http://geodesy.unr.edu/gps\\_timeseries/txyz/NA12](http://geodesy.unr.edu/gps_timeseries/txyz/NA12) with files names ending in NA12.txyz2 for UNR in the NA12 frame, and [http://geodesy.unr.edu/gps\\_timeseries/txyz/IGS08/](http://geodesy.unr.edu/gps_timeseries/txyz/IGS08/) with file names ending in IGS08.

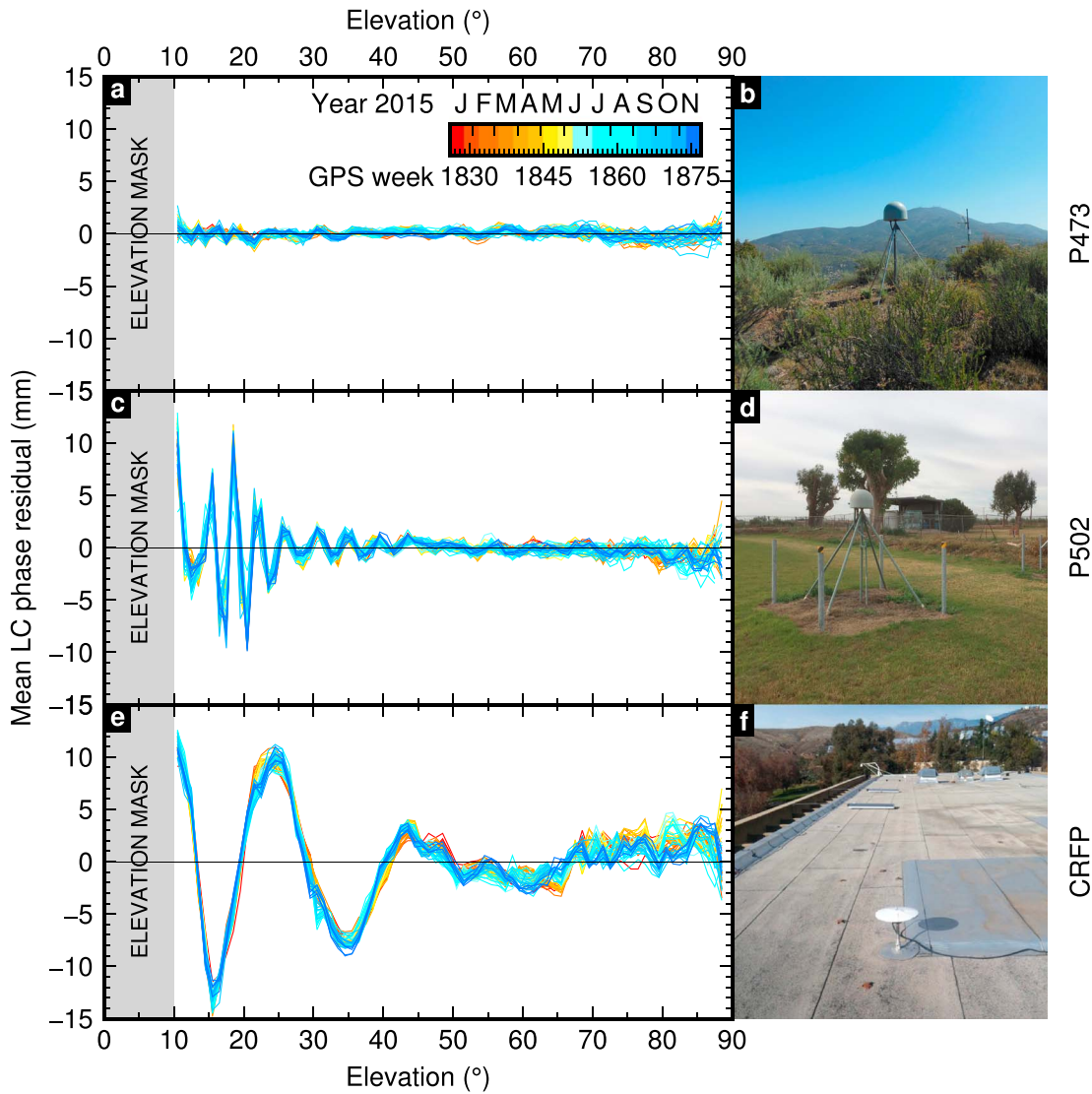


**Figure 13.** Mean ionosphere-free phase residuals for all satellites, averaged over each week of 2015 in 1° elevation angle bins above the horizon, and photographs of the antennas for (a and b) a station with a good scattering environment, P473; (c and d) a station with some multipath from a grassy plane, P502; and (e and f) a station in a poor signal reflection environment, CRFP, whose antenna is mounted near a metal covering on a roof, as shown in Figure 13f, resulting in large multipath effects at low-elevation angles. The color scale for Figures 13c and 13e is the same as shown in Figure 13a.

txyz2 for UNR in the IGS08 frame. The UNR NA12 frame is similar to the GAGE NAM08 frame except that the Euler pole used to rotate from IGS08 to a North America-fixed plate was derived by the UNR group using their own selection of stations [Blewitt et al., 2013]. The files from these stations are in different formats, and we convert them to PBO time series format for further analysis (thus the need for Cartesian coordinates). All of these additional time series align to their respective reference frames by estimating scale changes between the daily values in the reference frame realization on each day. For the height component, results in different reference frames (e.g., IGS08 or NA12) should be comparable without realigning the reference frames.

The size of the network used to estimate the scale changes affects the estimate of scale changes. The UNR and JPL IGS08 time series are derived from a global network, and therefore, scale estimates from these analyses are less sensitive to the average height variations of the North America region. There are, however, global scale variations seen in the IGS analysis, and at least some part of these variations are believed to arise from common snow and hydrological loading across the landmasses of the Northern hemisphere [Dong et al., 2002; Argus et al., 2014; Rebischung et al., 2012, 2016]. Some portion of these seasonal scale changes

**Table 8.** Effects Related to Changes of Common Antenna and Radome Types

From <sup>a</sup>	To <sup>a</sup>	# <sub>t</sub> <sup>b</sup>	# <sub>m</sub> <sup>b</sup>	N Mean mm	N RMS (mm)	E Mean (mm)	E RMS (mm)	U Mean (mm)	U RMS (mm)
TRM29659.00	TRM57971.00	11	10	1.6	3.9	3.2	3.5	-10.1	1.7
TRM41249.00	TRM29659.00	12	12	-0.4	2.8	-0.3	3.3	11.0	7.6
TRM41249.00	TRM55971.00	17	16	-0.7	2.0	1.5	1.8	3.9	5.0
TRM57971.00	TRM59800.00	20	20	0.2	2.3	-3.9	2.8	17.5	3.6
LEIAT504	LEIAR10	21	21	2.1	4.5	-0.1	2.5	3.7	4.2
TPSCR.G3	TRM57971.00	27	25	-0.1	2.2	0.7	1.6	-10.5	5.1
ASH700936C_M	ASH701945B_M	53	50	0.5	1.6	0.7	2.5	-1.0	6.3
ASH701945B_M	TPSCR.G3	53	51	0.1	1.9	1.5	1.4	1.2	5.2
TRM41249.00	TRM57971.00	70	68	-0.2	2.2	1.2	2.6	2.5	6.0
AOAD/M_T	AOAD/M_T	76	76	-2.1	3.8	0.6	3.2	-1.9	7.5
TRM29659.00	TRM59800.00	87	87	0.9	3.1	0.2	2.9	1.4	3.8
TRM29659.00	TRM59800.80	121	120	0.4	2.6	-0.2	3.1	1.6	2.9
TRM29659.00	TRM29659.00	196	196	0.5	2.7	0.5	2.9	-2.1	3.6
UNAV radome	SCIS radome	36	36	1.7	1.0	2.0	0.8	-5.3	2.1

<sup>a</sup>From and To columns show the change in antenna type (descriptions are available at [ftp://igs.org/pub/station/general/rcvr\\_ant.tab](ftp://igs.org/pub/station/general/rcvr_ant.tab)).

<sup>b</sup>#<sub>t</sub> column is the total number of events, and the second #<sub>m</sub> column is the number of events with absolute values less than 20 mm (to remove anomalous values).

<sup>c</sup>The N, E, and U columns give the RMS and mean of the estimated offsets (all calculations are weighted by the standard deviations of the offset estimates). The standard deviation of the means would be the RMS divided by the square root of the number of estimates if the estimates are uncorrelated.

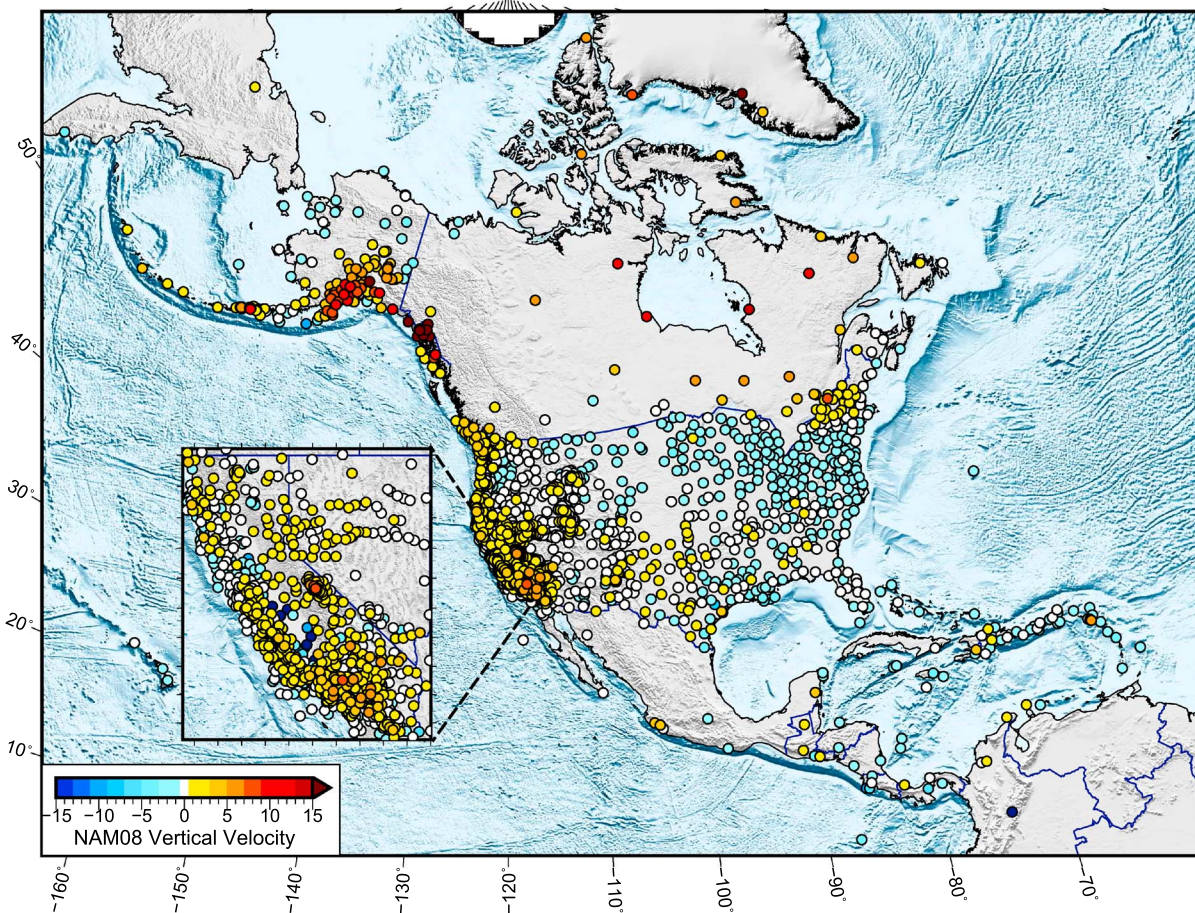


**Figure 14.** Geographic distribution of vertical velocities. Only those stations with vertical velocities with uncertainties <2 mm/yr are shown. Note the generally negative vertical velocities in the midwest and eastern part of the U.S. and the generally positive vertical velocities in the western US, with southern CA showing some of the highest positive values.

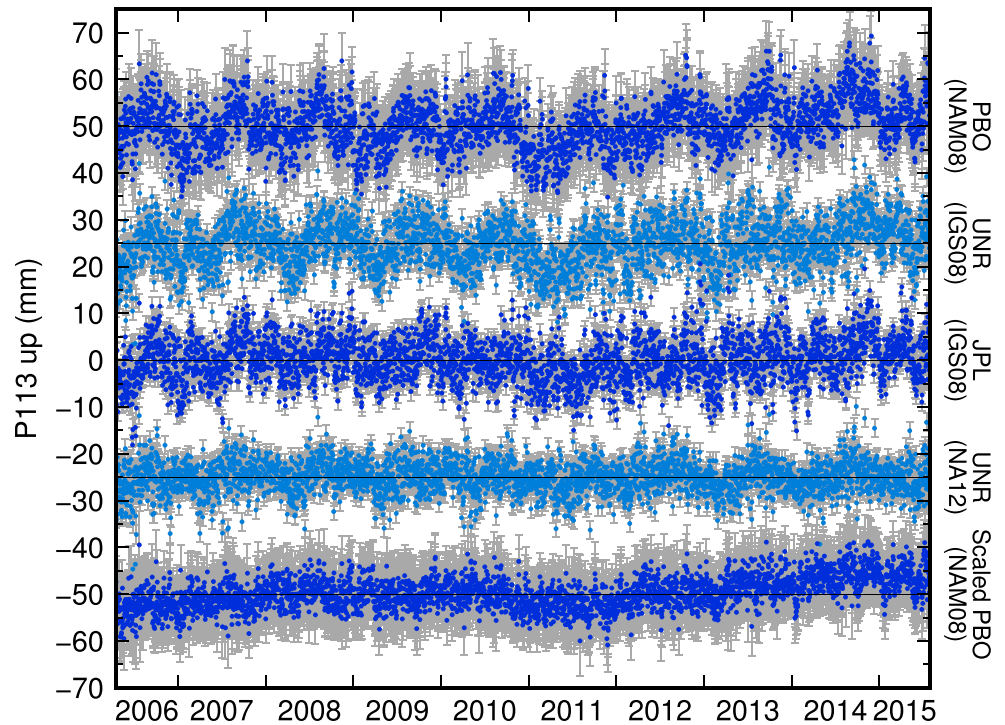


**Figure 15.** Estimates of the height differences from their mean values for the analyses discussed in the text. Daily values are shown with error bars in grey shown every 90 days. The time series have been offset by multiples of 25 mm for clarity. The PBO NAM08 series has no scale changes estimated, the IGS08 series have scale changes estimated using a global network of reference stations, and the bottom two time series have scale changes estimated using reference stations only in the North America region. Table 9 gives the statistics and parameter fits to the time series. See text for sources of UNR and JPL data.

may also result from modeling errors in the analyses of global GPS data. For example, the phase center locations of antennas on newer GPS satellites are typically processed using a nominal phase center offset (PCO) value rather than observationally calibrated values. Errors in these PCO values result in a seasonal-like signal in stations along the satellite ground-track.

For the discussion of the height comparisons between the analyses from various centers, we start with a specific example at one station, which is typical of the behavior we observe in many stations, and then we generalize the discussion to the ensemble average characteristics across the whole GAGE Facility network.

The height time series for P113, a PBO station in Utah, are shown in Figure 15, and the statistical parameters of the series are shown in Table 9. The analyses shown are the GAGE NAM08 standard product, the UNR analysis in the IGS08 frame, the JPL analysis in IGS08, the UNR analysis in NA12, and a test GAGE analysis processed with daily estimates of the scale differences between the daily positions and reference frame stations. The standard GAGE NAM08 results, where scale changes are not estimated, are closer in character to the

**Table 9.** Comparison of Effects of Scale Estimates on the Time Series of Height Estimates for Station P113<sup>a</sup>

Analysis	WRMS (mm)	dH/dT (mm/yr)	$\sigma_{dH/dT}$ (mm/yr)	Cos (mm)	$\sigma_{cos}$ (mm)	Sin (mm)	$\sigma_{sin}$ (mm)
PBO NAM08	4.46	0.78	0.25	-1.42	0.14	-2.98	0.14
UNR IGS08	4.94	0.85	0.23	0.02	0.07	-2.68	0.07
JPL IGS08	4.70	0.51	0.17	0.41	0.06	-1.21	0.06
UNR NA12	3.28	0.16	0.09	-0.14	0.05	-1.16	0.05
PBO scale estimated	2.97	0.85	0.19	-0.30	0.14	0.06	0.14

<sup>a</sup>The standard deviations of the estimates account for temporal correlations in the time series.

**Table 10.** Comparisons of the Secular Rates of the Differences in Height Estimates Between Different Analyses Centers Averaged Over the Number of Common Stations Given in the Second Column<sup>a</sup>

Analyses Differenced	No. of Stations	Mean $dH/dT$ (mm/yr)	WRMS (mm/yr)	NRMS
PBO-CWU	2140	-0.03	0.11	2.80
PBO-NMT	2139	-0.32	0.58	3.50
CWU-NMT	2143	-0.28	0.60	3.33
PBO-JPL IGS08	1574	-0.26	0.37	3.58
PBO-UNR IGS08	2123	-0.18	0.35	2.87
PBO-UNR NA12	2070	-0.48	0.67	4.13
CWU-NMT Scale estimated	2142	0.01	0.20	2.36

<sup>a</sup>The NRMS is computed from standard deviations of the velocity estimates that take into account temporal correlations.

times series of JPL and UNR in the IGS08 frame. The test GAGE analysis, where scale has been estimated, generates a time series that is similar to the UNR NA12 solution. The other analyses differ from the GAGE processing because they all estimate scale changes but use reference frames of different spatial extent.

The features apparent in the figure are that the GAGE NAM08 results are closer in character to time series in the IGS08 frame than to the series that have estimated scale changes using sites in the North America region. The UNR results in IGS08 are quite close to the GAGE NAM08 results, while the same UNR analysis in the NA12 frame is very different. In the IGS08 frame, the UNR estimate of the vertical rate is very close to the GAGE rate (0.85 versus 0.78 mm/yr with each having approximate uncertainty of  $\pm 0.25$  mm/yr), whereas the NA12 rate estimated by UNR is significantly lower (0.16 mm/yr). The amplitudes of the annual cosine and sine terms used to fit the time series also are much closer in the UNR IGS08 solution than the NA12 solution. When the GAGE analysis is performed with scale changes estimated, the annual signal is small and similar to the NA12 result from UNR. The WRMS scatter of the residual to the fits also depends on the treatment of the scale changes; we note that the GAGE analysis with scale changes estimated shows the smallest WRMS scatter (2.97 mm). The GAGE NAM08 analysis also has the smallest WRMS scatter of the IGS08-type solutions (4.6 mm). The GAGE time series with scale estimated have a secular rate very similar to the GAGE NAM08 and different to the UNR NA12 rate. This difference is most likely related to differences in the average secular rates in the reference frame stations between NA12 and NAM08. In general, since the North American frames are generated from the global no-net-rotation (NNR) frames by rotation only, height rate differences between the two frames are not expected.

To gain an overall assessment of the effects on height estimates when including daily scale changes, we generated the differences in the height estimates between different analyses, and then from these differences, we calculated mean offsets, secular rates, and annual cosine and sine terms. When computing the standard deviations for the estimates, we accounted for temporal correlations. The resulting NRMS scatter of the differences between estimates will be greatly affected by accounting for correlations, while the estimates of the weighted means and weighted RMS scatter are less affected. Table 10, height rates ( $dH/dT$ ), and Table 11, annual sine/cosine coefficients, summarize the statistics of the differences between series. There are

**Table 11.** Comparison of Estimates of Annual Terms From the Differences Between the Time Series Generated by Different Analysis Centers<sup>a</sup>

Analysis	No. of Stations	Cos Mean (mm)	Cos RMS (mm)	Sin Mean (mm)	Sin RMS (mm)
PBO-CWU	2139	-0.06	0.23	-0.07	0.29
PBO-NMT	2139	0.54	0.90	1.44	2.10
CWU-NMT	2135	0.63	1.08	1.48	2.20
PBO-JPL IGS08	1574	1.37	2.01	1.48	2.22
PBO-UNR IGS08	2118	0.83	1.41	1.72	2.64
PBO-UNR NA12	2066	2.44	3.55	1.64	2.55
PBO scale estimated-UNR NA12	2066	-0.67	1.20	0.45	1.10
NMT-CWU scale estimated	2135	-0.08	0.48	0.12	0.53

<sup>a</sup>The cosine and sine annual terms have zero phase on 1 January. The RMS values are from sum of the squares of the coefficients with no mean removed.

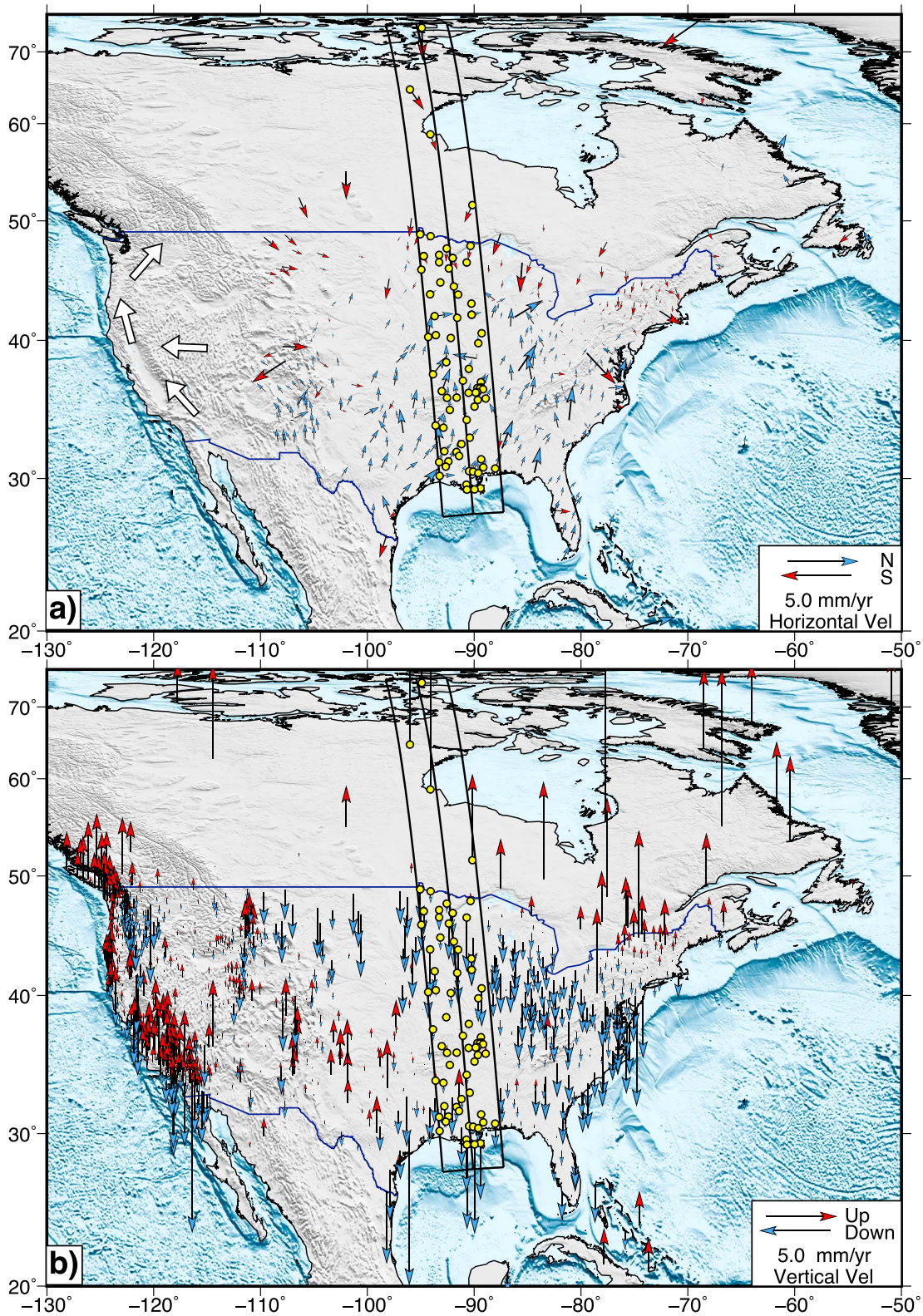


**Figure 16.** Map of stations used to estimate GIA effects (nearly NS profile) in cylindrical projection. (a) Horizontal velocities and (b) vertical velocities are shown. Arrowheads are color-coded to indicate whether a station has north (blue) versus south (red) motion, and uplift (red) versus subsidence (blue). Error ellipses/bars shown in the legend are 2-sigma, but error ellipses are not shown on the map for clarity. Only those stations with horizontal errors <0.5 mm/yr in both the north and east components are plotted. The more densely instrumented and faster moving stations east of 110°W are not shown in Figure 16a. Instead, the general sense of motion in the western U.S. is represented by the white arrows.

mean height rate differences from the PBO solution of  $-0.48$  mm/yr for the UNR NA12 solution, which as we have seen above, differs from other solutions due to North America region scale estimation. The PBO solution differs from other solutions by  $-0.18$  to  $-0.32$  mm/yr, except for the CWU solution ( $-0.03$  mm/yr). When scale changes are estimated in the GAGE analysis, the NMT and CWU solutions match much more closely (last line of each table) because they are both being aligned to the same reference frame stations. These average height rate differences are network wide and rate differences between stations in the same region agree much more closely.

In Table 11, the means and WRMS scatters of the estimated annual cosine and sine terms from the differences between the analyses are shown. Our conclusions here are similar to those above. The PBO combined results are dominated by the CWU solution, and those solutions that do not estimate scale changes or estimate scale changes in a global frame match more closely than the regional solutions that estimate scale changes. The WRMS differences between the UNR NA12 solution with the PBO solution without and with scale changes estimated drops from 3.55 and 2.55 mm to 1.20 and 1.10 mm. The mean values of the differences are also reduced considerably.

The estimation of scale changes in daily alignment to a reference frame has systematic effects on the estimates of station height and their temporal variations, although the derived linear velocity is unlikely to be significantly biased. The GAGE analyses do not estimate scale changes. For the other analyses shown here (JPL and UNR) the estimates of the scale changes that have been applied to their time series can be downloaded in the form of GIPSY X-files with one file per day from which the scale estimates can be extracted.

#### 4.6. GIA Effects Observed in GAGE Horizontal Velocities

One of the interesting results in the GAGE NAM08 velocity field that requires further discussion and study is the influence of glacial isostatic adjustment (GIA). The large number of CORS stations in the U.S. provides a dense network of stations across the North American midcontinent, which can be used to examine not only the vertical but also the horizontal velocities related to GIA [Snay *et al.*, 2016]. In Figures 16 and 17 we examine one way of looking at these signals. These figures show vertical and south directed velocities along a profile running from Resolute Bay in Canada to the Gulf of Mexico near Houston. Superimposed on the velocity estimates from the GAGE NAM08 velocity field are estimates from the GIA models ICE5G [Peltier, 2004] and ICE6G [Argus *et al.*, 2014; Peltier *et al.*, 2015]. For the south directed velocity profile, we also include GPS velocities after estimating (and removing) a best fitting North America Euler pole to align the horizontal motions to the GIA estimates in a least-squares sense. The Euler poles are estimated by using just the stations within the profile. Since only the rotation component of the pole is estimated, the height profile remains the same for all solutions. The WRMS differences (no means removed) between the GAGE NAM08 velocities and the GIA models are shown in Table 12. There is a dramatic improvement in the match between the south directed velocities in the NAM08 solution and prediction from the ICE6G versus ICE5G GIA models (2.74 mm versus 0.56 mm WRMS). Even if the Euler pole is estimated with the ICE5G model the WRMS difference is still twice as large as for the ICE6G model with or without an Euler pole estimated. The vertical rate WRMS differences also improve with ICE6G, but this might be expected because recent contemporary GPS vertical rates were used to constrain this model. With the ICE6G model, it would seem that the North America Euler pole derived in Altamimi *et al.* [2012] is a close approximation to the rigid plate at least in the region of this profile.

The portion of the southward velocity profile south of the U.S.-Canada border matches the ICE6G estimates well. However, stations north of the border, in Canada, do not match the ICE6G predictions at all. The spatial density of stations north of the U.S.-Canada border is very low principally because GPS data collected in Canada are not readily available. Thus, the accuracy of the analysis presented here requires that the data be processed in a unified fashion. Additional questions include (1) are northern stations inconsistent because processes other than GIA affect their horizontal motions or (2) are the current class of GIA models, with laterally homogeneous viscosity and uniform elastic plate thickness, too inadequate to match both horizontal and vertical motions derived from precise and self-consistent analysis such as that presented here?

#### 4.7. Comparison of Different Monument Types

The GAGE analysis includes stations that use many different types of monuments. The stations installed as PBO stations were mostly of two types: deep-drilled braced and shallow-drilled braced monuments. These monument types have also been used at a number of stations from other networks that are included in

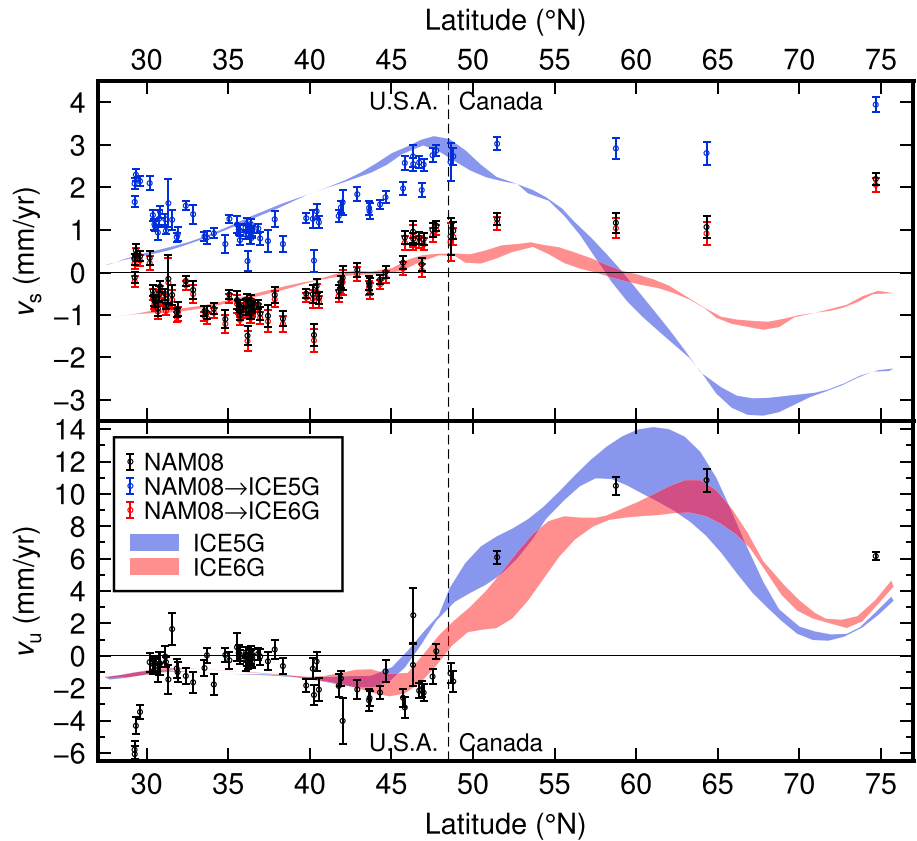


**Figure 17.** (top) Southward and (bottom) vertical velocities plotted as a function of latitude along a 5000 km profile from site RESO (Resolute Bay) in (right) Canada to the (left) Gulf of Mexico near LMCN and GRIS. The Canadian stations are RESO, BAKE, CHUR, and PICL. The width of the profile is ~1500 km and covers a box with longitude and latitude coordinates of 261.7156, 75.4857; 267.4151, 75.7914; 267.0573, 27.4141, and 272.7568, 27.7198 (deg). The profile is shown on the maps in Figure 16. The vertical profile clearly shows the collapse of the peripheral bulge (~45° latitude) related to GIA. The vertical rates at the end of the profile (latitude <30°) are mostly likely local to the Houston area and therefore not representative of GIA. The solid envelopes are from the ICE6G (red) and ICE5G (blue) GIA models, both of which have been tuned to match the vertical GPS motions. The circles with error bars are the GAGE NAM08 estimates (black), and these same estimates with a North America Euler pole estimated to best match the GIA horizontal motion estimates (blue for ICE5G, red for ICE6G). ICE5G and ICE6G results interpolated from the gridded velocity estimates available at <http://www.atmos.physics.utoronto.ca/~peltier/data.php>. [Peltier, 2004; Peltier et al., 2015]. The envelopes represent the ranges of the models within the width of the profile, not the uncertainties.

the GAGE analysis. In addition to deep- and shallow-drilled braced monuments, there are a variety of other monument types that have been used. While most stations in the GAGE analysis have a known monument type, for some nonPBO stations the monument type is not indicated in the station metadata and is unknown.

**Table 12.** WRMS Differences Between the NAM08 Velocity Estimates and the ICE5G and ICE6G GIA Models Without and With a North American Plate Euler Pole Estimated<sup>a</sup>

GIA Model	Euler Pole?	S WRMS (mm)	E WRMS (mm)	U WRMS (mm)
ICE5G	N	2.74	0.43	1.64
ICE5G	Y	1.10	0.37	1.64
ICE6G	N	0.56	0.40	1.11
ICE6G	Y	0.54	0.31	1.11

<sup>a</sup>Sixty-nine stations are used in the comparisons. Four stations (HOUM, BVHS, LMCN, and GRIS) are not included in the statistics or estimates because these are affected by local processes near the Gulf of Mexico.

The large number of stations and the long time span represented in the GAGE analysis allow us to derive some basic statistical information about the position time series associated with each different type of monument. Previous studies have also examined the character of position time series associated with different monument types [e.g., Beavan, 2005; Williams et al., 2004] and have concluded, based on smaller data sets than processed here,

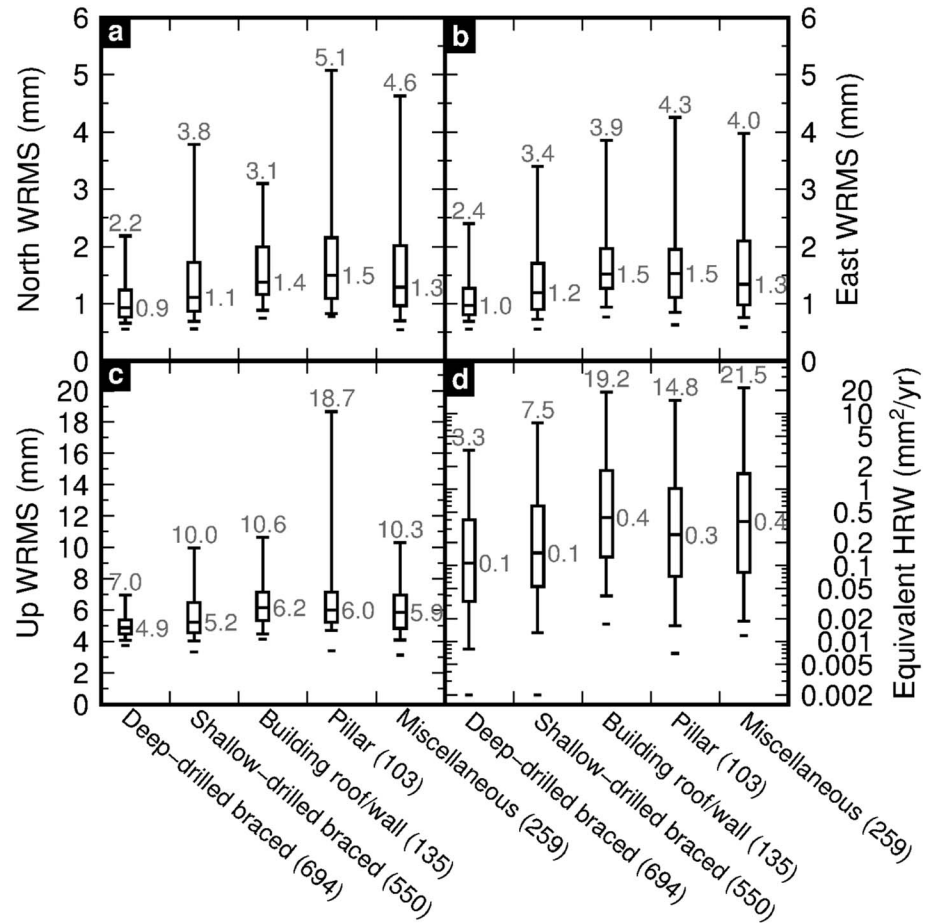


**Figure 18.** Box-and-whisker plots showing the distribution of weighted root-mean-square (WRMS) values estimated from the scatter of station time series residuals in the (a) north, (b) east and (c) up components, and (d) equivalent horizontal random walk (HRW), representing the time correlated noise. The WRMS scatter values are computed from the position residuals after removing a linear trend, discontinuities, annual signals, and for some stations, postseismic logarithmic functions. The HRW values are estimates of the random walk process noise value in the horizontal position estimates. The “Miscellaneous” category includes various types of other monuments including stations where the monument type is unknown. The line in the center of the box is the median value, the boxes encompass 50% of stations (25th to 75th percentiles), the whiskers encompass 90% of stations (5th to 95th percentiles), and the short horizontal line represents the minimum. Numbers in gray next to and above the box-and-whisker in each figure show the values below which are 50% and 95% of stations, respectively. Numbers in parentheses following the monument types are the total stations in that category.

that deep-drilled braced monuments are more stable than other monuments types. Our study supports that conclusion although much more detailed studies are possible. Figure 18 shows the basic statistics of the position time series of stations whose monument type is known. Since not all GAGE analysis stations are controlled by UNAVCO, the GAGE ACs do not know the monument types at some stations. Figure 18 shows a box-and-whisker plot of the WRMS scatters of the position residuals in north (N), east (E), and up (U) after fitting time series using the standard parameterization (see section 3) to the time series. The figure also includes statistics of the estimates of the random walk process noise values for the horizontal components. This latter statistic provides a good characterization of the longer-period systematic trends in each time series.

We do, however, note that caution should be used when interpreting the values in the figure because there are many other contributions to the noise in the position time series than monument stability. As discussed in section 4.2, there are geographic dependencies to the noise in the position time series reflecting the effects

of levels of vegetation and tropospheric water vapor variations. Station behavior will also depend on the material into which the monument is installed (e.g., sediments versus bedrock) and the detailed geology of each station is difficult to obtain. Nevertheless, Figure 18 shows that deep-drilled braced monuments have the smallest WRMS scatter and HRW values, followed by shallow-drilled braced monuments, suggesting that both of these monument types are more stable than other types. In addition, UNAVCO also collects data specifically aimed at comparing the relative motions between nearby monuments of different types (station separations of less than a few meters). The analysis of these data will be published elsewhere, but the time series for these stations appear in the standard products. The monument comparison sites are P591/P811/P812, P565/P809/P810, P804/P805/P806, P453/P813/P814, and P401/P815/P816. Differential motion between the stations at each site can be seen, but these relative motions are often small compared to longer period systematics in the time series. These comparison sites again highlight the idea that a simple interpretation of Figure 18 does not convey the full complexity of monument stability versus other sources of noise in position time series.

## 5. Considerations for Users of GAGE Products

The role of the GAGE Facility ACC/ACs is to provide a set of geodetic products, which may then be used by the scientific community and other interested stakeholders. Accordingly, several decisions were made before the GAGE analysis processing and combination stages regarding appropriate strategies, described in sections 2 and 3, which could directly affect the interpretation of geodetic products and therefore impact further geophysical analyses. In addition, there are some aspects of GPS that are beyond the control of the ACC/ACs, but nonetheless affect the outcome of the GAGE solution, often in significant and unintuitive ways, and these too must also be understood in order not to attach incorrect interpretations of apparent station motions to other known sources.

As stated in section 1, the intention of this paper is not to report any geophysical analysis and interpretation derived from the GAGE processing stream and data products. Rather, we hope and anticipate that this paper will support and encourage such studies; nevertheless, there are many caveats implicit in the distributed products of which users of these should be aware. We present and discuss these in this section. Throughout the process of generating the GAGE products, our intention is to leave as much physical signal intact for later analysis and interpretation by researchers investigating such signals, whether collectively or in isolation. The natural outcome of this approach, however, is that signals from sources that one might not be interested in modeling, and thus would otherwise attempt to remove, are still present in the products, and this must be taken into consideration when using the GAGE products.

### 5.1. User Resources Available Online via UNAVCO

The scope and extent of this paper are naturally limited and intentionally concise. Numerous detailed online resources, designed to inform and assist users of GAGE GPS data products, however, are available from the UNAVCO website. The GPS/GNSS Derived Data Products page (<http://www.unavco.org/revgeophys2016>) provides links to documentation, processing files, technical reports, links to products, User Notices and Advisories, the AC Products Log, and the GAGE GPS Products Technical News Google+ page. Documentation includes the latest GAGE GPS Analysis Plan, the latest Velocity Field release notes, and white papers such as the "Treatment of Scale in GAGE and by Other GPS Data Processing Groups" document. ZIP/tar files containing all the processing files used by the ACC/AC's to generate GAGE GPS data products are provided. Quarterly technical reports summarize statistics for all stations analyzed during the reporting period as well as processing notes, station offsets, etc. *User Notices and Advisories* are issued when there are major changes or issues affecting GAGE GPS data products. The AC Products Log is of particular value to data product users as it is updated in real time to report any and all changes or issues that affect products from a user perspective including product updates, new station additions, data access interruptions, processing method changes or updates, and so on. The Technical News Google+ page is meant to encourage communication among UNAVCO staff, GAGE and other analysis centers, and community users. This page features in-depth case studies of GPS station time series and discussion of significant developments related to data products among other topics. A unique feature of this page is that it is also interactive as comments and questions can be posted in response to technical news articles.

**Table 13.** Statistics of the Differences in Position Time Series From the GAGE Analyses and the JPL IGS08 Time Series Aligned to the NAM08 Reference Frame<sup>a</sup>

Analysis	No. of Stations	Mean N (mm)	WRMS N (mm)	Mean E (mm)	WRMS E (mm)	Mean U (mm)	WRMS U (mm)
CWU	1596	-0.04	1.10	-0.05	0.94	1.08	4.91
NMT	1603	0.09	0.95	-0.03	0.89	0.12	5.35
PBO	1603	0.01	0.90	-0.03	0.79	0.90	4.16

<sup>a</sup>The columns here show the median values of the mean offset between the series and the median WRMS scatter of the differences at each station.

## 5.2. Iteration Sequence of GAGE Products

Two forms of GAGE analysis iteration can result in updated products of which users may become aware during the course of their analyses: (1) rapid solutions support the near-real-time operational processing and monthly “snapshot” velocity solutions are eventually superseded by “final” products up to 6 months later, and (2) complete reprocessing efforts with updated global orbit and clock products. The latter usually occurs only after a major release of a new ITRF, for which orbit and clock products using updated processing models and antenna calibrations are also released or transitioned to in operational IGS processing, or a similar major reprocessing effort at a center upon whose orbit and clock products we also rely for our processing (e.g., JPL for GIPSY/OASIS). Therefore, a complete reprocessing effort will likely result in a new self-consistent set of products that supersede older versions, which may still be made available to users.

Supplementary solutions are necessary in circumstances such as when raw data files are not immediately available for operational processing. This may be due to, for example, a station having its telecommunications temporarily interrupted, causing lag time in incorporating files into data archives or problems with data server connectivity. Supplementary solutions also handle instances where metadata (e.g., equipment) information is found to be incorrect and the data are reprocessed accordingly. If a newer supplementary solution is available it supersedes all previous solutions.

## 5.3. Comparison With Other Analysis Methods and Groups

There are several institutions that undertake major processing of large continental-scale or even global-scale GPS/GNSS networks. These analyses range from the solutions submitted to the IGS by IGS analysis centers for combination into the final IGS products to university-based geodetic laboratories that provide their own processing results as free products for the community. The processing software, strategy, and standard of quality varies between each of these examples and must be considered when using any available products. We compare the GAGE results with such analyses from groups at JPL and at UNR. The results from these analyses are made available in geocentric Cartesian coordinates by the originating analysis group, facilitating these comparisons. URLs for obtaining these products are given in section 4.5.

In section 4.5 we compared vertical motions from analyses by JPL in the IGS08 reference frame and from UNR in both the IGS08 reference frame and UNR’s realization of a North America fixed frame referred to as NA12 [Blewitt *et al.*, 2013]. We present three statistical comparisons between these analyses and the GAGE analysis: (1) differences in the time series when the position time series are aligned to NAM08; (2) daily position residuals after fitting the GAGE velocity model, including discontinuities, logarithmic postseismic decay for the largest earthquakes, and annual sine and cosine terms; and (3) differences in the velocity estimates directly (i.e., simple differencing) and after estimating rotation and translation rates between the velocity fields (the latter is needed when the time series are in different reference frames).

Table 13 presents the statistics of the differences in the daily position estimates between these various analyses. For this comparison, all of the station positions each day are aligned to the NAM08 frame using the same methods used to align the GAGE solutions, as described in section 3.3. We can only compare the JPL solution in this manner because the UNR solutions are generated with an older version of the GIPSY software, which incorrectly applies the east component of ground station antenna PCOs with the wrong sign. This error can lead to centimeter-level position errors for some antenna types. In addition, Table 13 shows the median values of the mean difference and median WRMS scatter of differences in the daily position estimates. The medians are small (relative to position uncertainty) in the NE components, which would be expected because of the frame alignment. The median of the mean height differences are <1.1 mm for the ACs and the

**Table 14.** Statistics of the Position Residuals From the Fits to the GAGE Time Series Velocity Analyses for Different Solutions

Analysis	No. of Stations	N WRMS (mm)	N NRMS	E WRMS (mm)	E NRMS	U WRMS (mm)	U NRMS
CWU	2160	1.32	0.64	1.28	0.76	6.02	0.81
NMT	2169	1.11	0.59	1.18	0.67	5.83	0.86
PBO	2170	1.11	0.66	1.13	0.76	5.38	0.88
JPL NAM08	1636	1.27	1.91	1.19	2.20	5.64	2.66
UNR NA12	2116	1.38	2.14	1.31	2.50	5.21	2.51
UNR IGS08	2184	1.91	3.06	1.98	3.88	6.34	3.11
JPL IGS08	1636	1.85	2.88	1.97	3.85	5.55	2.67

combined PBO analysis. The NE median WRMS scatters are less than 1.1 mm. For height, the median WRMS scatters are <5.4 mm for all comparisons.

For these comparisons, we also calculate the WRMS scatter of the fits to the GAGE velocity model parameterization; i.e., for each data set, we estimate the parameters of the GAGE model and compute the statistics of the position residuals, for each station, for each analysis. We also compute the NRMS of the residuals. With the NRMS statistic, we note that if the error bars of each position estimate are truly representative of the scatter, then the NRMS will be approximately unity. The median WRMS and NRMS scatter results are shown in Table 14 for the GAGE, JPL, and UNR analyses. For the GAGE analyses, we have already scaled the position standard deviations to match, on average, the fit of the reference frame sites (see section 2.5) and so we would expect these NRMS values to be close to unity. However, we note that the NRMS scatters for the GAGE analyses are, in fact, somewhat smaller than unity (0.59–0.76). This could result from the fact that the scale factors were calculated based on just the reference frame stations (typically 575 stations) and a single scale factor was used for all of the CWU and NMT SINEX files. For all of the analyses in a North America frame (NAM08 or NA12) the WRMS scatters are similar, varying between 1.1 and 1.4 mm in NE and 5.2–6.0 mm in height. The WRMS in the IGS08 global reference frame is higher in the NE components because of the common mode errors removed when transforming into the North America frames. In addition, the NRMS scatters for the JPL and UNR solution are greater than unity because of the phase noise error model that is assumed during their processing. Had the same scale factor from the CWU analysis (2.2 for standard deviations) been used, the JPL and UNR analysis NRMS values would be closer to unity.

The final comparison gives the statistics of the differences between the velocity field estimates from each analysis. These results are given in Table 15. (These results are generated from a fit to time series rather than the estimates using the full variance-covariance matrices given in Table 4.) Results are shown as direct differences (North America frames only) and after estimating rotational and translational rates between the

**Table 15.** Statistics of the Differences in the Velocity Field Estimates Using Time Series From Different Analyses

Analyses	# <sup>a</sup>	N Mean <sup>c</sup> (mm/yr)	N WRMS <sup>c</sup> (mm/yr)	E Mean <sup>c</sup> (mm/yr)	E WRMS <sup>c</sup> (mm/yr)	U Mean <sup>c</sup> (mm/yr)	U WRMS <sup>c</sup> (mm/yr)
Direct difference <sup>b</sup>							
PBO-CWU	2140	0.00	0.04	−0.01	0.04	−0.04	0.25
PBO-NMT	2157	0.00	0.05	0.00	0.06	−0.22	0.66
PBO-JPL NAM08	1574	0.02	0.07	−0.01	0.06	−0.01	0.39
PBO-UNR NA12	2066	−0.70	0.71	−0.14	0.20	−0.47	0.76
Aligned Through Rotation and Translation Rate Estimation <sup>b</sup>							
PBO-UNR NA12	2066	0.01	0.09	0.00	0.10	−0.16	0.56
PBO-UNR IG08	2130	−0.00	0.15	0.00	0.25	0.07	0.55
JPL NAM08-UNR NA12	1558	0.00	0.09	0.00	0.09	−0.11	0.53
JPL NAM08-UNR IGS08	1600	−0.00	0.14	0.00	0.12	0.04	0.40
UNR IGS08-UNR NA12	2103	0.02	0.15	0.00	0.13	−0.22	0.43

<sup>a</sup>Number of common stations.

<sup>b</sup>The statistics for the first four entries are based on the direct difference in velocity estimates. The entries below the “Aligned” line are computed from differences after removing rotation and translation rates between the fields.

<sup>c</sup>Values shown are the weighted mean and WRMS scatter of the differences in velocity estimates using the number of common stations (# column) between the pairs of solutions list in the first column. The statistics are shown in north (N), east (E), and up (U).

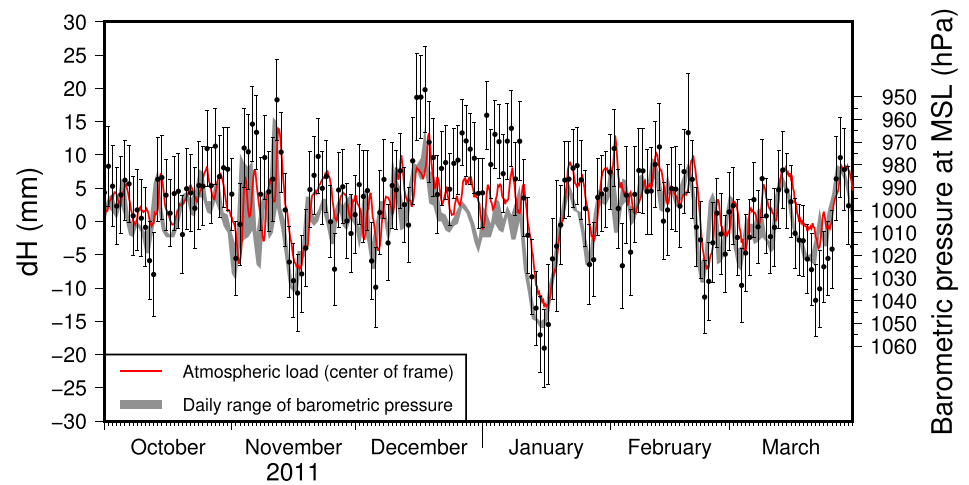


**Figure 19.** Example of height variations due to atmospheric pressure loading for site AB15. The observed GPS time series is shown by the black dots with one standard deviation error bars. The range of daily observed barometric pressure at a nearby meteorological station is shown in gray. The equivalent atmospheric load, calculated from the IERS geophysical fluids center and referenced to the center of figure frame [see *Blewitt, 2003*], is shown by the red line.

velocity fields. The agreement between the JPL NAM08 and PBO analysis is  $<0.1$  mm/yr in NE and 0.4 mm/yr in vertical. The UNR NA12 results do not match as well, but this is likely due to differences in the definition of stable North America. Allowing for rotation and translation rates reduces the WRMS scatter of the differences to less than 0.1 mm/yr NE and 0.6 mm/yr U. The agreement between the different analyses and to the PBO combined analyses are similar when the velocity fields are aligned.

#### 5.4. Atmospheric Loading Signals

Atmospheric loading terms (tidal and nontidal) are not applied to the phase data processing described in section 2 and Table 1. As a result, a portion of the observed vertical (and, to a lesser extent, the horizontal) position time series variation is the result of daily atmospheric pressure changes. This is an obvious example of how the products cater to the wider community rather than being tailored to suit a specialist subset of potential users, thus rendering the products uninformative to another group. For any researcher studying the effect of such atmospheric loading, these signals must remain in the raw time series, although for many solid Earth scientists this is considered unrelated noise. The vertical signal associated with the response to atmospheric pressure loading is also another example of the type of signal that may be suppressed if scaling of the network is not handled correctly (see section 4.5).

GPS stations at temperate and higher latitudes, which experience large atmospheric loading variations from migrating high- and low-pressure weather systems, show detectable variations in station position. GPS station AB15, located near Nyc in south west central Alaska, provides a good example of this effect on the temporal changes in station positions. Figure 19 shows AB15 over a short period during the winter of 2011–2012. Over a 4 day period between 11 and 16 January 2014, the station's height is observed to change by  $-22 \pm 8$  mm, while the load signal computed from atmospheric pressure changes is computed to be  $-16$  mm. Over the next 5 days the station height returns to its value before the high-pressure system passed through. At other times the station's height increases as low-pressure systems pass by. These short-period changes are seen frequently. Over longer periods of time other loading effects and possible GPS systematic errors introduce differences between the observed height changes and those predicted from simply atmospheric pressure loading. A number of studies have shown that even when loading contributions from oceans and hydrology are included in GPS analyses, there remains substantial unexplained signals in the GPS vertical time series [see e.g., *Dong et al., 2002; Williams and Penna, 2011*].

#### 5.5. Perturbations due to the Evolution of the GPS System

One aspect that users should be cautious of with operational GPS data processing is the impact of newly launched satellites. Errors in the model of the position of the satellite transmitting antenna map into ground station position estimates. When new satellites are launched only nominal satellite transmission antenna

calibrations are available and these are used in data analysis. Estimates of the positions of satellite phase center offsets (PCO) for individual satellites are made when new ITRFs are generated [Schmid *et al.*, 2007; Rebischung *et al.*, 2012]. The current set of PCO values used in that GAGE analyses are based on the ITRF2008 solutions. Since 2008, two Block II-RM and all 10 Block II-F satellites have been launched. No Block II-F satellites were in orbit at the time the analyses for ITRF2008 were completed and special analyses were performed, using results from just two IGS ACs, to estimate PCO values for the first two Block II-F satellites (PRNs 25 and 1; unique satellite vehicle numbers 62 and 63). These updated values were incorporated into the IGS antenna calibration files in September 2012. The remaining eight Block II-F satellites use nominal values, which will almost certainly be updated when ITRF2014 is released (expected late 2016).

Errors in radial position ( $Z$  coordinate) of the satellites' PCO values introduce apparent height changes in the terrestrial reference system. A constant  $Z$  offset to all satellites tends to generate a fixed global height change or, equivalently, a terrestrial network scale change [Ge *et al.*, 2005; Cardellach *et al.*, 2007]. When only one satellite has a  $Z$ -offset error, the ground stations under and near the track of the satellite will be more affected than other stations. Such a  $Z$ -offset can introduce a spatially correlated, time-dependent (for data collected before and after the satellite is launched) height errors. Although not obvious, there is a correlation between the estimates of radiation force model parameters and estimated satellite PCO values with the noise in the estimates of the radiation parameters depending on the angle between the Sun and the satellite orbit plane [Schmid *et al.*, 2007]. Consequently, this coupling of an error in the satellite PCO values and the radiation force estimates during orbit determination (either JPL or IGS) can lead to a quasi-annual signals in the estimates of the heights at stations near the ground track of the satellite [Cardellach *et al.*, 2007]. GPS ground tracks repeat every day, and consequently, errors in satellite PCO values can introduce geographically correlated errors in height estimates.

As GPS data collection gets further away in time from when major revisions of the ITRF are released, users should be cautious of possible systematic errors that might be introduced as new satellites are launched and prior to updates to the satellite PCO values that may be made.

### 5.6. Future and Frontier Science Applications

This paper has addressed the current state of the GAGE GPS analysis methods and models. These analysis methods are consistent with current international standards used for generating the ITRF2008 reference frame. We anticipate that the analysis methods will be updated to be consistent with ITRF2014 when it is released. Once ITRF2014 is available, a reprocessing of all available GAGE data will be performed with this ITRF and possibly with new analysis models.

An area that can be explored further is the estimation of atmospheric refractive delays from the data sets processed by GAGE. Currently, temporal variations in the zenith atmospheric delay and horizontal gradients, in accord with standard methods, are generated and made available in the GAGE products area. However, analysis of position time series shows that some GAGE stations have strongly skewed position residuals that suggest that the current parametrization used for atmospheric delay estimation is not adequate for these stations. Examples of sites with large skewness in both horizontal and vertical position estimates include P642/P643/P631 in California, P363 in Oregon, and RUBY in Nevada [Materna, 2014]. Other stations in the area around these sites show skewness as well. Data from these sites could be used to develop methods that generate estimates of the standard deviations of the positions that account for the effects of skewness. Ideally, methods that could be developed that remove the skewness from the position estimates by incorporating more elaborate atmospheric delay models.

Similarly, GPS stations on volcanoes often undergo rapid position changes for geophysical reasons (i.e., due to magmatic events) as well as meteorological reasons (i.e., snow and ice accumulation on the antenna). Position estimates affected by snow and ice are retained in the GAGE position time series and could be used to quantify the role of snow and ice on those estimates. Algorithms could be developed that robustly flag these data. Ideally, not only would data affected by snow and ice accumulation be recognized, independent of position changes, but possibly modeling techniques could be developed that would allow these data to be used to generate reliable position estimates.

In general, the vast majority of GAGE station time series show complexity beyond simple linear motion. Some of these deviations are understood to arise from physical processes such as earthquake coseismic and

postseismic motions, groundwater variations, and magmatic events. There are almost certainly to be other processes that have not yet been fully explored, and there are opportunities for revealing these processes especially when GPS results are combined with other data sets.

Currently, GAGE uses two analysis centers employing both different processing software and analysis methods. The comparison of the results from the two ACs has allowed errors in processing by one AC to be detected using the results of the other AC. The comparison of results also acts as a check on metadata consistency (e.g., antenna and receiver types at stations). However, the differences between the results of the ACs is often more reflective of the quality of data from a GPS station rather than fundamental differences in the models being used by either AC. The two analysis methods being used by the ACs, precise point positioning (PPP) versus double-difference network processing, are sensitive to models in different ways. For example, PPP analysis requires accurate orbit, clock, and wide lane phase bias (to allow ambiguity resolution) files and the models used in the GAGE processing must closely match those used in generating the PPP inputs. In contrast, the double-difference network approach requires accurate orbit information but estimates its own clock and ambiguity parameters.

These different approaches lead to different sensitivities. Specifically, if PPP clock products are generated with one antenna phase center model, the scale from that antenna model partially propagates into the PPP solutions even when an updated antenna phase center model is used. The double difference network approach is less sensitive to this scale propagation. This effect happened in transitioning the GAGE analysis from ITRF2005 to ITRF2008 and necessitated the transition to using JPL products generated in ITRF2008 for PPP solutions rather than the IGS products whose reprocessed results were generated in the ITRF2005 system. A similar transition will be needed when ITRF2014 is introduced. As noted in section 4.1, the double difference network solutions using just a regional array have a large uncertainty in the scale estimates. In future analyses, this uncertainty will be reduced by including a global distribution of sites in the double difference network solutions. Related to this same scale issue, methods still need to be explored that balance the weight of PPP network wide parameters, such as scale, with the double difference network solutions that include correlations between sites. The complexity here is that currently the PPP and double difference network solutions are balanced for single stations with both contributing equally to combined station time series. Only for network averaged parameters do the PPP results dominate the double difference network ones.

GAGE analyses are based purely on GPS L1/L2 code and phase observations at this time, but in the future a transition to full GNSS analysis capability will bring additional analysis complexity and will require upgrades to the currently installed receivers and antennas. This expansion will be challenging due to cost of equipment upgrades and the development of software that can process multiconstellation GNSS data as well as modernized GPS signals. Both of the software packages used by the GAGE ACs are being extended to process GNSS data but neither package has that capability now. The benefits of full GNSS processing will likely be most evident when there are sufficient data and constellations available to detect potential systematic errors in GPS results. Some errors in GPS can be difficult to diagnose due to the repeating ground track and common orbit characteristics of the satellites. For example, some errors in GPS manifest themselves as annual-like signals because of the difference between the data processing interval (24-solar hours) and two orbit periods (approximately 24 sidereal hours with adjustment for the precession of the nodes of satellite orbits). These repeating signals have the draconic period of the GPS satellite which is  $\sim 351$  days, and the repeat time differs by  $\sim 246$  s/d compared to 236 s expected for a sidereal repeat [Agnew and Larson, 2007; Larson et al., 2007]. Errors of these types can potentially be isolated through comparison with results from other constellations that have different characteristics including data from geostationary and geosynchronous satellites.

A final challenge to the full exploitation of GAGE products and data is the access to these results and the knowledge about the results. As we have discussed above, there are often very subtle effects imbedded in the GAGE analysis results that could be overlooked, possibly leading to incorrect conclusions. An example of such an effect has been noted above: that is, the impact of errors in PCO values for newly launched satellites and how these errors could lead to offsets and quasi-annual errors in position time series. In the future, methods will need to be developed that allow users to easily access this knowledge about such effects without overwhelming them with detail. Similarly, developing methods that allow discoverability of features in the results and the merging with other diverse data sets are needed. Efforts along these lines are underway with the GAGE products through the development of Web services to allow more insight into the processing and analysis methods associated with the GAGE ACs and ACC.

**Table A1.** Acronyms

Acronym	Description
AC	Analysis Center
ACC	Analysis Center Coordinator
AGU	American Geophysical Union
BARGEN	Basin and Range Geodetic Network
CDDIS	NASA Crustal Dynamics Data Information System
$\chi^2/f$	Chi-squared per degree of freedom (square root equals the normalized root-mean-square)
COCONet	Continuously Operating Caribbean GPS Observational Network
CORS	Continuously Operating Reference Station
CWU	Central Washington University. Also used as code for the solutions generated by this AC
DMC	Data Management Center
DOI	Digital Object Identifier
EOP	Earth Orbital Parameters
FRII	Front Range Internet, Inc.
GAGE	Geodesy Advancing Geosciences and EarthScope
GAMIT	"GPS At MIT" analysis package
GGN	Global GPS Network
GIA	Glacial Isostatic Adjustment
GPSY/OASIS	GPS Inferred Positioning System/Orbit Analysis and Simulation Software
GLOBK	"Global Kalman filter" used as an integral part of the GAMIT package and often linked as GAMIT/GLOBK
GLONASS	Globalnaya navigatsionnaya sputnikovaya sistema/Global Navigation Satellite System
GMF	Global Mapping Function
GMRT	Global Multi-Resolution Topography
GNSS	Global Navigation Satellite System
GPS	Global Positioning System
GPST	GPS time (This is written with a time: 12:00 GPST)
GPT2	A global tropospheric delay model.
HRW	Random walk process noise values in the horizontal position estimates for a station.
IERS	International Earth Rotation and Reference System
IGRF11/12	International Geomagnetic Reference Field
IGS	International GNSS Service
IGS08	IGS 2008 no net rotation reference frame aligned to ITRF2008 but with a scale change from the IGS reprocessed solutions.
IGb08	IGS 2008 refinement with added discontinuities and updated antenna calibration models for two antennas. The IGb08 coordinates used for the original position and velocity alignment are in igs08_noam.apr. See [IGSMail-6663] IGb08: an update on IGS08
INL	Idaho National Laboratory
IONEX	Ionosphere Map Exchange format
IRI2012	International Reference Ionosphere
IRIS	Incorporated Research Institutions for Seismology
ITRF	International Terrestrial Reference Frame
ITRF2008	International Terrestrial Reference Frame 2008 realization
ITRF2014	International Terrestrial Reference Frame 2014 realization in development
IUGG	International Union of Geodesy and Geophysics
InSAR	Interferometric Synthetic Aperture Radar
JGR	Journal of Geophysical Research
JPL	Jet Propulsion Laboratory
MHD	Mean Height Difference
MIT	Massachusetts Institute of Technology
MREFC	Major Research Equipment and Facilities Construction
MRI	Major Research Instrumentation grant
NA	North America
NA12	North America Reference frame defined <i>Blewitt et al.</i> [2013]
NAM08	North America Reference frame defined by the ITRF2008 Euler pole for North America [ <i>Altamimi et al.</i> , 2012]

**Table A1.** (continued)

Acronym	Description
NASA	National Aeronautics and Space Administration
NCEP/DOE	National Centers for Environmental Prediction/Department of Energy
NEIC	National Earthquake Information Center
NGS	National Geodetic Survey
NMT	New Mexico Institute of Mining and Technology. Also used as code for the solutions generated by this AC.
NNR	No-net-rotation
NOAA	National Oceanic and Atmospheric Administration
NRMS	Normalized root-mean-square (equal to the square root of chi-square per degree of freedom).
NSF	National Science Foundation
O&M	Operations and Maintenance
PANGA	Pacific Northwest Geodetic Array
PBO	Plate Boundary Observatory. This code is also used to refer to the combined GAGE analysis.
PCO	Phase center offset
PPP	Precise point positioning
PRN	Pseudo-random noise
QA	Quality assurance
QC	Quality control
RINEX	Receiver Independent Exchange Format (RINEX documentation)
RMS	Root-mean-square
RWPN	Random Walk time-step variances or Process Noise/Random Walk Process Noise (?)
SCIGN	Southern California Integrated GPS Network
SCIS	SCIGN Short
SINEX	Solution Independent Exchange Format (SINEX documentation)
SNR	Signal-to-noise ratio
SOPAC	Scripps Orbit and Permanent Array Center
SSA	Seismological Society of America
SV	Space vehicle
TEC	Total electron content
TLALOCNet	Trans-boundary Land and Atmosphere Long-term Observational and Collaborative Network
UNAM	Universidad Nacional Autónoma de México
UNAVCO	Not an acronym
UNR	University of Nevada, Reno
USGS	United States Geologic Survey
UT1	Universal time defined by the rotation of Earth. Differs from UTC by up to ~0.5 s depending on when leap seconds are inserted.
UTC	Coordinated universal time (Civilian atomic time).
VMF1	Vienna Mapping Function
VTEC	Vertical Total Electron Content
WLPB	Wide-Lane Phase Bias
WRMS	Weighted root-mean-square

## 6. Summary

The GAGE GPS data products are generated by merging data processing products from two analysis centers (ACs) using two different software packages, which in turn use different analysis methods. The primary products are daily station position estimates and aggregated quantities such as velocity fields. The two ACs are (1) Central Washington University (CWU), which applies a precise point positioning (PPP) methodology using the GIPSY/OASIS software, and (2) New Mexico Tech (NMT), which applies a double-difference network processing strategy with the GAMIT software package.

The results from the GAGE analysis for the period from 1996 to near the end of 2015 show agreement between the velocity estimates for the 2129 stations common to both the CWU and NMT analysis with weighted-root-mean-square (WRMS) differences of 0.1 mm/yr in both north and east (NE) components and

### Acknowledgments

This work was supported by the National Science Foundation (NSF) awards EAR-0350028 Collaborative Research: EarthScope-Acquisition, Construction, Facility Management, Operations and Maintenance/Plate Boundary Observatory (PBO MREFC); EAR-0732947 EarthScope Facility Operation and Maintenance (PBO O&M); EAR-1042906/9 Collaborative Instrumentation: COCONet (Continuously Operating Caribbean GPS Observational Network) An Infrastructure Proposal for a Multi-hazard Tectonic and Weather Observatory; EAR-1338091 MRI: TLALOCNet—Development of a continuous GPS-MET array in Mexico for atmospheric, climatic, and seismotectonic research in the Americas; and EAR-1261833 2013–2018 UNAVCO Community Proposal Geodesy Advancing Geosciences and EarthScope: The GAGE Facility (GAGE). The analysis comparison work was partly supported by NASA NNX14AQ03G, and the Southern California Earthquake Center and NSF cooperative agreement EAR-1033462. Most data used for this project were obtained from the UNAVCO archive. GPS data were also obtained from the NOAA National Geodetic Survey (NGS) Continuously Operating Reference Station (CORS) data center, the NASA Crustal Dynamics Data Information System (CDDIS), the U.S. Geological Survey, the Scripps Orbit and Permanent Array Center (SOPAC), and the International GNSS Service (IGS). Data products used for comparison purposes including GPS time series solutions were generated by and obtained from the Nevada Geodetic Laboratory at the University of Nevada Reno, the NASA Jet Propulsion Laboratory (JPL), and the U.S. Geological Survey. IGS products [Dow *et al.*, 2009] were used extensively in the analyses presented here. Figures were created by using the Generic Mapping Tools [Wessel *et al.*, 2013] and MATLAB™. Additional data and resources used for this project are cited as References. Gregory J. Anderson was the Data Products Manager at UNAVCO when this work was initially developed and implemented. He was instrumental to the success of this project through his leadership and contributions to helping design the systems, workflows, and product definitions still used to this day. Adrian Borsa coordinated this work during his tenure at UNAVCO as Data Products Manager and subsequently highlighted end-user requirements for vertical time series generation. Glen S. Mattioli, UNAVCO Director of Geodetic Infrastructure, was an invaluable

0.4 mm/yr in vertical (Kalman Filter SINEX analysis). The arithmetic means of the differences between the time series generated by each analysis center show median differences of < 0.1 mm in NE and < 1.0 mm in vertical. The median of the WRMS differences are < 1 mm in NE and 5.3 mm in vertical. These WRMS scatters of the differences are comparable in size to the standard deviation of their estimates. Comparisons of GAGE results with results from other analysis groups show similar levels of agreement.

The GAGE products differ from the analyses of other groups in that scale differences between daily position results and reference frame positions are not estimated, and this difference impacts the interpretation of height changes across the networks being analyzed. When scale is estimated by other groups, the average of the height differences at the reference frame sites is absorbed into the scale estimate. The impact of this removal of scale changes depends on the reference frame network. For example, a reference frame network that only spans North America will result in the average height changes across North America being absorbed into the scale estimates. The GAGE analyses retain these average height changes because the network scale is not removed. The GAGE position time series also retain estimates for all data that are collected even if these estimates might be affected by nongeophysical processes such as snow and ice on antenna or failed antennas. Loading effects, discontinuities due to earthquakes, equipment changes and other phenomena, and earthquake postseismic motions are not removed from the position time series. Efforts are made to account for these effects when velocity fields are determined.

This paper presents a snapshot and history of the GAGE analysis methods. Every effort has been made to document the methods used and to make processed results and explanations available. There is much more analysis that can be done on the GAGE products than the few small examples presented here. The products used to generate the results in this paper are being made available through supplemental material and on the UNAVCO GAGE products website (<http://www.unavco.org/revgeophys2016>). The analyses are ongoing with new data being added and refinements of earlier processed results being incorporated when necessary.

The next significant change to the GAGE processing will be the adoption of the ITRF2014 reference frame and the reprocessing (1996 to present) associated with this updated frame when IGS and JPL products in the ITRF2014 frame become available. This reprocessing is expected to begin before the end of 2016. There will be a transition period as new products are generated in the ITRF2014 system and older products are still being reprocessed. The UNAVCO products log will keep users informed of the status of this transition. It is expected that improved analysis methods will be incorporated into the reprocessing. In the future, it is also likely that full GNSS processing will be adopted and the new GNSS frequencies, signals, and orbits will complement the GPS system and help identify systemic errors and biases associated with the GPS system. Model improvements will likely be incorporated into future analyses to generate even higher-quality results than currently available.

## Appendix A

Table A1 lists the acronyms used in this paper along with explanatory text.

## References

- Agnew, D. C., and K. M. Larson (2007), Finding the repeat times of the GPS constellation, *GPS Solutions*, 11, 71–76.
- Aguilar, A., T. Melbourne, and C. Scrivner (2009), Moment release rate of Cascadia tremor constrained by GPS, *J. Geophys. Res.*, 114, B00A05, doi:10.1029/2008JB005909.
- Altamimi, Z., X. Collilieux, and L. Métivier (2011), ITRF2008: An improved solution of the international terrestrial reference frame, *J. Geod.*, 85, 457–473, doi:10.1007/s00190-011-0444-4.
- Altamimi, Z., L. Métivier, and X. Collilieux (2012), ITRF2008 plate motion model, *J. Geophys. Res.*, 117, B07402, doi:10.1029/2011JB008930.
- Amiri-Simkooei, A. R., C. C. J. M. Tiberius, and P. J. G. Teunissen (2007), Assessment of noise in GPS coordinate time series: Methodology and results, *J. Geophys. Res.*, 112, B07413, doi:10.1029/2006JB004913.
- Amos, C. B., P. Audet, W. C. Hammond, R. Bürgmann, I. A. Johanson, and G. Blewitt (2014), Uplift and seismicity driven by groundwater depletion in central California, *Nature*, 509, 483–486, doi:10.1038/nature13275.
- Argus, D. F., W. R. Peltier, R. Drummond, and A. W. Moore (2014), The Antarctica component of postglacial rebound model ICE-6G\_C (VM5a) based upon GPS positioning, exposure age dating of ice thicknesses, and relative sea level histories, *Geophys. J. Int.*, 198, 537–563, doi:10.1093/gji/ggu140.
- Barnhart, W. D., J. R. Murray, J. L. Svarc, B. A. Brooks, S.-H. Yun, E. J. Fielding, S. V. Samsonov, and P. Milillo (2015), Geodetic constraints on the 2014 M 6.0 South Napa earthquake, *Seismol. Res. Lett.*, 86, 335–343, doi:10.1785/0220140210.
- Beavan, J. (2005), Noise properties of continuous GPS data from concrete pillar geodetic monuments in New Zealand and comparison with data from U.S. deep drilled braced monuments, *J. Geophys. Res.*, 110, B08410, doi:10.1029/2005JB003642.

contributor to the development of this article from inception to final preparation and provided key strategic guidance, technical input, meticulous review, and critical editing. Charles M. Meertens, UNAVCO Director of Geodetic Services, and M. Meghan Miller, UNAVCO President provided strategic guidance and valuable input to the project and the preparation of this article. Frances M. Boler, David Maggert, Dan Reiner, and other UNAVCO Data Center staff provided critical support for data and metadata management. The acquisition of PBO, COCONet and TLALOCNet data is made possible by the entire team of individuals supporting these networks in numerous ways from field engineering to development and testing to permitting to data flow, and including UNAVCO staff and community partners. The GPS data processed for this review are available in open archives located at UNAVCO ftp://data-out.unavco.org/pub/rinex/obs, NASA CDDIS ftp://cddis.gsfc.nasa.gov/pub/gps/data/daily/, SOPAC ftp://garner.ucsd.edu/pub/rinex/, NGS CORS ftp://www.ngs.noaa.gov/cors/rinex/, and PANGA ftp://www.geodesy.cwu.edu/pub/data/. The products generated by the analyses discussed in this review are available through UNAVCO at ftp://data-out.unavco.org/pub/products/ for position time series, velocity fields, and processing script and discussions. These products are updated daily as new data become available and the specific release of the products used in this review are made available at <http://www.unavco.org/revgeophys2016>. The authors would also like to thank the Editor-in-Chief, Fabio Florindo, Tim Dixon, Jim Ray, and anonymous reviewer for their useful comments that helped clarify and improve this review.

- Bertiger, W., S. D. Desai, B. Haines, N. Harvey, A. W. Moore, S. Owen, and J. P. Weiss (2010), Single receiver phase ambiguity resolution with GPS data, *J. Geod.*, *84*, 327–337, doi:10.1007/s00190-010-0371-9.
- Beutler, G., M. Rothacher, S. Schaer, T. A. Springer, J. Kouba, and R. E. Neilan (1999), The International GPS Service (IGS): An interdisciplinary service in support of Earth sciences, *Adv. Space Res.*, *23*, 631–635, doi:10.1016/S0273-1177(99)00160-X.
- Bevis, M., S. Businger, T. A. Herring, C. Rocken, R. A. Anthes, and R. H. Ware (1992), GPS meteorology: Remote sensing of atmospheric water vapor using the global positioning system, *J. Geophys. Res.*, *97*, 15,787–15,801, doi:10.1029/92JD01517.
- Blewitt, G. (2003), Self-consistency in reference frames, geocenter definition, and surface loading of the solid Earth, *J. Geophys. Res.*, *108*(B2), 2103, doi:10.1029/2002JB002082.
- Blewitt, G., C. Kreemer, W. C. Hammond, H.-P. Plag, S. Stein, and E. Okal (2006), Rapid determination of earthquake magnitude using GPS for tsunami warning systems, *Geophys. Res. Lett.*, *33*, L11309, doi:10.1029/2006GL026145.
- Blewitt, G., C. Kreemer, W. C. Hammond, and J. M. Goldfarb (2013), Terrestrial reference frame NA12 for crustal deformation studies in North America, *J. Geodyn.*, *72*, 11–24, doi:10.1016/j.jog.2013.08.004.
- Bock, Y., S. A. Gorevitch, C. C. Counselman III, R. W. King, and R. I. Abbot (1986), Interferometric analysis for GPS phase observations, *Manuscr. Geod.*, *11*, 282–288.
- Bock, Y., L. Prawirodirdjo, and T. I. Melbourne (2004), Detection of arbitrarily large dynamic ground motions with a dense high-rate GPS network, *Geophys. Res. Lett.*, *31*, L06604, doi:10.1029/2003GL019150.
- Bock, Y., D. Melgar, and B. W. Crowell (2011), Real-time strong-motion broadband displacements from collocated GPS and accelerometers, *Bull. Seismol. Soc. Am.*, *101*, 2904–2925, doi:10.1785/0120110007.
- Boehm, J., B. Werl, and H. Schuh (2006), Troposphere mapping functions for GPS and very long baseline interferometry from European Centre for Medium-Range Weather Forecasts operational analysis data, *J. Geophys. Res.*, *111*, B02406, doi:10.1029/2005JB003629.
- Borsa, A. A., D. C. Agnew, and D. R. Cayan (2014), Ongoing drought-induced uplift in the western United States, *Science*, *345*, 1587–1590, doi:10.1126/science.1260279.
- Braun, J. J., E. Calais, K. F. Feaux, G. Mattioli, M. Miller, and G. Wang (2012), The Continuously Operating Caribbean Observational Network (COCONet): Improved observational capacity in the Caribbean, paper presented at 30th Conference on Hurricanes and Tropical Meteorology, Am. Meteorol. Soc., Ponte Vedra Beach, Fla.
- Brudzinski, M. R., and R. M. Allen (2007), Segmentation in episodic tremor and slip all along Cascadia, *Geology*, *35*, 907–910, doi:10.1130/G23740A.1.
- Calais, E., and J. B. Minster (1995), GPS detection of ionospheric perturbations following the January 17, 1994, Northridge earthquake, *Geophys. Res. Lett.*, *22*, 1045–1048, doi:10.1029/95GL00168.
- Calais, E., J. Y. Han, C. DeMets, and J. M. Nocquet (2006), Deformation of the North American plate interior from a decade of continuous GPS measurements, *J. Geophys. Res.*, *111*, B06402, doi:10.1029/2005JB004253.
- Cardellach, E., P. Elosegui, and J. L. Davis (2007), Global distortion of GPS networks associated with satellite antenna model errors, *J. Geophys. Res.*, *112*, B07405, doi:10.1029/2006JB004675.
- Chang, W.-L., R. B. Smith, J. Farrell, and C. M. Puskas (2010), An extraordinary episode of Yellowstone caldera uplift, 2004–2010, from GPS and InSAR observations, *Geophys. Res. Lett.*, *37*, L23302, doi:10.1029/2010GL045451.
- Chang, W.-L., R. B. Smith, and C. M. Puskas (2013), Effects of lithospheric viscoelastic relaxation on the contemporary deformation following the 1959  $M_w$  7.3 Hebgen Lake, Montana, earthquake and other areas of the intermountain seismic belt, *Geochem. Geophys. Geosyst.*, *14*, 1–17, doi:10.1029/2012GC004424.
- Chapman, J., and T. Melbourne (2009), Future Cascadia megathrust rupture delineated by episodic tremor and slip, *Geophys. Res. Lett.*, *36*, L22301, doi:10.1029/2009GL040465.
- Collilieux, X., T. van Dam, J. Ray, D. Coulot, L. Metivier, and Z. Altamimi (2011), Strategies to mitigate aliasing of loading signals while estimating GPS frame parameters, *J. Geod.*, *86*, 1–14, doi:10.1007/s00190-011-0487-6.
- Crowell, B. W., Y. Bock, and D. Melgar (2012), Real-time inversion of GPS data for finite fault modeling and rapid hazard assessment, *Geophys. Res. Lett.*, *39*, L09305, doi:10.1029/2012GL051318.
- Delouis, B., J. Nocquet, and M. Vallée (2010), Slip distribution of the February 27, 2010  $M_w$  = 8.8 Maule earthquake, central Chile, from static and high-rate GPS, InSAR, and broadband teleseismic data, *Geophys. Res. Lett.*, *37*, L17305, doi:10.1029/2010GL043899.
- Desai, S. D., W. Bertiger, and B. Haines (2014), Self-consistent treatment of tidal variations in the geocenter for precise orbit determination, *J. Geod.*, *88*, 735–747, doi:10.1007/s00190-014-0718-8.
- Dong, D., T. A. Herring, and R. W. King (1998), Estimating regional deformation from a combination of space and terrestrial geodetic data, *J. Geod.*, *72*, 200–214, doi:10.1007/s001900050161.
- Dong, D., P. Fang, Y. Bock, M. K. Cheng, and S. Miyazaki (2002), Anatomy of apparent seasonal variations from GPS-derived site position time series, *J. Geophys. Res.*, *107*(B4), 2075, doi:10.1029/2001JB000573.
- Dow, J. M., R. E. Neilan, and C. Rizos (2009), The International GNSS Service in a changing landscape of Global Navigation Satellite Systems, *J. Geod.*, *83*, 191–198, doi:10.1007/s00190-008-0300-3.
- Dragert, H., K. Wang, and T. S. James (2001), A silent slip event on the deeper cascadia subduction interface, *Science*, *292*, 1525–1528, doi:10.1126/science.1060152.
- Dreger, D. S., M.-H. Huang, A. Rodgers, T. Taira, and K. Woodell (2015), Kinematic finite source model for the 24 August 2014 South Napa, California, earthquake from joint inversion of seismic, GPS, and InSAR data, *Seismol. Res. Lett.*, *86*, 327–334, doi:10.1785/0220140244.
- Elliott, J. L., C. F. Larsen, J. T. Freymueller, and R. J. Motyka (2010), Tectonic block motion and glacial isostatic adjustment in southeast Alaska and adjacent Canada constrained by GPS measurements, *J. Geophys. Res.*, *115*, B09407, doi:10.1029/2009JB007139.
- Elósegui, P., J. L. Davis, J. X. Mitrovica, R. A. Bennett, and B. P. Wernicke (2003), Crustal loading near Great Salt Lake, Utah, *Geophys. Res. Lett.*, *30*(3), 1111, doi:10.1029/2002GL016579.
- Estey, L., and C. Meertens (1999), TEQC: The multi-purpose toolkit for GPS/GLONASS data, *GPS Solutions*, *3*, 42–49, doi:10.1007/PL00012778.
- Falck, C., M. Ramatschi, C. Subarya, M. Bartsch, A. Merx, J. Hoeberechts, and G. Schmidt (2010), Near real-time GPS applications for tsunami early warning systems, *Nat. Hazards Earth Syst. Sci.*, *10*, 181–189, doi:10.5194/nhess-10-181-2010.
- Farrell, J., R. B. Smith, T. Taira, W.-L. Chang, and C. M. Puskas (2010), Dynamics and rapid migration of the energetic 2008–2009 Yellowstone Lake earthquake swarm, *Geophys. Res. Lett.*, *37*, L19305, doi:10.1029/2010GL044605.
- Finlay, C. C., et al. (2010), International Geomagnetic Reference Field: The eleventh generation, *Geophys. J. Int.*, *183*, 1216–1230, doi:10.1111/j.1365-246X.2010.04804.x.
- Floyd, M. A., et al. (2016), Spatial variations in fault friction related to lithology from rupture and afterslip of the 2014 South Napa, California, earthquake, *Geophys. Res. Lett.*, *43*, 6808–6816, doi:10.1002/2016GL069428.

- Freyemueller, J. T., H. Woodard, S. C. Cohen, R. Cross, J. Elliott, C. F. Larsen, S. Hreinsdóttir, and C. Zweck (2008), Active deformation processes in Alaska, based on 15 years of GPS measurements, in *Active Tectonics and Seismic Potential of Alaska*, edited by J. T. Freyemueller et al., pp. 1–42, AGU, Washington, D. C., doi:10.1029/179GM02.
- Fritsche, M., R. Dietrich, C. Knöfel, A. Rülke, S. Vey, M. Rothacher, and P. Steigenberger (2005), Impact of higher-order ionospheric terms on GPS estimates, *Geophys. Res. Lett.*, *32*, L23311, doi:10.1029/2005GL024342.
- Fu, Y., D. F. Argus, and F. W. Landerer (2015), GPS as an independent measurement to estimate terrestrial water storage variations in Washington and Oregon, *J. Geophys. Res. Solid Earth*, *120*, 552–566, doi:10.1002/2014JB011415.
- Galvan, D. A., A. Komjathy, M. P. Hickey, and A. J. Mannucci (2011), The 2009 Samoa and 2010 Chile tsunamis as observed in the ionosphere using GPS total electron content, *J. Geophys. Res.*, *116*, A06318, doi:10.1029/2010JA016204.
- Ge, M., G. Gendt, G. Dick, F. P. Zhang, and C. Reigber (2005), Impact of GPS satellite antenna offsets on scale changes in global network solutions, *Geophys. Res. Lett.*, *32*, L06310, doi:10.1029/2004GL022224.
- Gomberg, J., the Cascadia 2007, and Beyond Work Group (2010), Slow slip phenomena in Cascadia from 2007 and beyond: A review, *Geol. Soc. Am. Bull.*, *122*, 963–978, doi:10.1130/B30287.1.
- Hernández-Pajares, M., J. M. Juan, J. Sanz, and R. Orús (2007), Second-order ionospheric term in GPS: Implementation and impact on geodetic estimates, *J. Geophys. Res.*, *112*, B08417, doi:10.1029/2006JB004707.
- Herring, T. A., R. W. King, M. A. Floyd, and S. C. McClusky (2015), *Introduction to GAMIT/GLOBK, Release 10.6*, Mass. Inst. of Technol., Cambridge.
- Holtkamp, S., and M. R. Brudzinski (2010), Determination of slow slip episodes and strain accumulation along the Cascadia margin, *J. Geophys. Res.*, *115*, B00A17, doi:10.1029/2008JB006058.
- Houlié, N., P. Briole, A. Nercessian, and M. Murakami (2005), Sounding the plume of the 18 August 2000 eruption of Miyakejima volcano (Japan) using GPS, *Geophys. Res. Lett.*, *32*, L05302, doi:10.1029/2004GL021728.
- IERS (2005), SINEX format. [Available at <https://www.iers.org/IERS/EN/Organization/AnalysisCoordinator/SinexFormat/sinex.html>.]
- Ji, K. H., and T. A. Herring (2011), Transient signal detection using GPS measurements: Transient inflation at Akutan volcano, Alaska, during early 2008, *Geophys. Res. Lett.*, *38*, L06307, doi:10.1029/2011GL046904.
- Ji, K. H., and T. A. Herring (2013), A method for detecting transient signals in GPS position time-series: Smoothing and principal component analysis, *Geophys. J. Int.*, *193*, 171–186, doi:10.1093/gji/ggt003.
- Johansson, J. M., et al. (2002), Continuous GPS measurements of postglacial adjustment in Fennoscandia, 1. Geodetic results, *J. Geophys. Res.*, *107*, 2157, doi:10.1029/2001JB000400.
- Kato, T., Y. Terada, K. Ito, R. Hattori, T. Abe, T. Miyake, S. Koshimura, and T. Nagai (2005), Tsunami due to the 2004 September 5th off the Kii peninsula earthquake, Japan, recorded by a new GPS buoy, *Earth Planets Space*, *57*, 297–301, doi:10.1186/BF03352566.
- Kedar, S., G. A. Hajj, B. D. Wilson, and M. B. Hefflin (2003), The effects of the second order GPS ionospheric correction on receiver positions, *Geophys. Res. Lett.*, *30*(16), 1829, doi:10.1029/2003GL017639.
- Lagler, K., M. Schindelegger, J. Böhm, H. Krásná, and T. Nilsson (2013), GPT2: Empirical slant delay model for radio space geodetic techniques, *Geophys. Res. Lett.*, *40*, 1069–1073, doi:10.1002/grl.50288.
- Langbein, J. (2004), Noise in two-color electronic distance meter measurements revisited, *J. Geophys. Res.*, *109*, B04406, doi:10.1029/2003JB002819.
- Langbein, J. (2008), Noise in GPS displacement measurements from Southern California and Southern Nevada, *J. Geophys. Res.*, *113*, B05405, doi:10.1029/2007JB005247.
- Langbein, J., and H. Johnson (1997), Correlated errors in geodetic time series: Implications for time-dependent deformation, *J. Geophys. Res.*, *102*, 591–603, doi:10.1029/96JB02945.
- Langbein, J., F. Wyatt, H. Johnson, D. Hamann, and P. Zimmer (1995), Improved stability of a deeply anchored geodetic monument, *Geophys. Res. Lett.*, *22*, 3533–3536, doi:10.1029/95GL03325.
- Larsen, C. F., R. J. Motyka, J. T. Freyemueller, K. A. Echelmeyer, and E. R. Ivins (2005), Rapid viscoelastic uplift in southeast Alaska caused by post-Little Ice Age glacial retreat, *Earth Planet. Sci. Lett.*, *237*, 548–560, doi:10.1016/j.epsl.2005.06.032.
- Larson, K. M., P. Bodin, and J. Gomberg (2003), Using 1-Hz GPS data to measure deformations caused by the Denali fault earthquake, *Science*, *300*(5624), 1421–1424, doi:10.1126/science.1084531.
- Larson, K. M., A. Bilich, and P. Axelrad (2007), Improving the precision of high-rate GPS, *J. Geophys. Res.*, *112*, B05422, doi:10.1029/2006JB004367.
- Larson, K. M., E. E. Small, E. Gutmann, A. Bilich, J. Braun, and V. Zavorotny (2008), Use of GPS receivers as a soil moisture network for water cycle studies, *Geophys. Res. Lett.*, *35*, L24405, doi:10.1029/2008GL036013.
- Larson, K. M., E. D. Gutmann, V. U. Zavorotny, J. J. Braun, M. W. Williams, and F. G. Nievinski (2009), Can we measure snow depth with GPS receivers?, *Geophys. Res. Lett.*, *36*, L17502, doi:10.1029/2009GL039430.
- Leick, A., L. Rapoport, and D. Tatarnikov (2015), *GPS Satellite Surveying*, 840 pp., John Wiley, Hoboken, N. J.
- Liu, J.-Y., Y.-B. Tsai, K.-F. Ma, Y.-I. Chen, H.-F. Tsai, C.-H. Lin, M. Kamogawa, and C.-P. Lee (2006), Ionospheric GPS total electron content (TEC) disturbances triggered by the 26 December 2004 Indian Ocean tsunami, *J. Geophys. Res.*, *111*, A05303, doi:10.1029/2005JA011200.
- Lohman, R. B., and J. R. Murray (2013), The SCEC geodetic transient-detection validation exercise, *Seismol. Res. Lett.*, *84*, 419–425, doi:10.1785/0220130041.
- Mannucci, A. J., B. D. Wilson, D. N. Yuan, C. H. Ho, U. J. Lindqwister, and T. F. Runge (1998), A global mapping technique for GPS-derived ionospheric total electron content measurements, *Radio Sci.*, *33*, 565–582, doi:10.1029/97RS02707.
- Mao, A., C. G. A. Harrison, and T. H. Dixon (1999), Noise in GPS coordinate time series, *J. Geophys. Res.*, *104*, 2797–2816, doi:10.1029/1998JB900033.
- Materna, K. (2014), Analysis of atmospheric delays and asymmetric positioning errors in the global positioning system, BSc thesis, 51 pp., Mass. Inst. of Technol. [Available at <http://hdl.handle.net/1721.1/90657>.]
- Nandy, D., A. Muñoz-Jaramillo, and P. C. H. Martens (2011), The unusual minimum of sunspot cycle 23 caused by meridional plasma flow variations, *Nature*, *471*, 80–82, doi:10.1038/nature09786.
- Niell, A. (1996), Global mapping functions for the atmosphere delay at radio wavelengths, *J. Geophys. Res.*, *101*, 3227–3246, doi:10.1029/95JB03048.
- Nievinski, F. G., and K. M. Larson (2014a), Inverse modeling of GPS multipath for snow depth estimation—part I: Formulation and simulations, *IEEE Trans. Geosci. Remote Sens.*, *52*, 6555–6563, doi:10.1109/TGRS.2013.2297681.
- Nievinski, F. G., and K. M. Larson (2014b), Inverse modeling of GPS multipath for snow depth estimation—Part II: Application and validation, *IEEE Trans. Geosci. Remote Sens.*, *52*, 6564–6573, doi:10.1109/TGRS.2013.2297688.
- Nishimura, T., H. Munekane, and H. Yari (2011), The 2011 off the Pacific coast of Tohoku Earthquake and its aftershocks observed by GEONET, *Earth Planets Space*, *63*, 631–636, doi:10.5047/eps.2011.06.025.

- Orús, R., M. Hernández-Pajares, J. M. Juan, J. Sanz, and M. García-Fernández (2002), Performance of different TEC models to provide GPS ionospheric corrections, *J. Atmos. Sol. Terr. Phys.*, *64*, 2055–2062, doi:10.1016/S1364-6826(02)00224-9.
- Ouellette, K. J., C. de Linage, and J. S. Famiglietti (2013), Estimating snow water equivalent from GPS vertical site-position observations in the western United States, *Water Resour. Res.*, *49*, 2508–2518, doi:10.1002/wrcr.20173.
- Ozeki, M., and K. Heki (2012), GPS snow depth meter with geometry-free linear combinations of carrier phases, *J. Geod.*, *86*, 209–219, doi:10.1007/s00190-011-0511-x.
- Peltier, W. R. (2004), Global glacial isostasy and the surface of the Ice-Age Earth: The ICE-5G (VM2) model and GRACE, *Annu. Rev. Earth Planet. Sci.*, *32*, 111–149, doi:10.1146/annurev.earth.32.082503.144359.
- Peltier, W. R., D. F. Argus, and R. Drummond (2015), Space geodesy constrains ice-age terminal deglaciation: The global ICE-6G\_C (VM5a) model, *J. Geophys. Res. Solid Earth*, *120*, 450–487, doi:10.1002/2014JB011176.
- Peyret, F., D. Baille, and G. Hintzy (2000), High-precision application of GPS in the field of real-time equipment positioning, *Automat. Constr.*, *9*, 299–314, doi:10.1016/S0926-5805(99)00058-8.
- Pritchard, M., et al. (2012), Open access to geophysical data sets requires community responsibility, *Eos Trans. AGU*, *93*(26), 243, doi:10.1029/2012EO260006.
- Radhakrishna, B., F. Fabry, J. J. Braun, and T. M. Vanhove (2015), Precipitable water from GPS over the continental United States: Diurnal cycle, intercomparisons with NARR, and link with convective initiation, *J. Clim.*, *28*, 2584–2599, doi:10.1175/JCLI-D-14-00366.1.
- Rebischung, P., J. Griffiths, J. Ray, R. Schmid, X. Collilieux, and B. Garayt (2012), IGS08: The IGS realization of ITRF2008, *GPS Solutions*, *16*, 483–494, doi:10.1007/s10291-011-0248-2.
- Rebischung, P., Z. Altamimi, J. Ray, and B. Garayt (2016), IGS contribution to ITRF2014, *J. Geod.*, *90*, 611–630, doi:10.1007/s00190-016-0897-6.
- Rocken, C., T. Van Hove, and R. Ware (1997), Near real-time GPS sensing of atmospheric water vapor, *Geophys. Res. Lett.*, *24*, 3221–3224, doi:10.1029/97GL03312.
- Rogers, G., and H. Dragert (2003), Episodic tremor and slip on the cascadia subduction zone: The chatter of silent slip, *Science*, *300*, 1942–1943, doi:10.1126/science.1084783.
- Sagiya, T. (2004), A decade of GEONET: 1994–2003—the continuous GPS observation in Japan and its impact on earthquake studies—, *Earth Planets Space*, *56*, xxix–xli, doi:10.1186/BF03353077.
- Sauber, J. M., and B. F. Molnia (2004), Glacier ice mass fluctuations and fault instability in tectonically active Southern Alaska, *Global Planet. Change*, *42*, 279–293, doi:10.1016/j.gloplacha.2003.11.012.
- Schmid, R., P. Steigenberger, G. Gendt, M. Ge, and M. Rothacher (2007), Generation of a consistent absolute phase center correction model for GPS receiver and satellite antennas, *J. Geod.*, *81*, 781–798, doi:10.1007/s00190-007-0148-y.
- Sella, G. F., S. Stein, T. H. Dixon, M. Craymer, T. S. James, S. Mazzotti, and R. K. Dokka (2007), Observation of glacial isostatic adjustment in “stable” North America with GPS, *Geophys. Res. Lett.*, *34*, L02306, doi:10.1029/2006GL027081.
- Shao, G., X. Li, C. Ji, and T. Maeda (2011), Focal mechanism and slip history of the 2011 Mw 9.1 off the Pacific coast of Tohoku Earthquake, constrained with teleseismic body and surface waves, *Earth Planets Space*, *63*, 559–564, doi:10.5047/eps.2011.06.028.
- Silver, P. G., et al. (1998), A plate boundary observatory, *IRIS Newsl.*, *XVI*, 3.
- Simons, M., et al. (2011), The 2011 magnitude 9.0 Tohoku-Oki earthquake: Mosaicking the megathrust from seconds to centuries, *Science*, *332*, 1421–1425, doi:10.1126/science.1206731.
- Small, E. E., K. M. Larson, and J. J. Braun (2010), Sensing vegetation growth with reflected GPS signals, *Geophys. Res. Lett.*, *37*, L12401, doi:10.1029/2010GL042951.
- Snay, R. A., J. T. Freymueller, M. R. Craymer, C. F. Pearson, and J. Saleh (2016), Modeling 3-D crustal velocities in the United States and Canada, *J. Geophys. Res. Solid Earth*, *121*, 5365–5388, doi:10.1002/2016JB012884.
- Vey, S., R. Dietrich, A. Rülke, M. Fritsche, P. Steigenberger, and M. Rothacher (2010), Validation of precipitable water vapor within the NCEP/DOE reanalysis using global GPS observations from one decade, *J. Clim.*, *23*, 1675–1695, doi:10.1175/2009JCLI2787.1.
- Vigny, C., et al. (2005), Insight into the 2004 Sumatra–Andaman earthquake from GPS measurements in southeast Asia, *Nature*, *436*, 201–206, doi:10.1038/nature03937.
- Wahr, J., S. A. Khan, T. van Dam, L. Liu, J. H. van Angelen, M. R. van den Broeke, and C. M. Meertens (2013), The use of GPS horizontals for loading studies, with applications to northern California and southeast Greenland, *J. Geophys. Res. Solid Earth*, *118*, 1795–1806, doi:10.1002/jgrb.50104.
- Wei, S., S. Barbot, R. Graves, J. J. Lienkaemper, T. Wang, K. Hudnut, Y. Fu, and D. Helmberger (2015), The 2014 Mw 6.1 South Napa earthquake: A unilateral rupture with shallow asperity and rapid afterslip, *Seismol. Res. Lett.*, *86*, 344–354, doi:10.1785/0220140249.
- Wessel, P., W. H. F. Smith, R. Scharroo, J. F. Luis, and F. Wobbe (2013), Generic Mapping Tools: Improved version released, *Eos Trans. AGU*, *94*, 409–410, doi:10.1002/2013EO450001.
- Williams, M. L., K. M. Fischer, J. T. Freymueller, B. Tikoff, and A. M. Tréhu (2010), Unlocking the Secrets of the North American Continent: An EarthScope Science Plan for 2010–2020, 78 pp.
- Williams, S. (2008), CATS: GPS coordinate time series analysis software, *GPS Solutions*, *12*, 147–153.
- Williams, S. D. P., and N. T. Penna (2011), Non-tidal ocean loading effects on geodetic GPS heights, *Geophys. Res. Lett.*, *38*, L09314, doi:10.1029/2011GL046940.
- Williams, S. D. P., Y. Bock, P. Fang, P. Jamason, R. M. Nikolaidis, L. Prawirodirdjo, M. Miller, and D. J. Johnson (2004), Error analysis of continuous GPS position time series, *J. Geophys. Res.*, *109*, B03412, doi:10.1029/2003JB002741.
- Wolfe, D. E., and S. I. Gutman (2000), Developing an operational, surface-based, GPS, water vapor observing system for NOAA: Network design and results, *J. Atmos. Oceanic Technol.*, *17*, 426–440, doi:10.1175/1520-0426(2000)017<0426:DAOSBG>2.0.CO;2.
- Wright, T. J., N. Houlié, M. Hildyard, and T. Iwabuchi (2012), Real-time, reliable magnitudes for large earthquakes from 1 Hz GPS precise point positioning: The 2011 Tohoku-Oki (Japan) earthquake, *Geophys. Res. Lett.*, *39*, L12302, doi:10.1029/2012GL051894.
- Zhang, J., Y. Bock, H. Johnson, P. Fang, S. Williams, J. Genrich, S. Wdowinski, and J. Behr (1997), Southern California permanent GPS geodetic array: Error analysis of daily position estimates and site velocities, *J. Geophys. Res.*, *102*, 18,035–18,055, doi:10.1029/97JB01380.
- Zumberge, J. F., M. B. Heflin, D. C. Jefferson, M. M. Watkins, and F. H. Webb (1997), Precise point positioning for the efficient and robust analysis of GPS data from large networks, *J. Geophys. Res.*, *102*, 5005–5017, doi:10.1029/96JB03860.